UNIVERSITA' DEGLI STUDI DI NAPOLI"FEDERICO II"

DIPARTIMENTO DI INGEGNERIA ELETTRICA E DELLE TECNOLOGIE DELL'INFORMAZIONE

DOTTORATO DI RICERCA IN INGEGNERIA ELETTRICA

XXVII CICLO

"The use of axial flux machine in high reliability mechatronic actuators"

SUPERVISOR

Chiar.mo Prof. Andrea Del Pizzo

Ph.D. CANDIDATE

Luigi Pio Di Noia

Ph.D. COORDINATOR

Ch.mo Prof. Claudio Serpico

A.A. 2014-2015

INDEX

List of figures

Fig.1.4) a) Harmonic content of the stator magneto motive force for a 24 slots- 20 poles machine; b)Winding factor of the stator windings for a 24 slots- 20 poles machine.
Fig.2.4) On the left is shown the total view of magnetic flux density in the machine MFA3500-159; on the right a tooth particular is shown
Fig.3.4) Electromagnetic torque obtained with a transient analysis at rated speed of 590 rpm and rated current of 5,6 A
Fig.4.4) On the left is shown the total view of magnetic flux density in the machine MFA3500-159CT; on the right a tooth particular is shown
Fig.5.4) Electromagnetic torque obtained with a transient analysis at rated speed of 590 rpm and rated current of 5,6 A
Fig.6.4) On the left is shown the total view of magnetic flux density in the machine MFA3500-109; on the right a tooth particular is shown
Fig.7.4) Electromagnetic torque obtained with a transient analysis at rated speed of 590 rpm and rated current of 5,6 A
Fig.8.4) Mean values of electromagnetic torque [Nm] computed for the three machine: MFA3500-159, MFA3500-159CT, MFA3500-109
Fig.9.4) Maximum values of cogging torque [Nm] computed for the three machine: MFA3500-159, MFA3500-159CT, MFA3500-109.
Fig.10.4) Torque constant [Nm/A] computed for the three machine: MFA3500-159, MFA3500-159CT, MFA3500-109.
Fig.11.4) EMF constant [V/rpm] computed for the three machine: MFA3500-159, MFA3500-159CT, MFA3500-109.
Fig.12.4) Joule losses [W] and Iron losses [W] computed for the three machine: MFA3500-159, MFA3500-159CT, MFA3500-109.
Fig.13.4) Fill factor of the three machine: MFA3500-159, MFA3500-159CT, MFA3500-109.
Fig.14.4) Synchronous inductances of the machines: MFA3500-159, MFA3500-159CT, MFA3500-109.
Fig.15.4) Electromagnetic torque in the flux weakning operation zone, at maximum speed of 900 rpm and Id equal to 6,86 A: MFA3500-159, MFA3500-159CT, MFA3500-109.
Fig.16.4) Single coil of windings (each phase is constituted by four type of this coil)
Fig.17.4) In the figure is shown a single coil which is wrapped around the teeth of machine
Fig.18.4) Frontal view of a single coil wrapped around the teeth of machine
Fig.19.4) View of machine 3d printer prototype
Fig.20.4) On the left is shown the 3D view of a slot and on the right 2D section of slot
Fig.21.4) The average diameter (red circle) is linearized and the 2D view is shown on the right

Fig.1.5) Stator linearization: τ_p is the polar pitch, α_{ele} is the slot electrical angle, θ_{ele} is the stator electrical angle.
Fig.2.5) Magneto motive force distribution for 24 slots-20 poles three phase machine (a) and for 6 slots-4 poles three phase machine (b).
Fig.3.5) Magneto motive force distribution for 24 slots-20 poles three phase machine (a) and for 6 slots-4 poles three phase machine (b).
Fig.4.5) Magneto motive force distribution for10 slots-4 poles three five machine (a) and for 20 slots-18 poles five phase machine (b).
Fig.5.5) Magneto motive force distribution for10 slots-4 poles three five machine (a) and for 20 slots-18 poles five phase machine (b).
Fig.6.5) Magneto motive force distribution for10 slots-4 poles three five machine (a) and for 20 slots-18 poles five phase machine (b).

Fig.1.6) Three phase AC Drives with a connection between the neutral point and the middle point of DC-Link; a)without triac on neutral b) with triac on the neutral.

List of Tables

Author's Note

This thesis contains the results of my PhD experience at the Department of Electrical Engineering and Information Technology of University of Naples Federico II. The PhD was funded by the Italian Ministry of Education (MIUR).

Some topics shown in the thesis are partially related to the PON 01_02886 "Attuatori meccatronici ad elevate prestazioni per applicazioni aeronautiche" in collaboration with Umbra Cuscinetti S.p.A.

1. Introduction

In recent years, the wide availability and the cost reduction of rare earth materials have made permanent magnet machine a cost effective alternative for motor and generator application, in particular for the applications where an high power density and high efficiency are required. The permanent magnet motor are divided in two main categories: the radial flux machines and the axial flux machines. The first kind is characterized by radial magnetic field paths; instead in the axial flux machine the magnetic field paths are parallel to the axial direction. In many situations, the specific power of axial flux machine is better than the specific power of radial flux machine and the particular geometry permits to utilize the axial flux machine in some applications where direct drives are required.

The basic axial flux machine comprises one rotor disk and one fixed stator. Usually the stator and rotor are made with ferromagnetic material, but different ironless configuration of the stator or rotor could be take into account. Regarding the stator windings, all the windings arrangement can be utilized (lap per pole windings, concentrated windings, torus windings for slotless stator, fractional slot windings). The most interesting configuration for axial flux machine comprises the use of double rotor or double stator. The double rotor machine is realized with two external rotor disk and a central fixed stator. The two rotor can be realized with the same polarity exposes on the airgap (homopolar configuration , fig.1.1a) or with the two different polarity exposes (heteropolar configuration , fig. 1.b); in this configuration the stator can be made with a torus configuration (fig.2.1) or with a double side windings arrangement (fig.3.1a and 3b.1):

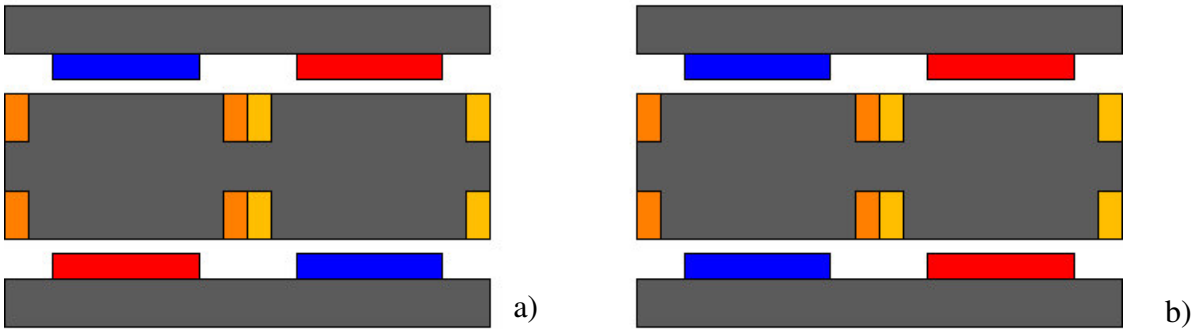

Fig.1.1a) Heteropolar axial flux rotor (2D view); 1.1b) homopolar axial flux rotor (2D view)

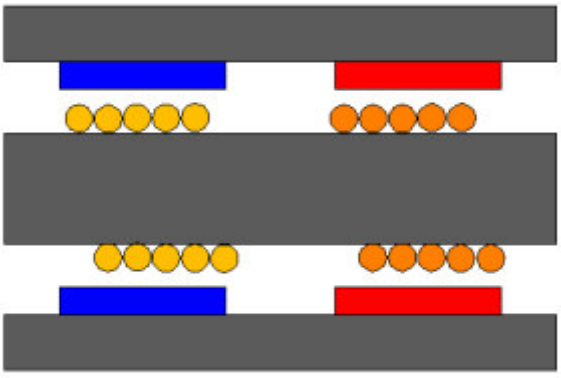

Fig.2.1) Homopolar rotor with slotless stator configuration and torus windings

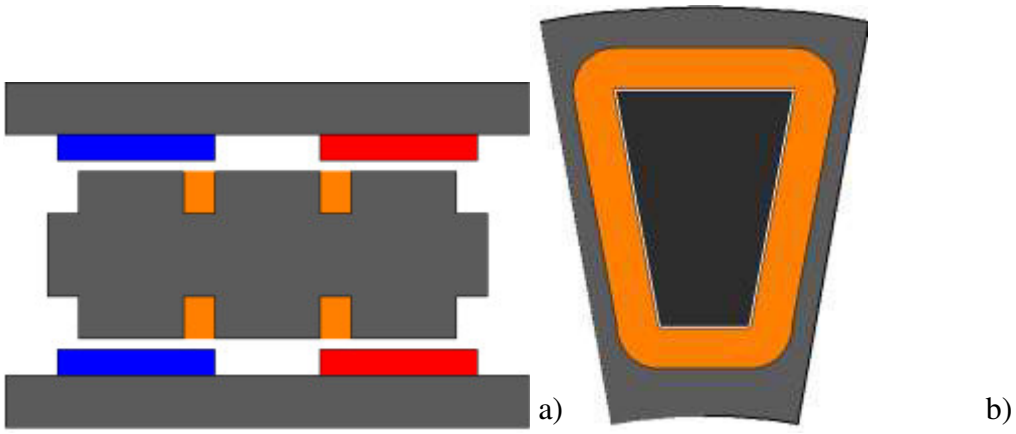

Fig.3.1)a Homopolar rotor with slotted stator and concentrated windings; b) section of stator slot with concentrated windings

The latter configuration permits to obtain the higher value of machine reliability, because it is possible to divide the windings into two independent windings fed by the same inverter of by more different inverter. Furthermore, if the rotors are mechanically separated, it is possible to design the two rotor with a different number of pole pairs in order to create a different speed.

The machine with double stator is made with a central rotor disk and two stator (fig.4.1), for which are applied the same consideration of the stator of double rotor machine.

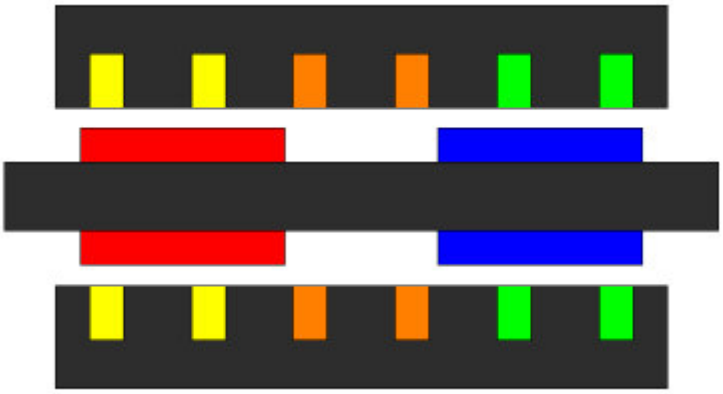

Fig.4.1) Double stator machine with internal homopolar rotor

Many applications of axial flux machines are found in literature. Various study are performed to model the axial flux machines. For example in [1] is described the magnetic behavior (considering a no constant magnetic potential in the airgap) of a permanent magnet d.c. machine where the lamination iron stack is substituted with iron powder and epoxy resine; in [2] is performed an analysis based travelling waves of an axial flux double stator machine with a very light internal rotor. Furlani in [3] presents a method for obtaining the field in the coil region of permanent-magnet axial-field motors. The method is based on the use of an analytical two-dimensional field formula coupled with an empirical procedure. This method allows the possibilities of rapid parametric studies of field strength relative to variations in motor dimensions and magnet materials. Instead in [4] he presented a formula for optimizing the filed generates by NdFeB magnets; the formula is based on a 3D analytical analysis. Referring to the 3D analytical analysis, in [5] is considered *a* three-dimensional magnetic field problem in an axial flux machine with a toroidal

winding. Using the iterative Schwartz algorithm has been joined the precise solutions generated by the integral transform and Fourier methods in elementary subregions. From the comparison the 3D and the 2D model, the author proposes a correction factor for the 2D analysis. The manufacturing of axial flux machine is usually associated with the use of iron powders magnetic material; this is due to the fact that is complicated to make laminated iron stacks which have the shapes of stators and teeth utilized in axial flux machine. The papers [5] and [6] analyze the effect and the behavior of axial flux machines with the wedges make with iron powder materials and [7] it is shown the design and the thermal behavior of an axial flux machine with single rotor and single stator where the stator is made with iron powder materials. In [8] a 2D and 3D finite element analysis are performed on an iron powders DC brushless axial flux machine used in servo system application; in order to reduce the iron losses and for application where an high speed and a low power are required, it is possible to make an ironless machine where the iron parts are substituted with plastic or with no magnetic materials as shown in [9]. Thanks to the reduced axial length, the high torque density and an excellent efficiency, the axial flux permanent magnet synchronous machines are particularly suitable for propulsion systems such as wheel motors and direct drive applications. In [10] the authors make a comparison between the induction and the synchronous axial flux machine with double rotors utilized in wheel application; the induction machine is well suitable for wheel direct drive application because it can behave as an electromagnetic differential supplied by a single inverter, but the only limitation is due to the large external diameter of the machine. In [11] and [12] for the in-wheel applications is proposed the used of an axial flux machine with a slotless stator; in particular the axial flux machine proposed in [11] has a multistage structure and a water-cooled toroidal ironless stator where the heat is removed directly from the interior surface of the stator winding and the high efficiency of the machine cooling arrangement permits a reduction of the machine weight and an overload operation with an high duty cycle. The axial flux machine can be also used in the application where a contra rotating or counterrotating shaft are required, for example in the naval propulsion systems. In [13] the use of axial flux machine permits to remove an epicycle gear box which is characterized by an high weight and a low efficiency, while in [14] it is studied a multistage machine composed by slotless stator utilized in marine applications. In [15] is presented a direct drive application of an axial flux machine for an elevator system which allows the possibilities to eliminate the machine room and in [16] is shown an high speed direct drive application for exhaust gas energy recovery.

Various design to improve the performance of axial flux machine are proposed in literature. For example, in [17] is obtained an optimum value for the thickness of magnet and windings in order to reduce the losses in the machine. The aims of various papers are inherent of the cogging torque reduction of axial flux machine: in [18] and [19] are proposed some experimental validation and finite element analysis of various techniques which permits the reduction of cogging torque, in [20] is validated the use of magnetic wedges.

A particular configurations of axial flux machine are reported in [21] and in [22]. In the paper [21] is proposed a modular axial flux generator where the windings of each module can have one or more phases; in particular it is presented the case of a three module machine with one phases for each module. The paper [22] shows an axial flux machine realized with a lamination stacks and characterized by a variable air gap between the inner and outer radius of the machine in order to avoi the saturation of the magnetic circuit, obtaining thath the core losses are reduce by 8%.

In these thesis is presented the use of axial flux machine for high reliability applications, in particular for the application in linear actuators systems bases on ball screw. The following chapters are divided as:

- Chapter 2: Introduction to the high reliability configuration using the axial flux machine and making of a design procedure of axial flux permanent magnet machines;
- Chapter 3: Introduction to the linear actuators;
- Chapter 4: FEM analysis of obtained machines and 3D printer prototyping;
- Chapter 5: Model of single layer, teeth concentrated windings;
- Chapter 6: Control algorithm of a particular configuration using the double rotor axial flux permanent magnet machines.

References of Introduction

[1] Campbell P., M.A., "*The Magnetic Circuit of an Axial Field D.C. Electrical Machine*", IEEE Transactions on Magnetics, vol. Mag-11, no. 5, September 1975

[2] Platt D., "*Permanent Magnet Synchronous Motor with Axial Flux Geometry*", IEEE Transactions on Magnetics, Vol. 25, No. 4, July 1989

[3] Furlani E.P., "*A Method for Predicting the Field in Permanent Magnet Axial-Field Motors*", IEEE Transactions on Magnetics, Vol. 28, No. 5, September 1992

[4] Furlani E.P., "*Field Analysis and Optimization of NdFeB Axial Field Permanent Magnet Motors",* IEEE Transactions on Magnetics, Vol. 33, No. 5, September 1997

[5] Campbell P. , Nafisi A., "*The Effect of Iron Powders on the Utilization of Permanent Magnet Materials in Advanced Motors*", IEEE Transactions on Magnetics, Vol. MAG-16, No. 5, September 1980.

[6] Nafisi A., Campbell P., "Composite Iron Powder Materials for the Armature of Axial-Field Permanent Magnet Machines" IEEE Transactions on Magnetics, Vol. mag-21, No. ***5,*** September 1985

[7] Di Stefano R., Marignetti F., "*Electromagnetic Analysis of Axial-Flux Permanent Magnet Synchronous Machines With Fractional Windings With Experimental Validation*" IEEE Transactions on Industrial Electronics, Vol. 59, No. 6, June 2012

[8] Z.Zhang, F.Profumo and A.Tenconi, "*Analysis and experimental validation of Performance for an Axial Flux Permanent Magnet DC Brushless Motor with Powder Iron Metallurgy Cores*", IEEE Transactions on Magnetics, Vol. 33, No. **5,** September 1997

[9] Lombard N.F., Kamper M.J., "*Analysis and Performance of an Ironless Stator Axial Flux PM Machine*" IEEE Transactions on Energy Conversion, Vol. 14, No. 4, December 1999

[10] Profumo F., Zhang Z., Tenconi A., "*Axial Flux Machines Drives: A New Viable Solution for Electric Cars*", IEEE Transactions on Industrial Electronics, Vol. 44, No. 1, February 1997

[11] Caricchi F., Crescimbini F., Mezzetti F., Santini E., "Multistage Axial-Flux PM Machine for Wheel Direct Drive", IEEE Transactions on Industry Applications, Vol. *32,* No. **4,** July/August 1996

[12] Caricchi F., Crescimbini F., Honorati O., Di Napoli A., Santini E., "*Compact Wheel Direct Drive for EVs*", IEEE Industry Applications Magazine, November/December 1996

[13] Caricchi F., Crescimbini F., Santini E., "*Basic Principle and Design Criteria of Axial-Flux PM Machines Having Counterrotating Rotors*", IEEE Transactions on Industry Applications, Vol. 31, No. 5, September-October 1995

[14]] Caricchi F., Crescimbini F., Honorati O., "*Modular Axial-Flux Permanent-Magnet Motor for Ship Propulsion Drives*", IEEE Transactions on Energy Conversion, Vol. 14, No. 3, September 1999

[15] Ficheux R.L., Caricchi F., Crescimbini F., Honorati O., "*Axial-Flux Permanent-Magnet Motor for Direct-Drive Elevator Systems Without Machine Room*", IEEE Transactions on Industry Applications, Vol. 37, No. 6, November/December 2001

[16] Crescimbini F., Lidozzi A., Lo Calzo G., Solero L., "*High-Speed Electric Drive for Exhaust Gas Energy Recovery Applications*" IEEE Transactions on Industrial Electronics, Vol. 61, No. 6, June 2014

[17] Takano H., Itoh T., Mori K., Sakuta A., Hirasa T., "*Optimum Values for Magnet and Armature Winding Thickness for Axial-Field Permanent Magnet Brushless dc Motors*", IEEE Transactions on Industry Applications, Vol. **28,** No. 2, March-April 1992.
[18] Caricchi F., Capponi F.G., Crescimbini F., Solero L., "*Experimental Study on Reducing Cogging Torque and No-Load Power Loss in Axial-Flux Permanent-Magnet Machines With Slotted Winding*" IEEE Transactions on Industry Applications, Vol. 40, No. 4, July/August 2004
[19] Aydin M., Zhu Z.Q., Lipo T.A., Howe D., "*Minimization of Cogging Torque in Axial-Flux Permanent-Magnet Machines: Design Concepts*", IEEE Transactions on Magnetics, Vol. 43, No. 9, September 2007
[20] De Donato G., Capponi F.G., Caricchi F., "*No-Load Performance of Axial Flux Permanent Magnet Machines Mounting Magnetic Wedges*" , IEEE Transactions on Industrial Electronics, Vol. 59, No. 10, October 2012
[21] Muljadi E., Butterfield C. P., Wan Y., "*Axial-Flux Modular Permanent-Magnet Generator with a Toroidal Winding for Wind-Turbine Applications*", IEEE Transactions on Industry Applications, Vol. 35, No. 4, July/August 1999
[22] Vansompel H., Sergeant P., Dupré L., Van den Bossche A., "*Axial-Flux PM Machines With Variable Air Gap*", IEEE Transactions on Industrial Electronics, Vol. 61, No. 2, February 2014

2. Design of multi stack axial flux permanent magnet machine

The design of electrical machines is based on the calculation of main machine dimensions with some assumptions regarding the electromagnetic and thermal behavior. Until some decades ago, the designed machines are usually made with a radial air gap flux; the used of permanent magnet has permitted the development of new machines topologies, like axial flux machine and transverse flux machine. Due to this, new sizing equations are required for this kind of machine. A machine sizing procedure includes the electromagnetic design, where are performed the calculation of main machine sizes, the windings configuration, the losses determination, the verify of working limits and also the verify of thermal and mechanical limits. In the following sections is reported the sizing procedure utilized for the application presented in this thesis; in particular are reported the sizing equations which provide the main sizes, and the equations utilized to verify the thermal and mechanical constrained.

- *Electromagnetic design procedure for axial flux permanent machine*

Different electromagnetic design procedure are presented in [1] and in [2]. The procedure presented in [1] is developed in order to introduce a systematic method to compare the capabilities of machines with different topologies; moreover with this equation it is possible to account the effect of power converters which feed the machine. In [2] the typical size equation referred to an AC machines are adopted and particularized to the axial flux machine case.

The sizing procedure shown in [1] gives the output power equation neglecting the stator leakage inductance and resistance, obtaining:

$$P_R = \eta \frac{m}{T} \int_0^T e(t)\, i(t) dt \qquad (1.2)$$

whit m is the phases number, T is the waveform period, η is the performance, e(t) is the back emf waveform, i(t) is the current waveform. The (1.2) can be written as :

$$P_R = \eta \frac{m}{T} E_m I_m \int_0^T f_e(t)\, f_i(t) dt \qquad (2.2)$$

where E_m and I_m are the peak values of back emf and machine current, while $f_e(t)$ and $f_i(t)$ are the ratio between the back emf and machine current divide for the respective peak values. The values of $f_e(t)$ and $f_i(t)$ can be particularized to a typical waveforms of current and back emf, obtaining a precision raise in the design procedure. In the thesis, the size procedure is based on the equations given by [2], but those equations are particularized to the case of multi stacks machines and with the thermal and mechanical limits. In particular, if m is the number of phases, the mechanical output power is:

$$P_r = mE_n I_n \cos\Psi \qquad (3.2)$$

In (3.2) E_n is the no-load back emf, I_n is the nominal current (for a multi stack machine, I indicates the phase current and not the single stack current) and Ψ is the angle between the current and the back emf (considering the maximum torque per ampere control, it is possible to consider that the angle Ψ is equal to zero). The values of E_n depends by the type of stack connections and for a double side its values is affected also by the stator windings connections; table 1 shows the values of back emf and of current of a single stack in the different configurations (the symbol *h* indicates the generic stack, *k* indicates the generic sides of the stator of the stack and *l* is the total number of stator sides):

Series connection between the windings of each stacks		**Parallel connection between the windings of each stacks**	
Series connection between the two stator side	*Parallel connection between the two stator side*	*Series connection between the two stator side*	*Parallel connection between the two stator side*
$E_{tot} = \sum_{h=1}^{n}\sum_{k=1}^{l} E_{h,k}$	$E_{tot} = \sum_{h=1}^{n} E_{h,l}$	$E_{tot} = 2E_{h,l}$	$E_{tot} = E_{h,l}$
$I_k = I_n$	$I_k = \frac{I_n}{2}$	$I_k = \frac{I_n}{n}$	$I_k = \frac{I_n}{2n}$

Table 2.1 Values of back emf and stator side current in the different connections between the stator sides and between the stack of a multi stack machine

Moreover in a multi stack machine, the total mechanical power can be computed as the sum of the power of the single stator stack; the power of a single stack side results:

$$P_{r,ss} = mE_{h,l} I_k \cos\Psi \qquad (4.2)$$

The proposed design procedure starts with the sizing of a single stack in order to guarantee that the multistacks machine gives the total amount power.
The rms value of no-load back emf can be computed by the instantaneous value obtainable as:

$$e(t) = -\frac{d\varphi_c(t)}{dt} = -\frac{d}{dt}\left(N \iint_S B_g(t)\hat{n}\, dS \right) \qquad (5.2)$$

In (5.2), φ_c is the total linkage flux of a generic phase, *N* is the number of turn per phase, B_g is the air gap magnetic flux density due to the rotor and considering only the first harmonic, it is equal to:

$$B_g(t) = B_{g,m}\cos(p_r\,\omega t) \qquad (6.2)$$

Referring to the concentrated tooth winding utilized in the application with high reliability , the relation (1.2) can be written taking into account the generic winding function and the transformation into polar reference frame:

$$e(t) = -\frac{d}{dt}\left(N \int_0^{2\pi} \int_{\frac{D_{in}}{2}}^{\frac{D_{out}}{2}} B_{g,m} \cos\left(p_r\, \omega_r t\right) \rho\, d\, \rho d\theta \right) = 2 p_r\, \omega_r\, m_l\, t\, B_{g,m} S_{slot} N_c \sin\left(p \omega_r t\right) \qquad (7.2)$$

Where the symbols utilized are referred respectively to:

-N_c is the number of turns around one tooth;

-p_r is the number of rotor poles pairs;

-w_r is the mechanical angular frequency;

-m_l is the number of winding layers;

-t is the machine periodicity, computed as the maximum common divisor of slots number and rotor poles pairs;

-$B_{g,m}$ is the maximum value of air gap magnetic flux density;

-D_{out} ,D_{in} are respectively the internal and the external diameter of the machine

- S_{slot} is the area of a slots, computed as:

$$S_{slot} = \frac{\pi\left(D_{out}^2 - D_{in}^2\right)}{4Q} \qquad (8.2)$$

where Q is the total number of machine slots.

- ρ is the radius in polar coordinates system, comprises in the range [R_1, R_2];

- θ is the angle in polar coordinates system, comprises in the range [0, 2π];

Considering the rms value of equation (7.2) and substituting this value in equation (4.2), it is possible to obtain the sizing equation for the single side of a generic stack:

$$P_{r,ss} = \frac{2}{\sqrt{2}} p \omega_r m m_l t B_{g,m} N_c I_k S_{slot} \quad (9.2)$$

Generally, the current is expressed by the linear current density of the machine and for an axial flux machine is equal to:

$$A_k = \frac{2 m m_l N I_k}{\pi\left(D_{out} + D_{in}\right)} = \frac{m m_l N I_k}{\pi D_g} \qquad (10.2)$$

With (8.2) and (10.2), the equation (9.2) become:

$$P_{r,ss} = \frac{\pi^2}{4\sqrt{2}} p \omega_r B_{g,m} A_k D_g \frac{\left(D_{out}^2 - D_{in}^2\right)}{Q} = \frac{\pi^2}{4\sqrt{2}} p \omega_r B_{g,m} A_k \frac{\left(D_{out} + D_{in}\right)\left(D_{out}^2 - D_{in}^2\right)}{Q} = \frac{\pi^2}{4\sqrt{2}} p \omega_r B_{g,m} A_k \frac{(1+\lambda)\left(1-\lambda^2\right) D_{out}^3}{Q} \qquad (11.2)$$

where λ is the ratio between the internal and external diameter.

To use of formula (11.2), it is necessary to fixed the maximum values of the parameters : usually the number of poles pairs and the angular mechanical speed are fixed by the application. The maximum value of air gap magnetic flux density due to the magnets is comprised in the range of 0.6 T -1 T, and depends by the magnets utilized and by the maximum operation temperature. The ratio between the internal and the external diameter can be optimized with an iteration process: usually the minimum internal diameter is fixed by the required shaft diameter and the maximum external diameter is equal to the maximum axial size allowed, therefore the optimum λ is obtained by a mathematical procedure. For example, it is possible to calculate the maximum value from equation (11.2), or introduce new consideration as shown in [3] and [4]. In [3] is calculated the optimum ratio of 0,57 and in [4] the optimum ratio is 0,68. In the design procedure, an important parameters is the linear current density A_k. In the proposed procedure, this value is fixed tacking into account the respect of thermal limits. In fact, supposing that the mechanical losses are dissipated by the shaft of the machine, the total losses dissipated by the surface of the machine are:

$$P_{d,losses} = H \cdot S_{tot} \qquad (12.2)$$

with S_{tot} is the total external surface of the machine [m^2], H is the global exchange coefficient [W/m^2] and $P_{d,losses}$ indicates the sum of iron losses, Joule losses and magnet losses. The total external surface of an axial flux machine is equal to:

$$S = 2\pi \cdot D_o \cdot l_{tot} + \frac{\pi}{2} \cdot D_o^2 \cdot \left(1 - k_d^2\right) \qquad (13.2)$$

where l_{tot} is the total length of the machine. Specifying with l_{rot}, h_c, g, l_{gs} the rotor axial length, the slot deep, the air gap length and the stator axial length, for a double rotor machine the total length is:

$$l_{tot} = 2 \cdot l_{rot} + 2 \cdot h_c + 2 \cdot g + 2 \cdot l_{mag} + l_{gs} \qquad (14.2)$$

The global exchange coefficient depend by the machine cooling system. The relation (15.2) become:

$$P_{d,losses} = \iiint_{V_{cu}} \eta J^2 dV + \iiint_{V_{Fe}} f_{Fe}(B, f, \rho) dV + \iiint_{V_{mag}} f_{mag}(B, f, \rho) dV \qquad (16.2)$$

Neglecting the magnets losses, it is possible to explain the Joule losses in function of current density J [A/m^2] as:

$$\eta \cdot J^2 \cdot m \cdot m_l \cdot N \cdot S_{Cu} \left(\frac{l_{med,sp}}{2} \right) = H \cdot S - \iiint_{V_{Fe}} f_{Fe}(B, f, \rho) dV \qquad (17.2)$$

where S_{cu} is the conductor section in m^2, $l_{med,sp}$ is the average length of a turns. Referring to (11.2), the relation (16.2) become:

$$A_k \cdot J = \frac{H \cdot S - \iiint_{V_{Fe}} f(B, f, \rho) dV}{\eta \cdot \pi \cdot l_{med,sp} \cdot D_g} \qquad (17.2)$$

Examining the relation (17.2) , in order to respect the temperature limits it is necessary that the product between the linear current density and the current density in the conductors will be below to a function which depends by the exchange coefficient H, the external surface, the conductors resistivity and by some machine sizes, like the average diameter and the average length of a turn.

The second limits to check are the mechanical limits. Referring to the values of external and internal diameter, the radial and the hoop stresses depended by the generic diameter D are expressed as [5]:

$$\sigma_H = \frac{\rho\omega^2}{8}\left[(3+\nu)\left(\frac{D_2^2}{4}+\frac{D_1^2}{4}+\frac{D_1^2 D_2^2}{4D^2}\right)-(1+3\nu)\frac{D^2}{4}\right] \qquad (18.2)$$

$$\sigma_r = \frac{\rho\omega^2}{8}(3+\nu)\left[\frac{D_2^2}{4}+\frac{D_1^2}{4}-\frac{D_1^2 D_2^2}{4D^2}-\frac{D^2}{4}\right] (19.2)$$

From the relation (18.2), it easy to verify that the maximum and minimum hoop stress occur on the inside and outside diameter respectively; the values of this stress are equal to:

$$\sigma_{H,\max} = \frac{\rho\omega^2}{16}\left[(3+\nu)D_2^2+(1-\nu)D_1^2\right] \qquad (20.2)$$

$$\sigma_{H,\min} = \frac{\rho\omega^2}{16}\left[(3+\nu)D_1^2+(1-\nu)D_2^2\right] \qquad (21.2)$$

The maximum radial stress is obtained at the geometric mean of external and internal radius; this value is expressed in the following formula (22.2):

$$\sigma_{r,\max} = \frac{\rho\omega^2}{32}(3+\nu)[D_2-D_1]^2 \qquad (22.2)$$

Fig.(1.2) shows the variation of hoop stress and radial on an half diameter:

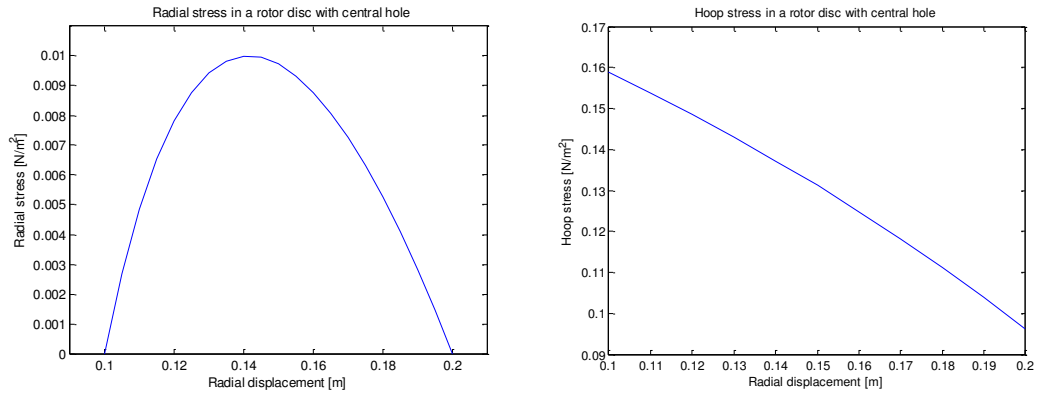

Fig.1.2)Radial stress and hoop stress in the axial flux rotor, along the radial displacement

Referred to the axial flux machine, the relation (20.2) and (22.2) can be written as:

$$\sigma_{H,\max} = \frac{\pi^2\rho f_r^2}{4} D_o^2\left[(3+\nu)+(1-\nu)\lambda_d^2\right] \qquad (23.2)$$

$$\sigma_{r,\max} = \frac{\pi^2 \rho f_r^2}{4}(3+\nu) D_o^2 [1-\lambda_d]^2 \qquad (24.2)$$

During the design procedure, it is necessary the knowledge of other machine sizes like the rotor length, the tooth area, the slot deep, the magnet height and the stator length. The rotor length l_{rot} is calculated by the formula (25.2):

$$l_{rot} = \pi \frac{B_{m,r}}{B_{\max,rot}} \frac{(D_{out} - D_{in})}{8p} \alpha_{span} \qquad (25.2)$$

In the relation (25.2), $B_{m,r}$ is the residual magnetic flux density, $B_{max,rot}$ is the maximum value of magnetic flux density in the rotor yoke and α_{span} is the ratio between the magnet area and the rotor poles area. It is important to remark that in a radial flux machine, the α_{span} is equal to the ratio of magnet polar arc and rotor polar arc, while in axial flux machine it is necessary to related this value to the ratio between the magnet area and the rotor poles area because in this case the magnet radial extension does not coincide always with rotor axial extension. The tooth area A_{tooth} is calculated supposing that all the magnetic flux which linkage the total slot area, cross through the tooth area:

$$A_{tooth} = \frac{B_g}{B_{\max,tooth}} \frac{\left(D_{out}^2 - D_{in}^2\right)}{2Q} \qquad (26.2)$$

In formula (26.2), $B_{max,tooth}$ is the maximum value of magnetic flux density in the tooth. Obtained the tooth area, it is necessary to design the tooth: the fist step is the choice of toot shape which can be round, trapezoidal, trapezoidal chamfered (fig. 2).

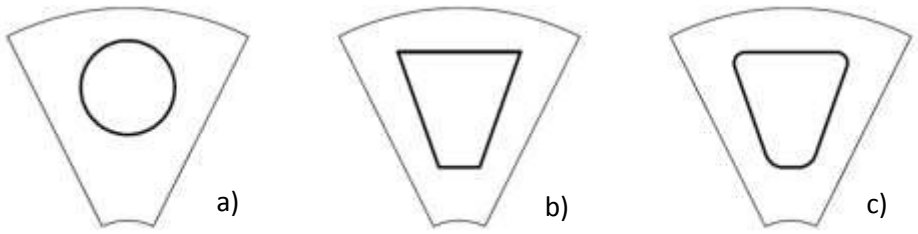

Fig.2.2 a) Round tooth; b) Trapezoidal tooth; c) Trapezoidal chamfered tooth.

Considering a trapezoidal tooth, the most important things to check during the design is the saturation of tooth base; the length of tooth base is related to the maximum tooth magnetic flux density and by the width of slot overlapped to the base of tooth (fig.3.2):

$$b_1 = \frac{B_{med}}{B_{\max,tooth}} \alpha_0 \qquad (27.2)$$

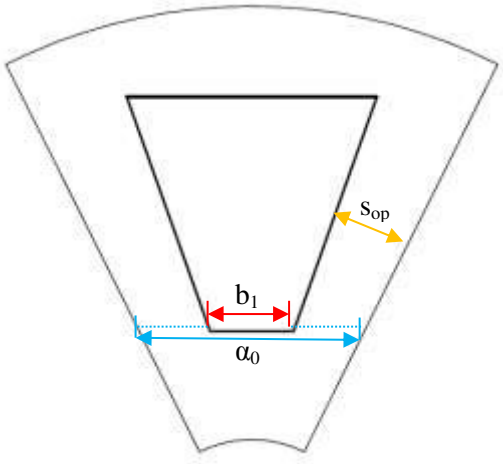

Fig.3.2) Zoom of a trapezoidal slot: b_1 is the width of base, α_0 is the slot opening overlapped to the slot base and s_{op} is the slot opening.

The height of the slot depends by the tooth area and by the fact that the slot opening must be constant along the radial direction (s_{op} in fig.7.2).The slot depth depends directly by the number of turns, the number of layers of the machine, by the slot openings and by the type of conductor utilized. Fixed the slot opening, the slot depth is equal to:

$$s_{depth} = \frac{m_l m N S_{Cu}}{k_{fill} s_{op} Q} \qquad (28.2)$$

where k_{fill} is the fill factor of the slot. This coefficient taking into account the volume between the conductors, the space filled by the conductors insulation and by the coil and slots insulation. The variation range of fill factor is between 0,30 and 0,70: for circular conductors k_{fill} is nearest the lower value but it increase to the upper limit for flat conductors. The sizing of magnet happens with the solution of magnetic circuit of axial flux machine where it is necessary to know the reluctance of all parts included in the circuit; the main size of magnet are the polar arc α_{span} , the height of magnet l_m and the difference between the external radius and internal radius of magnet; generally the last size is imposed equal to the height of slot. The polar arc is choice in order to reduce the harmonic content of magnetic flux density generated in the air gap and to minimize the height of magnet. The magnet height is calculated through the solution of a magnetic circuit which comprises the magnetic air gap (obtained with the product between the geometric air gap and the Carter's coefficient) , the slots depth, the stator and the rotor cores. The machine stator length l_{gs} is calculated with the relation (29.2):

$$l_{gs} = \frac{\pi}{8 p_{sta}} \frac{B_{med}}{B_{\max,gs}} \left(D_{out} + D_{in}\right) \qquad (29.2)$$

In the relation (29.2) p_{sta} is the stator poles pairs, $B_{max,gs}$ is the maximum value of magnetic flux density in stator yoke. Obviously the formula (25.2) and (29.2) depend by the type of machine choice: in fact, for a homopolar machine with double rotor (double stator), the stator yoke (rotor woke) has only a structural purpose and the respective sizing formula are not used.

The results obtained by the proposed design procedure are verified with a finite element analysis and are shown in chapter 3.

2.1 Axial flux machine in mechatronic: multi stacks machines

The axial flux permanent magnet machine can be really important in mechatronic systems, because the predominant radial dimensions respect the axial dimensions permits to design very compact motor which can be installed for the direct drive coupling in gaps where it is impossible to use the normal radial flux machine without the use of mechanical gear. In this thesis is presented the possibility to design a multi stacks machine which is a machine compound based on different axial flux machines whom are jointed between them in order to create a machine with a total power equal to the sum of each stacks power (fig. 4.2). This kind of machines could be realized with internal and external rotor. Both in the case of external and internal rotor machine, the stator can be divided in two independent sides: this create the possibilities to feed each side with a different inverter.

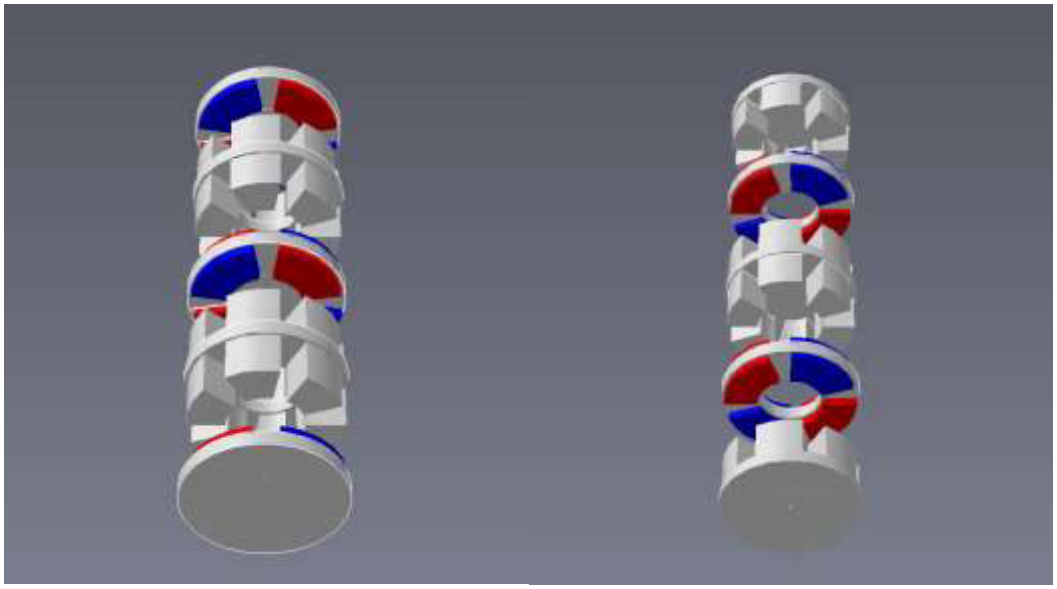

Fig.4.2)Multi-stacks machine: on the right there is a double stator, internal rotor machine with homopolar configuration; on the left is presented a double rotor, internal stator machine with heteropolar configuration.

In literature, there are some applications [6],[7], regarding the use of induction machines where a single inverter supply the machine with series or parallel connection of windings: each machine has a no common mechanical load and for the series connection, a phase shift in the windings machine is necessary to give the possibility to separate the machines control.

The use of a multi -stacks is quite different because the mechanical load is the same for each stack and the series connection between the windings it is utilized only in the application where the reliability required isn't very high. In fact the most important novelty of multi stacks machines is the rise of machines reliability. Considering the axial flux stack whit an internal rotor and two separated stator; the windings of each stator side are connected in series or in parallel to the respective inverter leg: the parallel configuration determines the highest reliability values, because

the stack is similar a dual *m*-phase machine with the same axis. With a machine composed by *n* axial flux stacks, which double side *m*-phases stator, it is possible to create different configurations presented in the following, where the case of two stacks-three phases machine is considered.

Moreover, the multi stacks machine can improve the industrial manufacturing of electrical machines. The ability to assemble different machine stacks gives the opportunity to realize easily various machines with different power; in fact it is possible to realize different stacks which the same external and internal diameter and the same slot/poles configuration but with different power and combining the different stacks it is possible to reach various levels of powers. In order to show the goodness of multi stack axial flux machine, in the following are reported the reliability analysis of many configuration of double rotor , three phase axial flux machine composed by two stack.

- Single Inverter with Series connection between each stack and each stack side (SISS)

This configuration provides the possibility to link all the different phases of each stack side in series (fig.5.2) . The vantage of this configuration regard the total back EMF which is equal to the sum of back EMF of each sides phases; in this way it is possible to guarantee that in rated conditions, the nominal voltage value is similar to the total back EMF and this implies the possibility to work with a low load angle and with an high power factor.

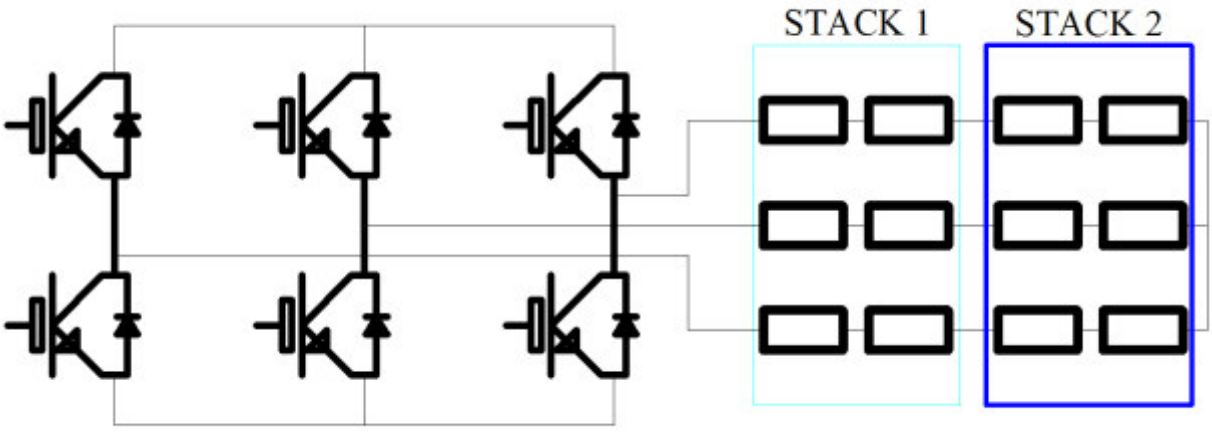

Fig.5.2) Schematic of SISS configuration

The disadvantages comes from the low value of reliability. As shown in fig.6.2, if a problem occurs on a phase windings of a stator side, the phase become completely unusable on each stacks.

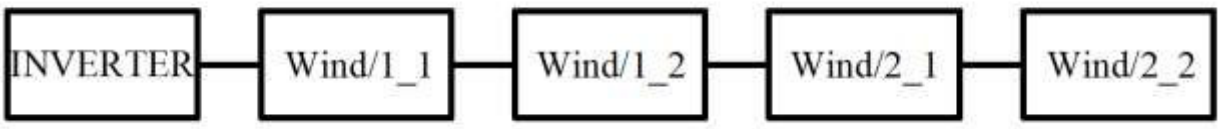

Fig.6.2) Block diagram of SISS configuration: the symbol Wind/a_b indicates the generic phase of stack "a" and stator side "b"

If this situation occurs, it is possible to act on the control in order to improve the machine performance. In fact considering a three phase machine and supposing that a fault occurs on the third phase : to guarantee that the rotating magnetic field remain the same, it is necessary to feed the machine with the follow symmetrical component vector:

$$\mathbf{i}_s = \frac{2}{3}\left(i_1' e^{j\frac{\pi}{6}} + i_2' e^{j\frac{\pi}{2}} \right) \qquad (30.2)$$

The symmetrical component imposes that the current in the first and second phase must be shifted by an angle of 30° and 90° respectively and the value of current are amplified by $\sqrt{3}$. The amplification of current value deeply affects the machine control: if the maximum torque per ampere strategy is considered, for respect the current limits it is necessary to divide the fixed current limit by $\sqrt{3}$ and this increased the base speed and reduced the maximum torque of motor. Taking into account the mathematical model in d-q reference frame of a permanent magnet motor where the phase resistance is neglecting and where V_n, L_s, p, ϕ_r are the rated phase voltage, the phase inductance (sum of the leakage inductance and of synchronous inductance), the number of rotor pole pairs and the no-load magnetic flux due to the magnets, it is possible to compute the base speed as:

$$\omega_{r,b} = \frac{V_n}{\sqrt{\left(p L_s I_{\lim}\right)^2 + \left(p \phi_r\right)^2}} \qquad (31.2)$$

In the working domain, the base speed is the maximum speed where it is possible to work with the total limit current in quadrature and therefore it is possible to obtain the maximum torque. If the current limit is reduced, also the maximum torque of motor decreases and the working domain undergoes the variation in fig.7.2:

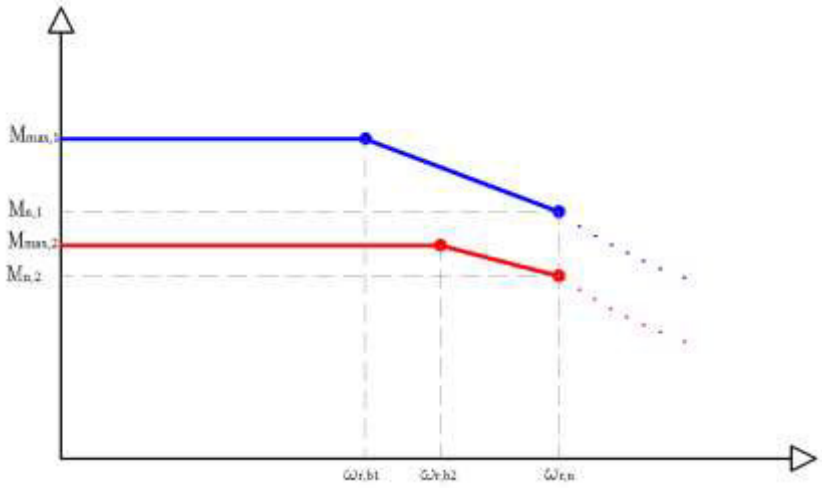

Fig.7.2)Variation of working domain: the rated and maximum torque after a fault ($M_{max,2}$,$M_{n,2}$) decrease

- Single Inverter with Series connection between each stack side and Parallel between each stack (SISP)

The SISP (fig.8.2) derived directly from the SISS configuration, but the stack windings are connected in parallel on the same inverter leg. The main advantage is the rise of configuration reliability (fig.9.2).

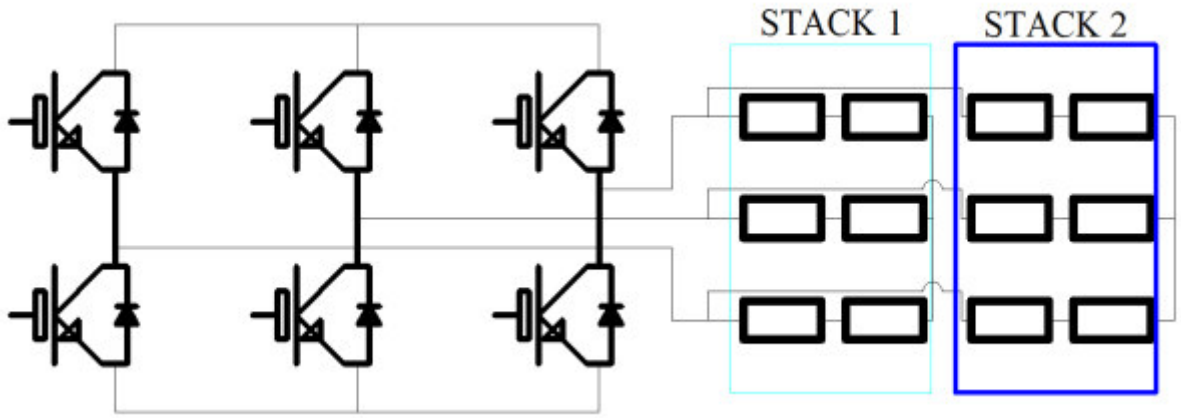

Fig.8.2) Schematic of SISP configuration:

In fact, if a fault occurs on Wind/1_1, the generic phase of stack 1 is unserviceable, but the stack 2 is healthy. Obviously if a fault occurs on an inverter legs, both the stack are compromises.

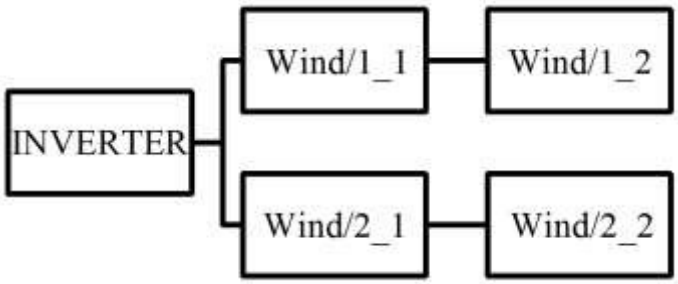

Fig.9.2) Block diagram of SISP configuration: the symbol Wind/a_b indicates the generic phase of stack "a" and stator side "b"

Considering fig.8.2 and 9.2, the maximum torque of motor is the sum of torque expressed by the two stacks, and imposing that the torque of two stack is equal, the following expression is valid:

$$M_{\max,tot} = M_{\max,1} + M_{\max,2} = \frac{M_{\max,tot}}{2} + \frac{M_{\max,tot}}{2} \qquad (32.2)$$

If a one phase fault occurs on the windings of stack 2, the expression (32.2) become:

$$M_{\max,tot\_pf} = M_{\max,1} + \frac{M_{\max,2}}{\sqrt{3}} = \frac{M_{\max,tot}}{2} + \frac{M_{\max,tot}}{2\sqrt{3}} = \left(\frac{3+\sqrt{3}}{6}\right) M_{\max,tot} = 0,78 M_{\max,tot} \qquad (33.2)$$

Instead, taking into account the fault on one inverter legs, the maximum torque is the 57 % of torque generated in no fault condition and it is equal to te maximum torque reached when the windings are all connected in series (SISS configuration).

- Single Inverter with Parallel connection between each stack side and Parallel between each stack (SIPP)

The configuration called SIPP, allows the highest reliability in the single inverter configurations. The greater disadvantage is about the value of back emf phase in the windings: in fact the total emf is equal to the emf of each phase winding (the windings of each side are considered similar) and to obtain an high value of back emf which permits to reduce the machine rated current and the load angle, an high number of turns per phase is necessary. Moreover, considering the SISS and the SIPP configuration and supposing that the back emf, the load angle and the power factor of machine is the same, also the rated current of the machine is the same: in the SISS configuration, each windings conductors are sized for the nominal current but in SIPP the current of each side is equal to the nominal current divided by the number of stacks and the number of sides; in this way the windings conductors are designed for a parts of nominal current and the size is less than in SISS. Combining these features with the high number of turns request, involves that in the SIPP configuration the resistance and inductance of a phase is higher than the phase resistance and inductance in SISS, with an increase of losses and a variation of working domain.

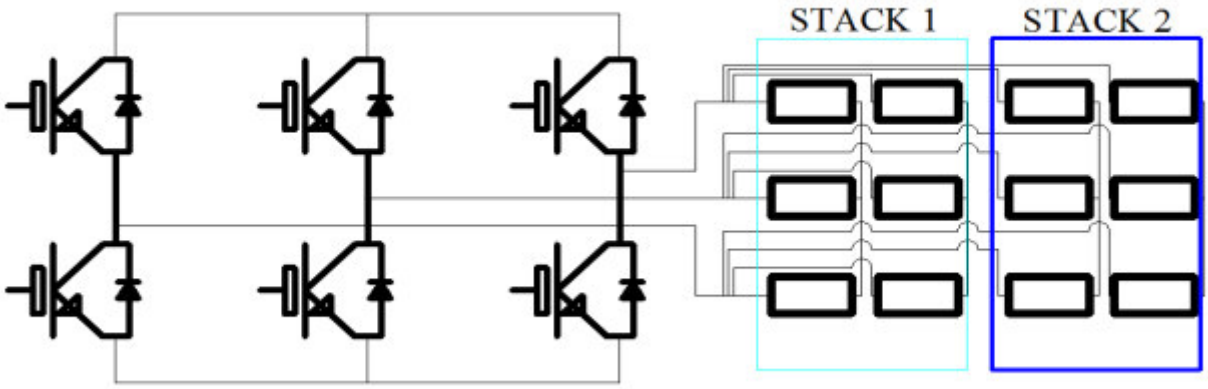

Fig.10.2) Schematic of SIPP configuration

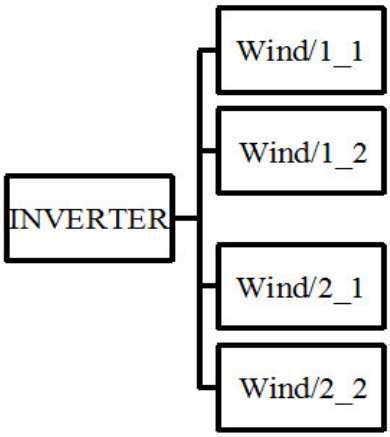

Fig.11.2) Block diagram of SIPP configuration: the symbol Wind/a_b indicates the generic phase of stack "a" and stator side "b"

Referring to the relation (32.2) and (33.2) and taking into account that a fault occurs on a single phase, in the SIPP configuration the relation (34.2) and (35.2) are valid:

$$M_{\max,tot} = M_{\max,1} + M_{\max,2} + M_{\max,3} + M_{\max,4} = \frac{M_{\max,tot}}{4} + \frac{M_{\max,tot}}{4} + \frac{M_{\max,tot}}{4} + \frac{M_{\max,tot}}{4} \tag{34.2}$$

$$M_{\max,tot\_pf} = M_{\max,1} + M_{\max,2} + M_{\max,3} + \frac{M_{\max,4}}{\sqrt{3}} = \frac{M_{\max,tot}}{4} + \frac{M_{\max,tot}}{4} + \frac{M_{\max,tot}}{4} + \frac{M_{\max,tot}}{4\sqrt{3}} = \frac{9+\sqrt{3}}{12} M_{\max,tot} \approx 0,89 M_{\max,tot} \tag{35.2}$$

From (35.2) it is possible to note that the maximum torque value in one phase post fault operation is about the 89% of maximum torque in healthy condition. Analog consideration due for the SISP can be made for the fault of one inverter leg.

- Dual Inverter with Series connection between each stacks side and Parallel between each stack (DISP)

The DISP provides the use of two inverter; each inverter supplies one or more than one stacks. This configuration increase considerably the reliability, in particular against the inverter faults and it is also the best solution for the single stack double rotor machine, with the two rotors mechanically separated and where is necessary to move the two rotors with a different angular speed.

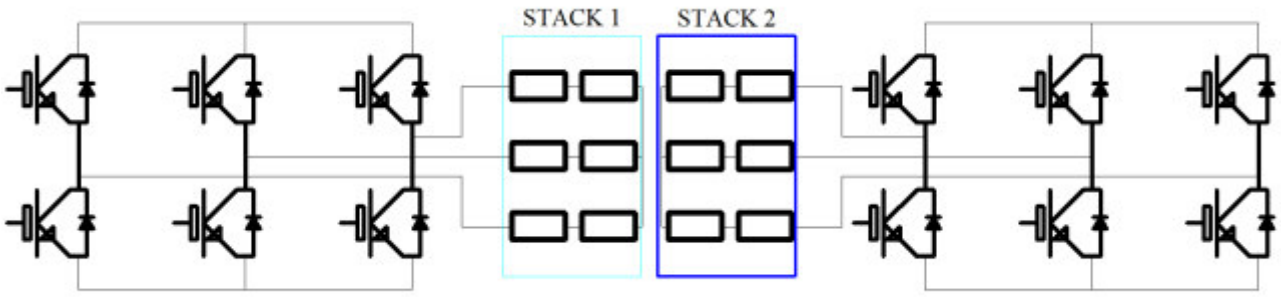

Fig.12.2) Schematic of DISP configuration

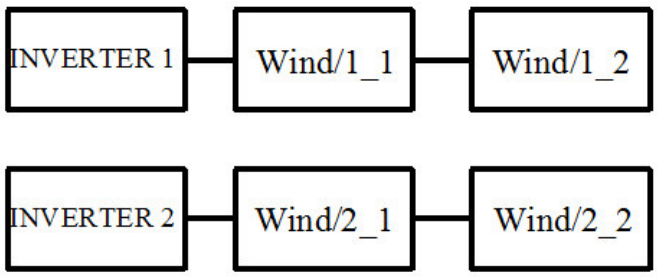

Fig.13.2) Block diagram of DISP configuration: the symbol Wind/a_b indicates the generic phase of stack "a" and stator side "b"

In the DISP configuration, the maximum torque available in a one-phase post fault condition is the same of SISP configuration , expressed with formula (33.2). As mentioned before, if the single

phase fault occurs on inverter there is an improvement of maximum torque allowable. In fact, if one of the two inverter lost one leg, the maximum torque available is the 78% of maximum torque in health condition.

- Multi Inverter with Parallel connection between each stack side and Parallel between each stack (MIPP)

The MIPP configuration is the configuration with the highest reliability obtainable in a multi stacks machines. Each stator side of a stack is fed by a single inverter and acts like an independent winding of the machine; the disadvantages are the same describe for the other configuration where the windings of each stator side are connected in parallel; besides, the configuration introduces also a difficulty in the control, which has to operate in synchronous manner to avoid the loss of synchronism in the machine.

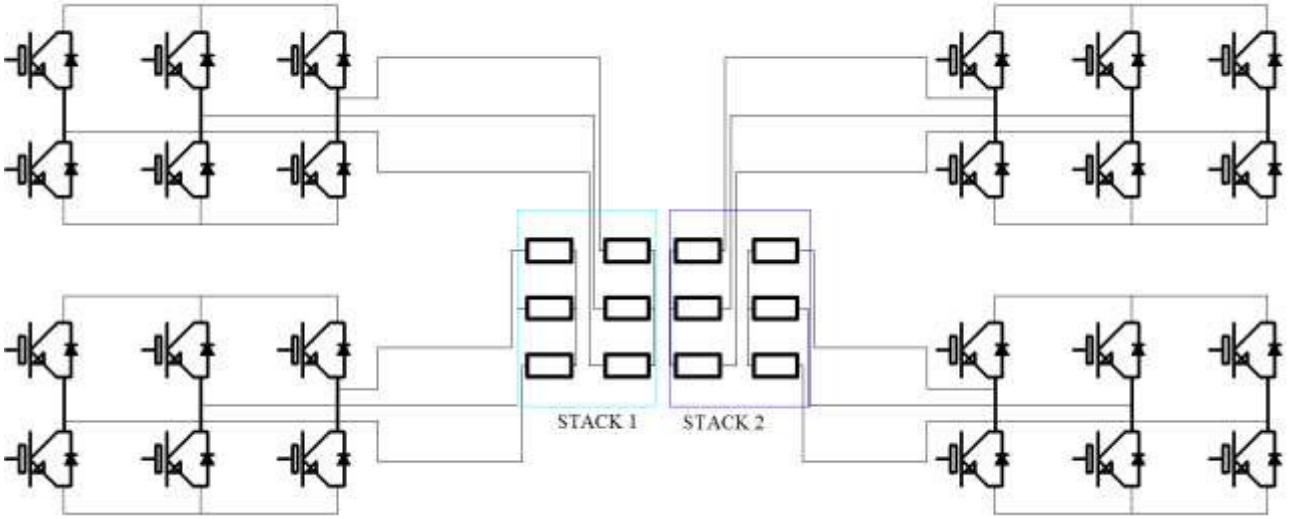

Fig.14.2) Schematic of MIPP configuration

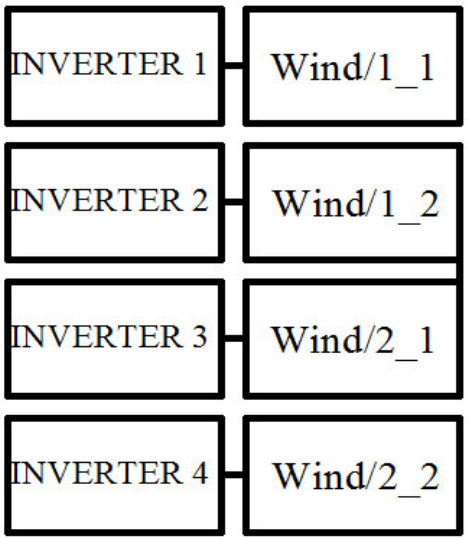

Fig.15.2) Block diagram of MIPP configuration: the symbol Wind/a_b indicates the generic phase of stack "a" and stator side "b"

Supposing that a fault occurs on the one phase winding of one side stack, the maximum torque is the same obtained in (35.2); while if one inverter legs is damaged the maximum torque available equal to the 89% of maximum torque in health mode (and this is the maximum value obtainable respect the other configurations presented when the one phase fault occurs in the inverter).

References of Chapter 2

[1] Surong Huang , Jian Luo , Leonardi, F. ,Lipo, T.A., "*A comparison of power density for axial flux machines based on general purpose sizing equations* ", IEEE Transactions on Energy Conversion, Vol.14, Issue:2, pp.185-192, January 1999

[2] **Gieras**, Jacek F., **Wang**, Rong-Jie, **Kamper**, Maarten J., "*Axial Flux Permanent Magnet Brushless Machines*", 2008 ,2nd ed. , Springer

[3] P. Campbell, "*Principle of a Permanent Magnet Axial Field DC Machine*", Proceeding of Institute of Electrical Engineers, vol. 121,No. 12, Dec. 1974, p 1489-1494

[4] F. Caricchi, F. Crescimbini , E. Fedeli, G. Noia, "*Design and Construction of a Wheel-Directly Coupled Axial-Flux PM Motor Prototype for EVs* ", Conference Record of the 1994 IEEE Industry Applications Society Annual Meeting, 2-6 October 1994, Denver (USA)

[5] E. J. Hearn, "*Mechanics of Materials 2: The Mechanics of Elastic and Plastic Deformation of Solids and Structural Materials*", Third Edition, Butterworth-Heineman, 1997

[6] E. Levi, M. Jones,S.N. Vukosavic, "*Even-phase multi-motor vector controlled drive with single inverter supply and series connection of stator windings* " IEE Proceedings Electric Power Applications, Vol.150, Issue:5, pp.580-590

[7] M. Jones, S.N. Vukosavic, E. Levi, "*Parallel-Connected Multiphase Multidrive Systems With Single Inverter Supply* " IEEE Transactions on Industrial Electronics, Vol.56, Issue:6,pp.2047-2057

3. Linear mechatronic actuators

The linear motion is really important for the industrial application and many mechatronic system needs a linear actuator. To create the linear motion it is possible to carry out or a linear motor or a rotational motor joint with a mechanical gear.(es. lead screw, ball screw, roller screw).

The linear motor is indicated generally for short track and usually result more expensive than the rotational motor with mechanical gear which are adopted in many applications. The linear actuator constituted by a rotational motor are divided in three different categories: 1) actuators with lead screw; 2) actuators with ball screw; 3) actuators with roller screw.

$$\text{Linear actuators} \rightarrow \begin{cases} \text{Linear motor} \\ \text{Rotational motor} + \begin{cases} \text{Lead screw} \\ \text{Ball screw} \\ \text{Roller screw} \end{cases} \end{cases}$$

The lead screw is a mechanical actuator which permits to transform the rotational motion into linear motion with the contact between the screw and the nuts and a larger part of energy is dissipated by friction losses. This kind of component is used for low power actuators (e.g. electronic device as DVD reader) and where a cheap solution is required.

The mechanical actuators called ball screw is composed by a screw and a nut which is fixed to the moving object. The nut is composed by an external case with an internal helical path for the ball bearings; the movement of ball bearings transmits the rotational movement of screw to the linear motion of nut. This transformation happens with a very low value of friction and with a good precision in the positioning.

The characteristic of high performance and high precision are also typical of roller screw. The roller screw is constituted by an internal screw and an external planetary roller screw. Both ball screw and roller screw are the most suitable technology for linear actuators but due to the expensive costs, the roller screw is used only for particular application where a very high precision and high speed are required. In these thesis the ball screw actuators are considered.

3.1 Ball screw actuators

As previous mentioned, the ball screw actuators are composed by a screw and a nut. The two possible configuration are [1]:

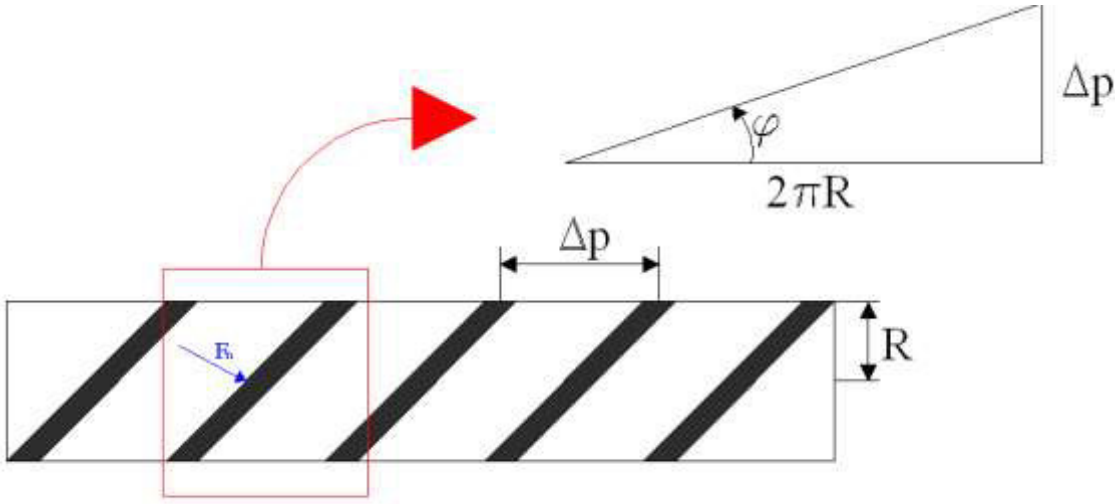

Fig.1.3 2D view of a screw: Fn is the force that acting between the screw and the nuts, Dp is the screw pitch, R is the screw radius and φ is the helical angle

- *ball screw driving*: the screw has a rotational motion and transmit a linear motion to the nuts, that is fixed to the moving object; in this case the contact force between the screw and nut acts on the nuts in the same direction of nut movement. In particular, the axial and tangential forces on the contact surface are:

$$F_{ax} = F_n \cos\varphi - \mu F_n \sin\varphi \qquad (1.3)$$

$$F_{\tan} = F_n \sin\varphi + \mu F_n \cos\varphi \qquad (2.3)$$

Referring to fig.1.3, it is possible to evaluate the helical angle as:

$$\cos\varphi = \frac{2\pi R}{\sqrt{\Delta p^2 + (2\pi R)^2}} \qquad (3.3)$$

$$\sin\varphi = \frac{\Delta p}{\sqrt{\Delta p^2 + (2\pi R)^2}} \qquad (4.3)$$

and the relation (1.3) and (2.3) become:

$$F_{ax} = \frac{F_n}{\sqrt{\Delta p^2 + (2\pi R)^2}}\left[2\pi R - \mu \Delta p\right] \qquad (5.3)$$

$$F_{\tan} = \frac{F_n}{\sqrt{\Delta p^2 + (2\pi R)^2}} \left[\Delta p + \mu 2\pi R \right] \qquad (6.3)$$

- *ball screw driven:* the nut transmit the motion to the screw; this configuration is used in some applications like sea waves generator; in these configuration the contact force acts on the opposite direction of nut movement. The axial and tangential force between the nuts and screw are:

$$F_{ax} = \frac{F_n}{\sqrt{\Delta p^2 + (2\pi R)^2}} \left[2\pi R + \mu \Delta p \right] \qquad (7.3)$$

$$F_{\tan} = \frac{F_n}{\sqrt{\Delta p^2 + (2\pi R)^2}} \left[\Delta p - \mu 2\pi R \right] \qquad (8.3)$$

In both configurations, the screw is joined to an electric motor with or without the use of a mechanical gear. The most interesting solutions is the actuators composed by a permanent magnet motor joined directly to the screw: this solution permits to avoid the mechanical gear and to increase the efficiency of the mechatronic systems.

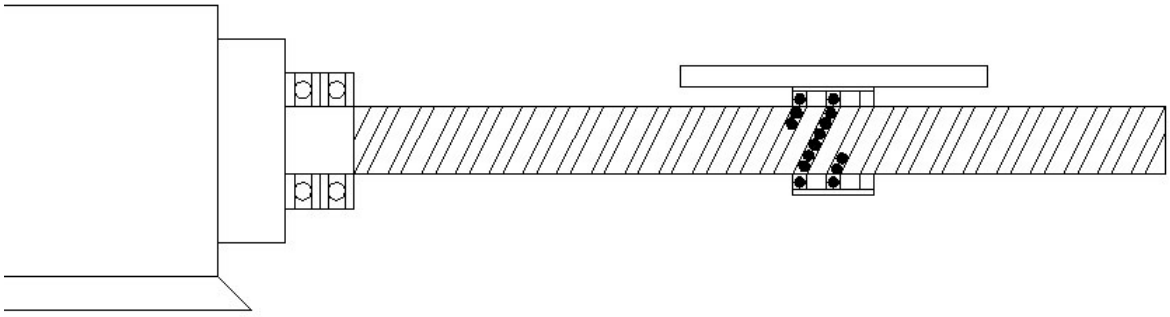

Fig.2.3 Electric motor joint with a ball screw with a free terminal

The possible arrangement of the screw depend by the type of fixed supported and if both the extremity of screw are fixed. In particular, one type of arrangement provides a screw terminal fixed with a bearings (generally with a pre-loaded bearing) and the second terminal is free (as shown in fig.2.3) ; the other possibility arrangement are constituted by the two terminal fixed with different bearings configurations. The vibration and mechanical behavior of actuator depend by the utilized configuration and also the model utilized in the simulation of system depends by the chosen configuration. Referred to [2], it is considered the following model for the ball screw with a free terminal:

$$\begin{cases} J_m \ddot{\theta}_1 - k_{rot}(\theta_2 - \theta_1) = M_m \\ J_s \ddot{\theta}_2 + k_{rot}(\theta_2 - \theta_1) = -i F_l \\ m_s \ddot{x}_1 - k_{nut}(i\theta_2 + x_2 + x_1) - k_{ax} x_1 = 0 \\ m_t \ddot{x}_2 + k_{nut}(-x_1 + x_2 + i\theta_2) + F_l = 0 \end{cases} \qquad (9.3)$$

where:

J_m = [kgm^2] inertia of electric motor rotor

J_s = [kgm^2] inertia of screw

M_m = [Nm] motor torque

Fl = [N] resistive force (sum of load force and weight of nut)

m_s = [kg] mass of the screw

m_t = [kg] sum of the nut mass and moving object mass

i = [m/rad] ratio between the helical step and the rotor angle in radians

x_1 = [m] screw axial movement

x_2 = [m] nut axial movement

θ_1 = [rad] angle of the rotation of rotor of electric motor

θ_2 = [rad] angle of the rotation of the screw

k_{rot} = [kg/s^2] rotor stiffness

k_{ax} = [kg/s^2] axial stiffness

k_{nut} = [kg/s^2] nut stiffness

The value of k_{rot} depend by the torsional stiffness of rotor shaft and by the coupling between the rotor of the motor and the screw:

$$k_{rot} = \left(\frac{1}{k_{shaft\_rot}} + \frac{1}{k_{coupl}} \right)^{-1} \qquad (10.3)$$

instead k_{ax} is equal to:

$$k_{rot} = \left(\frac{1}{k_{shaft\_screw}} + \frac{1}{k_{bearings}} \right)^{-1} \qquad (11.3)$$

where k_{shaft_ax} and $k_{bearings}$ are respectively the stiffness of screw and the stiffness of bearings. The model is realized as show in fig. 3.3 and 4.3:

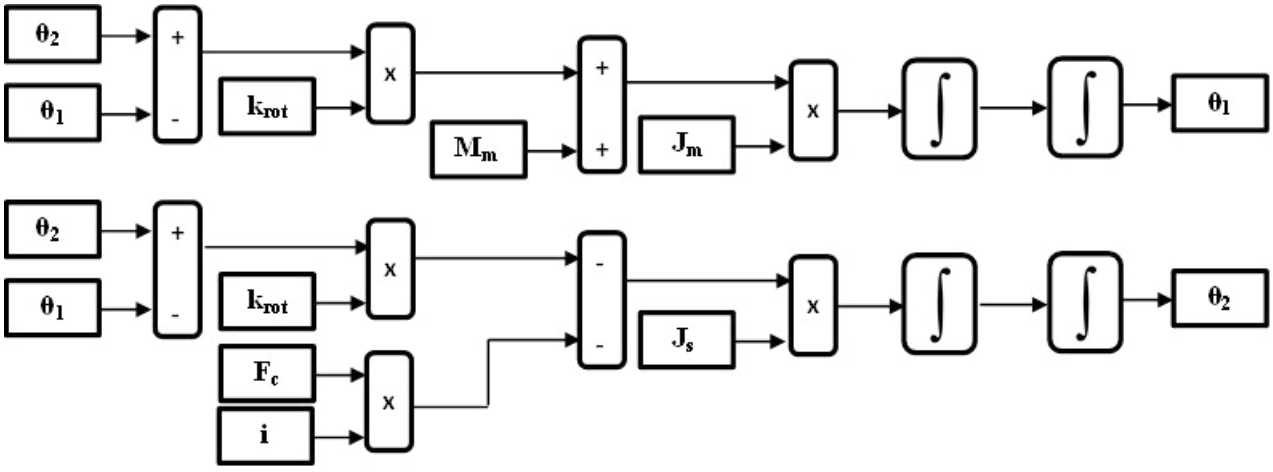

Fig.3.3 Simulation of coupling between the electric motor rotor and the screw

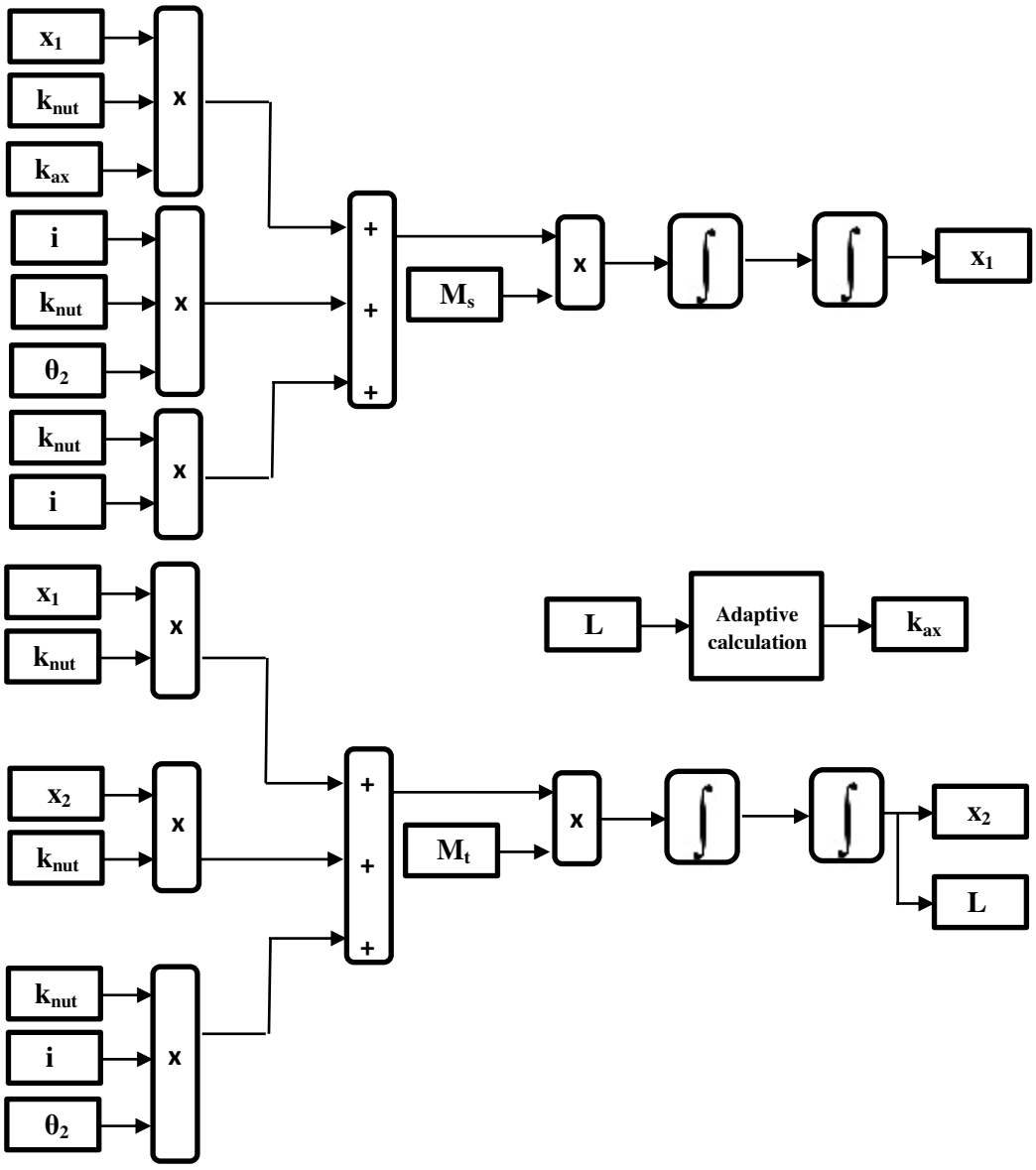

Fig.4.3 Simulation of mass-spring system which describe the screw and the nut behavior; the adaptive calculation permits to obtain the value of variable stiffness k_{ax}

The fig. 3.3 shows the simulation of rotational coupling between the electric motor and the screw. The angle θ_1 and θ_2 are calculated during the simulation, the motor torque and the load force are imposed by the external load and the rotational stiffness is considered constant. In the fig.4.3 is modeled the mass spring systems which describe the screw and the nuts. In the model an adaptive calculation of axial stiffness is necessary because its value depend by the nut position.

3.2 Coupling between the permanent magnet motor and the ball screw

As previous mentioned, the new applications in mechatronic provide the direct coupling between the ball screw and the electric motor; this solution permits to avoid the use of mechanical gear and increased the efficiency of the system. The direct coupling or direct drive solution become possible with the utilized of permanent magnet motor. Generally, the mechanical gear are required because the rated electric motor speed and the required speed for the screw are quite different; with the permanent magnet motor is very simple the realization of motor with an high number of pole pairs which permits to obtain a low speed and to couple directly the load to the motor shaft. The main limitation to make an high pole pairs number machine is the necessity to use an high number of stator slots (and also an high number of rotor bars for asynchronous machines); with an high number of slots, become very difficult the respect of stator main size and in particular it is very difficult avoid the magnetic saturation of teeth and to respect the axial and radial limit due to the end windings length which increased with the raise of stator slots number. This problem can be solve with the use of machine which presents a different stator and rotor pole pairs number (in literature this kind of machines are defined as fractional slot windings machine because the number of slot per pole and phase is calculated referred to the rotor poles pair number) and where the electromagnetic coupling between the stator and rotor happens on a spatial harmonic depending by the ratio between the stator and rotor pole pairs. Otherwise this kind of machines are generally realized with a concentrated tooth windings and for the use in application where an high reliability is required the windings is made by a single layer. The machine with different stator and rotor pole pairs are characterized by an increase of harmonic content in the torque; this is very important in the actuators, where exist a high risk that a resonant occurs between the machine and the linear actuator. In order to avoid that a resonant happens, is required the study of resonant frequencies of the ball screw and the comparison with the forcing frequencies . The frequency components in the air gap magnetic flux density and in the torque can be calculated referred to the model presented in chapter 4 and particularizing the model at the slot/poles configuration chosen. The natural frequencies of ball screw can be determine from equation (9.3), using the model in frequency domain:

$$\mathbf{M}\mathbf{X}(\omega)^2 + \mathbf{K} = 0 \qquad (12.3)$$

where **M** is the mass matrix which contains the mass terms and the inertia terms:

$$\mathbf{M} = \begin{bmatrix} J_m & 0 & 0 & 0 \\ 0 & J_s & 0 & 0 \\ 0 & 0 & m_s & 0 \\ 0 & 0 & 0 & m_t \end{bmatrix} \qquad (13.3)$$

And **K** is the stiffness matrix:

$$\mathbf{K} = \begin{bmatrix} krot & krot & 0 & 0 \\ -krot & krot & 0 & 0 \\ 0 & -knut \cdot i & -(knut + kax) & -knut \\ 0 & knut \cdot i & -knut & knut \end{bmatrix} \qquad (14.3)$$

The fig. 5.3 and 6.3 show the resonant frequencies obtained by the system (12.3) with a variable screw length and a variable mass of nut and of the moving object. As is possible to note, there is one frequencies which remain substantially stable at variable of length and mass, but the other one has a meaningful variation and could create problem during the actuator performance. In fig. 5.3 and 6.3 are reported also the frequency of the first four harmonic presents in the motor torque.

For the coupling between the axial flux permanent magnet motor and the ball screw is also really important to analyze the electromagnetic axial force which acts on the rotor and the stator. In fact, in radial flux permanent magnet motor the axial force are negligible, but in axial flux motor the forces due to the axial magnetic pressure are very high. To compute the axial force is necessary the calculation of magnetic pressure. The magnetic pressure which acts in an axial flux machine is expressed for an isotropic machine (surface mounted permanent magnet machine) as :

$$p(\theta,t)=\frac{B_{airgap}^2(\theta,t)}{2\mu_0}=\frac{\left\{\lambda_0\sum_{n=1}^{+\infty}B_{s,n}\Re\left[e^{-jnp_{sta}\theta}\mathbf{i_s}\right]+\sum_{n_r=1}^{+\infty}B_{n_r}\Re\left[e^{jn_rp_r\theta_r}\right]\right\}^2}{2\mu_0} \qquad (15.3)$$

Using formula (15.3), the axial force are calculated with the product between the magnetic pressure and stator disc surface.

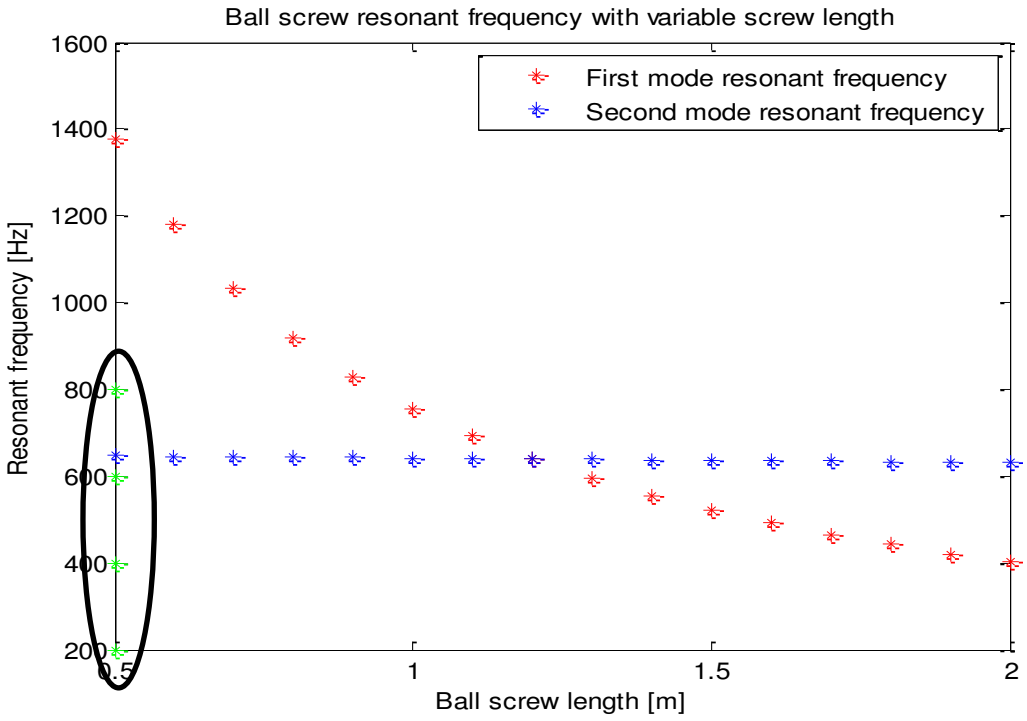

a)

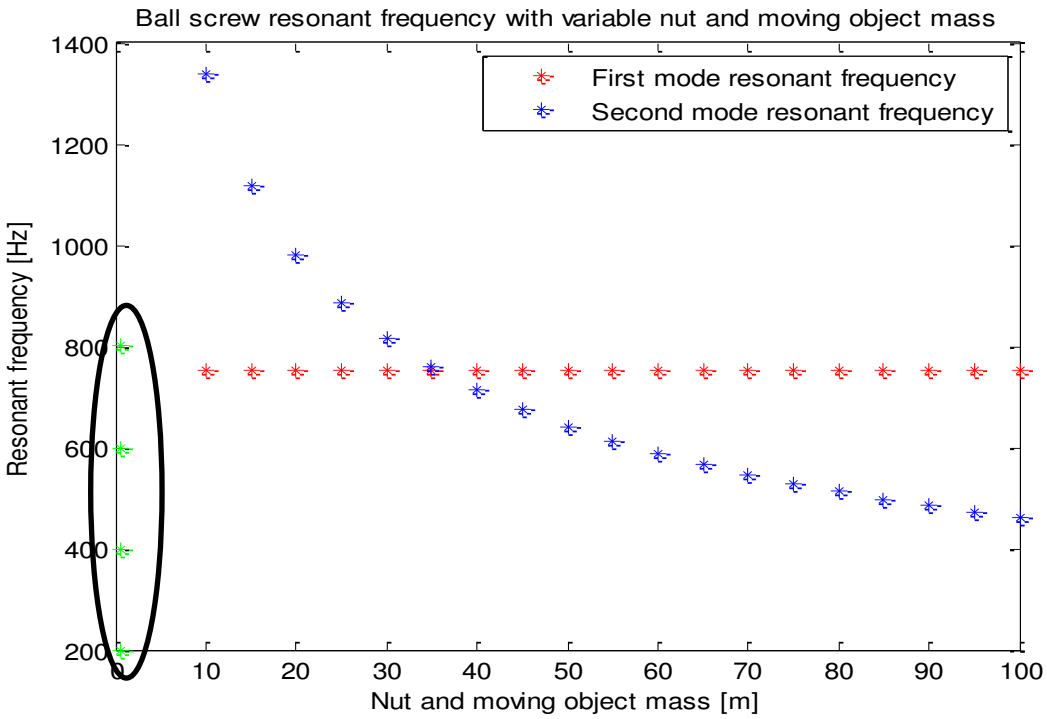

b)

Fig.5.3 Comparison between the resonant frequency of ball screw with variable length (a) and variable nut(b) and moving object mass and the torque frequencies of 24 slots-20 poles three phase machine. The black ellipses indicate the main torque frequencies of the motor.

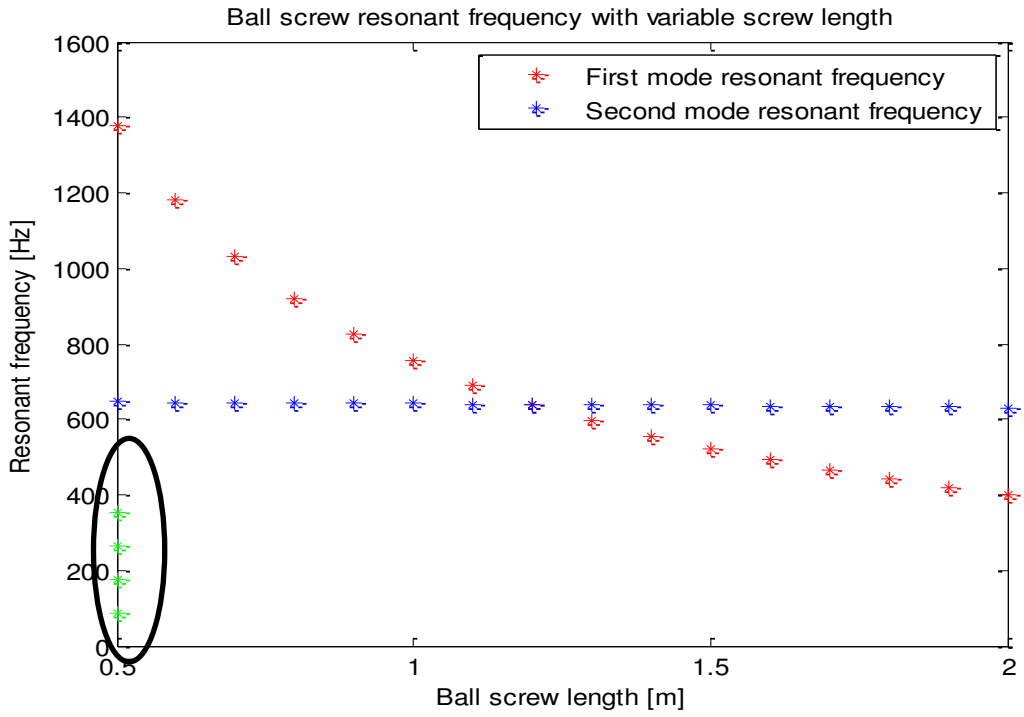

a)

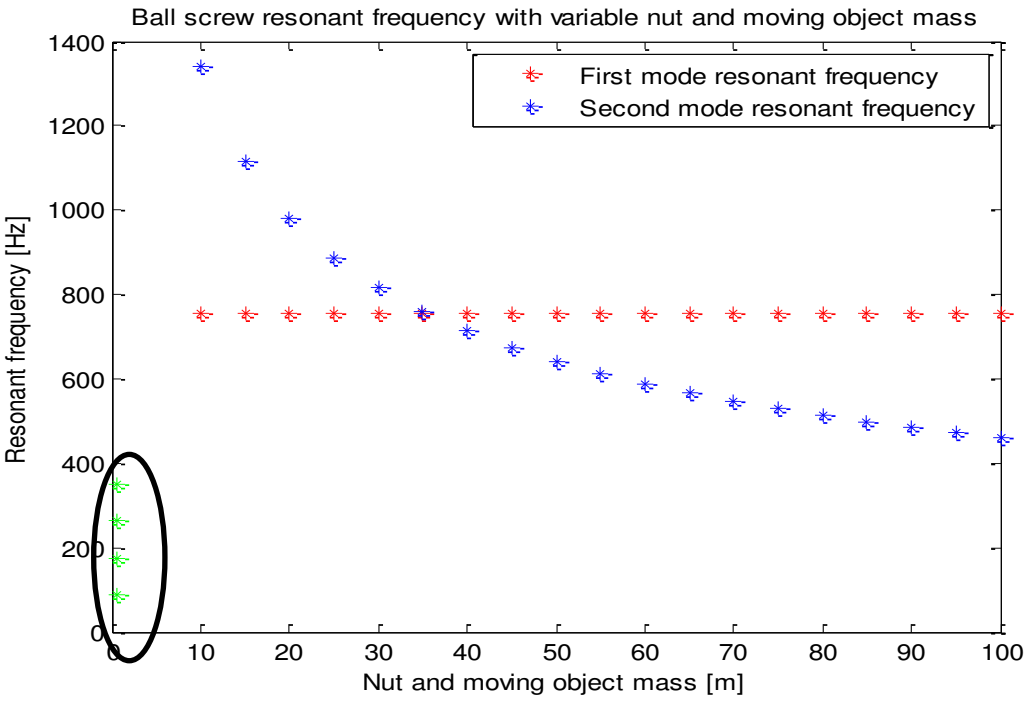

b)

Fig.6.3 Comparison between the resonant frequency of ball screw with variable length(a) and variable nut(b) and moving object mass and the torque frequencies of 20 slots-18 poles five phase machine. The black ellipses indicate the main torque frequencies of the motor.

In fig. 7.3 and 8.3 are reported the axial force frequencies for a three phases 24 slots-20 poles machine and for a five phases 20 slots-18 poles machine. This figures show that in the choice screw length range and mass range there aren't overlaps between the ball screw frequencies and the axial force frequencies; in particular the performed analysis show that only the torque contain frequencies which in some conditions could create resonance phenomena.

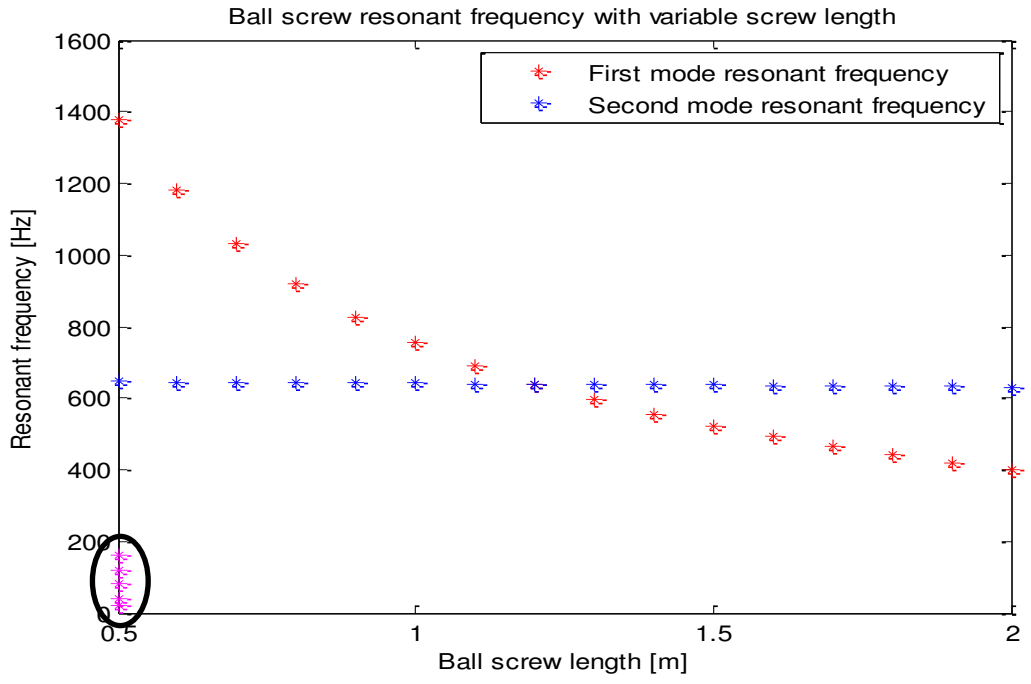

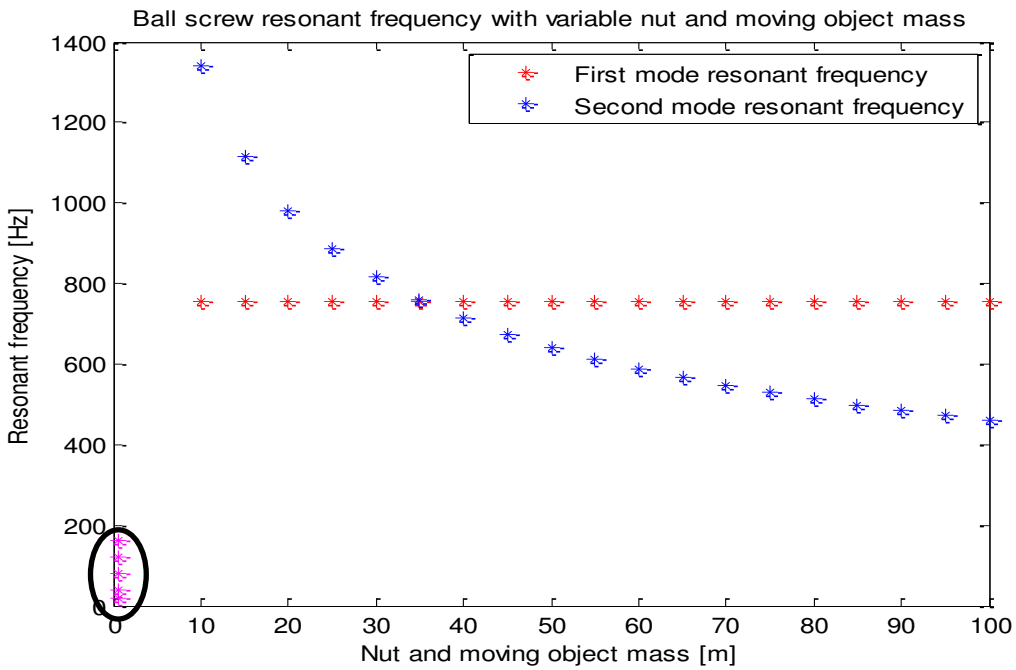

Fig.7.3 Comparison between the resonant frequency of ball screw with variable length (a) and variable nut (b) and moving object mass and the axial force frequencies of 24 slots-20 poles three phase machine. The black ellipses indicate the main axial force frequencies which act in the motor.

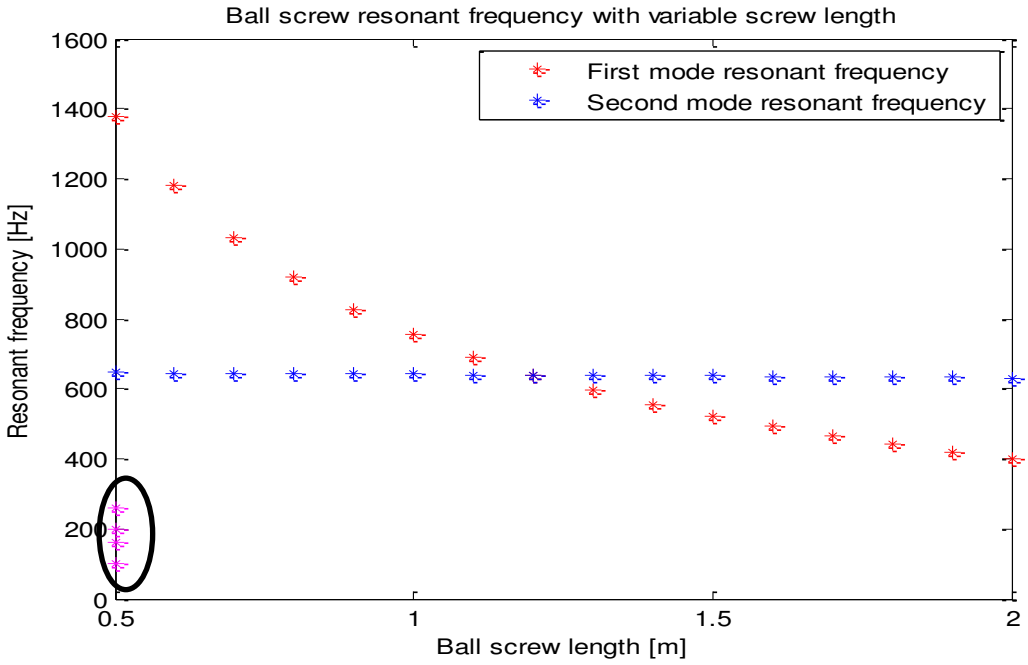

a)

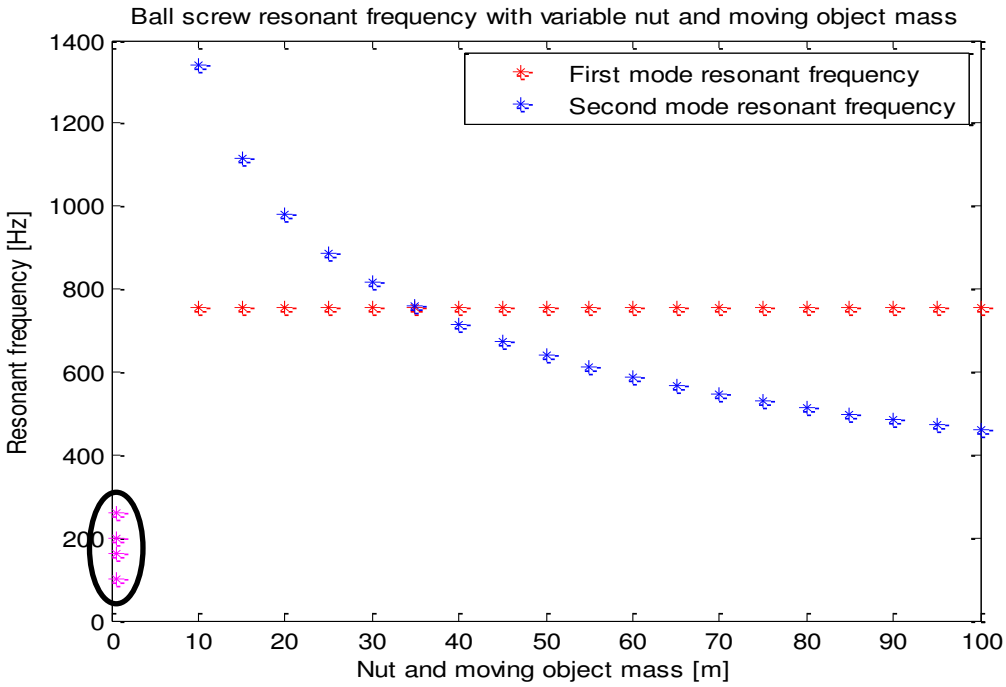

b)

Fig.8.3 Comparison between the resonant frequency of ball screw with variable length (a) and variable nut (b) and moving object mass and the axial force frequencies of 20 slots-18 poles five phase machine. The black ellipses indicate the main axial force frequencies which act in the motor.

References of Chapter 3

[1] Geoffrey Holroyd, "*The modelling and correction of ball-screw geometric, thermal and load errors on cnc machine tools*", Phd thesis, University of Huddersfield

[2] S. Frey, A. Dadalau ,A. Verl ,"*Expedient Modeling of Ball Screw Feed Drives*", Issue No. 2009-19 Stuttgart Research Centre for Simulation Technology (SRC SimTech)

4. Design of axial flux machine for ball screw actuator

The aim of the thesis is the design of an axial flux multi stack machine which can be used to substitute a radial permanent magnet machine jointed with a ball screw. Taking into account the radial permanent magnet motor characteristic, the design constraints obtained are shown in tab.4.1:

Total machine output power	10000 W
External maximum diameter	280 mm
Internal minimum diameter	120 mm
Axial length	<350 mm
Thermal class	B
Rated phase to phase voltage	440 V
Rated speed	590 rpm
Maximum speed	900 rpm
Cooling	Natural cooling

Tab4.1. Design constraints for the multi stacks machine

The output mechanical power of radial flux permanent magnet motor is 10 kW and the motor is coupled directly with a ball screw actuators and generally a preload on the bearing is request to guarantee the movement of actuator screw: some experimental test have detected that the greatest part of machine losses shall be counted by the mechanical losses in the bearings due to the preload and this must be taking into account during the torque validation with finite element analysis and also in the thermal analysis of machine. The machine cooling is performed with natural air and without the use of fun: in this way it is possible to realize a totally enclosed motor and to shield the permanent magnet against dust or other contingencies (like the ice in aerospace applications), but this implies to limit the current density in the conductor and the linear current density of machine with an increase of machine sizes. The geometric constraints are obtained with some considerations about the maximum dimension of frame and the diameter required for the ball screw. The radial flux machine is made with 24 slots-20 poles and has two poles pairs on the stator and ten poles pair on the rotor; the phases coil are concentrated around the stator teeth and are realized with a single layer windings. The coupling between the rotor and stator happens on the fifth stator magnetic field harmonic which correspond to the 100 Hz frequency (fig.1.4 a).

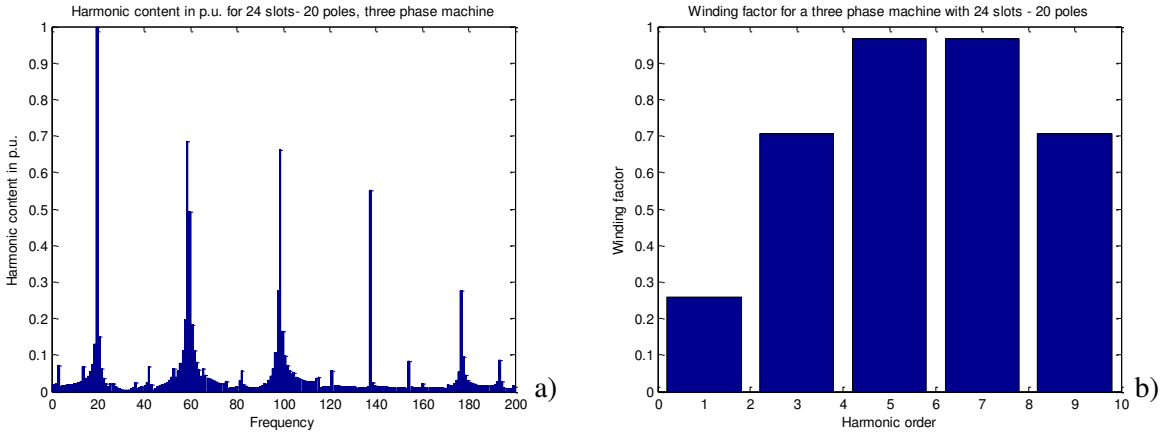

Fig.1.4 a) Harmonic content of the stator magneto motive force for a 24 slots- 20 poles machine; b)Winding factor of the stator windings for a 24 slots- 20 poles machine.

The fig. 1.4b) show the variation of winding factor for the first 10 harmonics. Obviously, only the odd harmonics number are contained in the magneto motive force. As it is possible to note from fig. 1.4 b), the winding factor of 5^{th} and 7^{th} harmonics is the same: this gives us the possibility to create a coupling on the 7^{th} magnetic field harmonic utilizing a rotor with 14 poles pairs.

In order to compare the radial flux motor and the multi stacks machine, it was decided to maintain the same slots/poles configuration in each stack which has a mechanical power of 3500 W and the topologies chosen is the axial flux double rotor machine; also the current density imposed in the conductor is the same utilized in the conductors of radial flux machine (5 A/mm^2). Regarding the maximum values of magnetic flux density in the machine, it was decided to size the machine with a maximum value of 1,6 T in the rotor yokes, 1,4 T in the tooth and 0,9 T in the air gap. The design procedure provided three different machine which are analyzed with a finite element analysis and compared between them. The differences between the three machine are related to the outer stator and rotor diameter and to the shape of teeth. In the following paragraphs are reported the main machine sizes and the results obtained with finite element analysis:

- *Axial flux double rotor machine:* ***MFA3500-159***

The single stack of these machine has the following features:

MFA3500-159 Features

Stack power	3500 W
External diameter	240mm
Internal minimum diameter	120 mm
Axial length	114 mm
Number of turns per phase	636
Slots/poles configuration	24/20
Slot length	43 mm
Tooth area	417 mm^2
Air gap	1 mm
Type of magnets	N38SH
Magnet polar arc	11,3°
Length of magnet	3,1 mm
Thermal class	B
Rated phase to phase voltage	440 V
Rated current	5,6 A
Rated speed	590 rpm
Maximum speed	900 rpm
Cooling	Natural cooling

Tab.4.2 MFA3500-159 features

The magnetic flux density in the machine and in the tooth are given in fig. 2.4. The results show that the imposed maximum values of magnetic flux density are respected in the main part of the machine, but a very high magnetic saturation occurs at the base of tooth. In order to guarantee the machine performance, each phase is composed by 636 turns which are wrapped around four teeth. The fill factors obtained is equal to 0,57 and this value is very high for round conductor and probably, only the use of flat conductors could permits the realization of the windings.

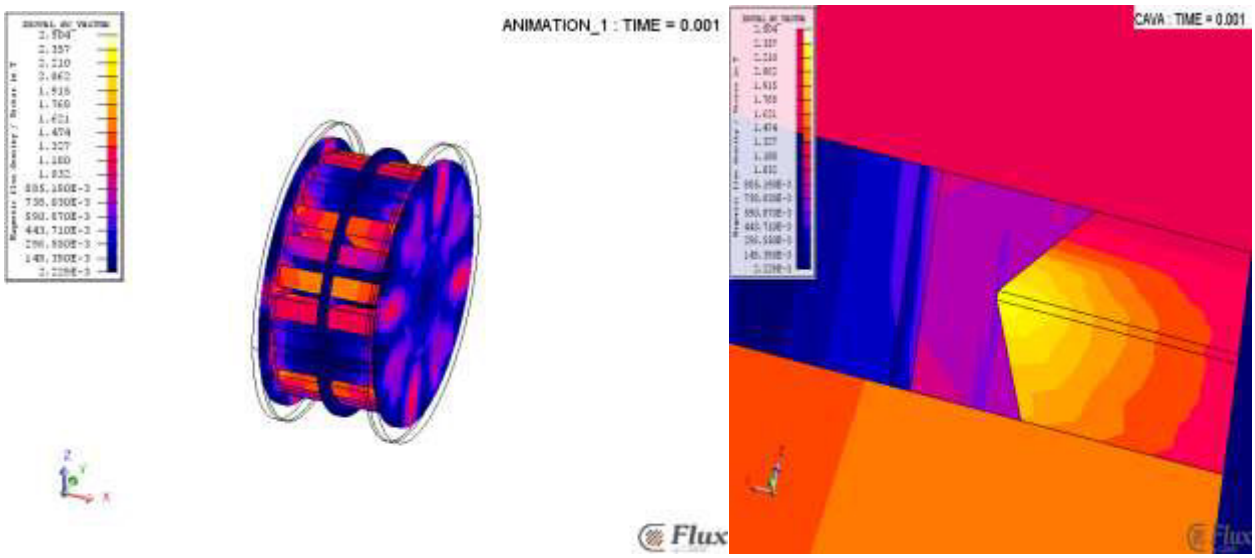

Fig.2.4On the left is shown the total view of magnetic flux density in the machine MFA3500-159; on the right a tooth particular is shown

The single stack electromagnetic torque is calculated with a transient analysis, imposing the rated speed and the rated current and the result is shown in fig.3.4. The maximum torque ripple is around 10 Nm.

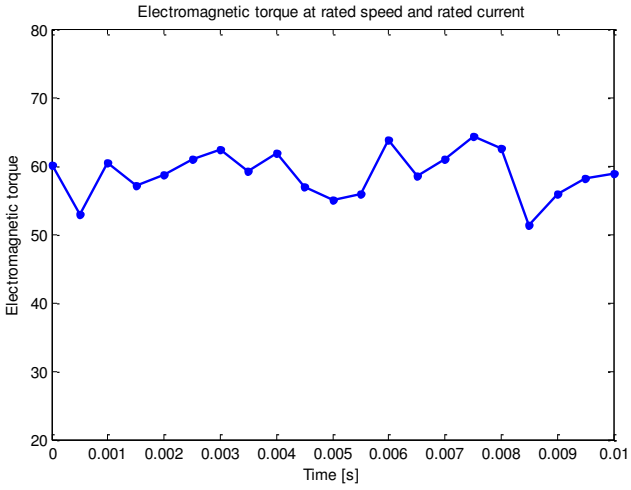

Fig.3.4 Electromagnetic torque obtained with a transient analysis at rated speed of 590 rpm and rated current of 5,6 A

- *Axial flux double rotor machine:* ***MFA3500-159CT***

The second machine designed and analyzed is similar to the previous machine but some modifies has been executed on the teeth shape. The stator and rotor main sizes are the same of first machine, and also the number of turns is the same.

MFA3500-159CT Features

Stack power	3500 W
External diameter	240mm
Internal minimum diameter	120 mm
Axial length	114 mm
Number of turns per phase	636
Slots/poles configuration	24/20
Slot length	43 mm
Tooth area	360 mm^2
Air gap	1 mm
Type of magnets	N38SH
Magnet polar arc	11,3°
Length of magnet	3,1 mm
Thermal class	B
Rated phase to phase voltage	440 V
Rated speed	590 rpm
Maximum speed	900 rpm
Cooling	Natural cooling

Tab.4.3 MFA3500-159CT features

The new tooth shape permits to reduce the magnetic saturation at the base of tooth but the reduction of tooth area increased the average value of magnetic flux density respect the previous machine, as shown in fig.4.4. In this case the obtained fill factor is equal to 0,53.

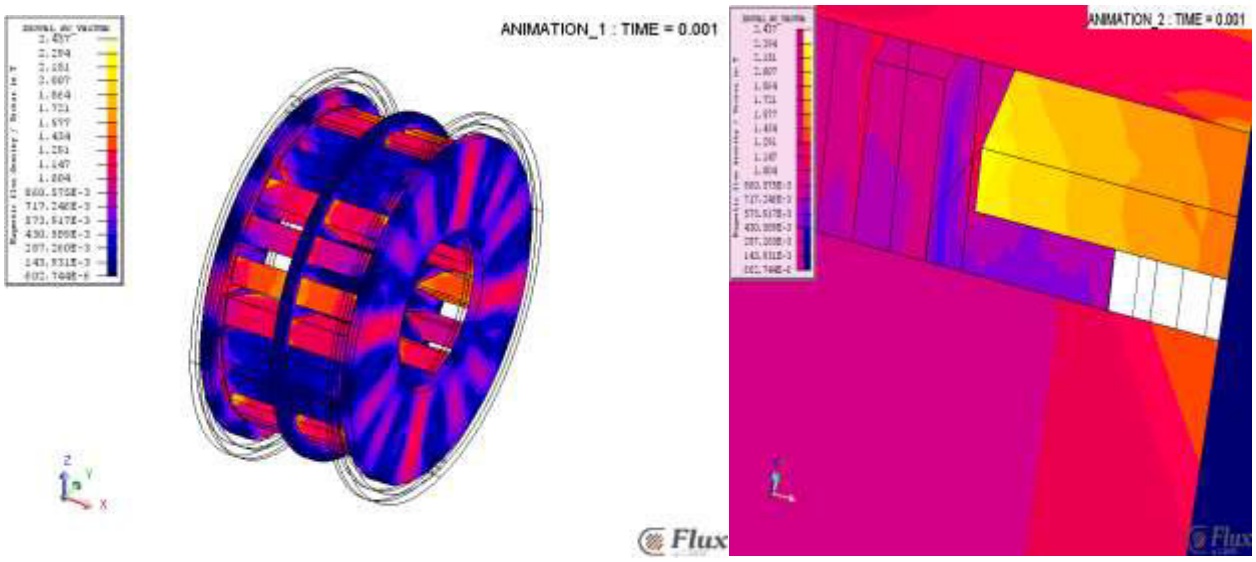

Fig.4.4 On the left is shown the total view of magnetic flux density in the machine MFA3500-159CT; on the right a tooth particular is shown

The fig.5.4 shows the electromagnetic torque obtained by the analysis of a single stack.

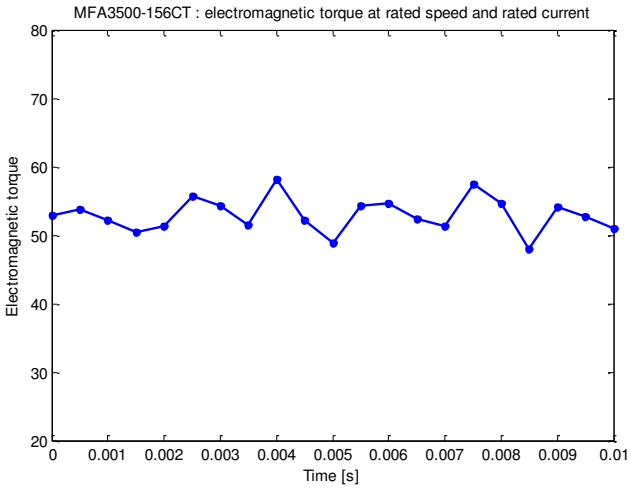

Fig.5.4 Electromagnetic torque obtained with a transient analysis at rated speed of 590 rpm and rated current of 5,6 A

- *Axial flux double rotor machine:* ***MFA3500-109***

The last machine is obtained with a variation of stator and rotor external diameter and with a reduction of number of turns per phase. This changes permit to reduce the axial length of the machine and also the fill factor in the slots (0,32).

MFA3500-109 Features

Stack power	3500 W
External diameter	280mm
Internal minimum diameter	120 mm
Axial length	97 mm
Number of turns per phase	436
Slots/poles configuration	24/20
Slot length	34 mm
Tooth area	514 mm^2
Air gap	1 mm
Type of magnets	N38SH
Magnet polar arc	11,3°
Length of magnet	3,1 mm
Thermal class	B
Rated phase to phase voltage	440 V
Rated speed	590 rpm
Maximum speed	900 rpm
Cooling	Natural cooling

Tab.4.4 MFA3500-109CT features

As shown in fig.6.4, the maximum value of magnetic flux density in the machine is lower than the other two machines and the magnetic saturation is not reached in the slots. The diameter of rotor and stator are different: this configuration permits to bind the stator at the machine frame and if a forced cooling is required, it is possible to create a path for air flow along the rotors and the sides of the stator. In this machine, the slots width are greater than the other machines obtained: in this way

it is reached a low value of fill factor which is required for round conductor but this allows a high torque ripple as shown in fig.7.4.

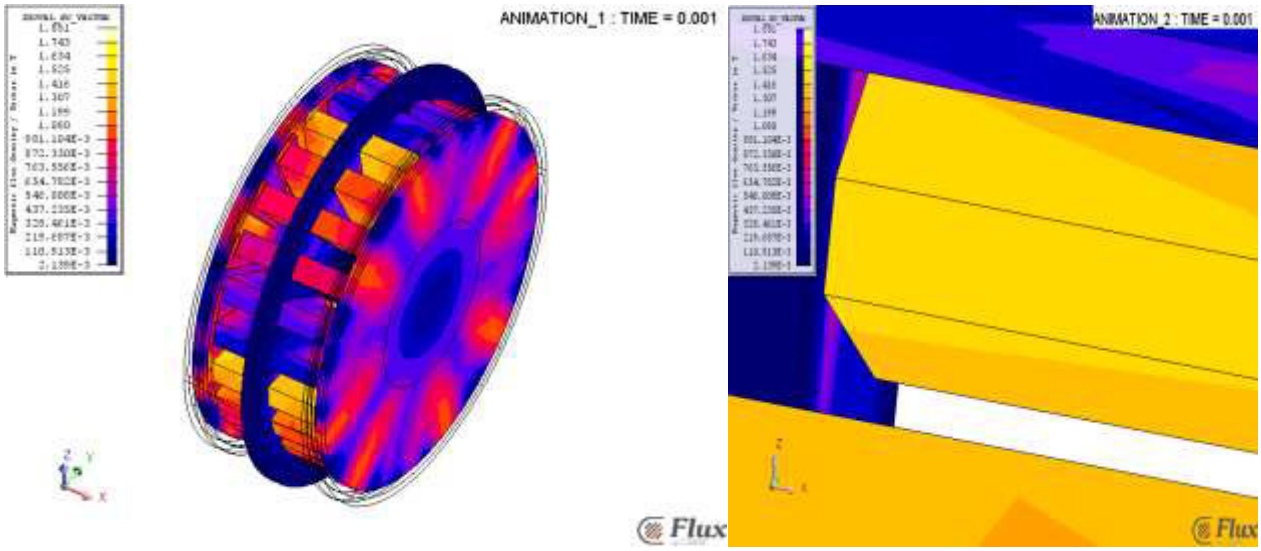

Fig.6.4 On the left is shown the total view of magnetic flux density in the machine MFA3500-109; on the right a tooth particular is shown

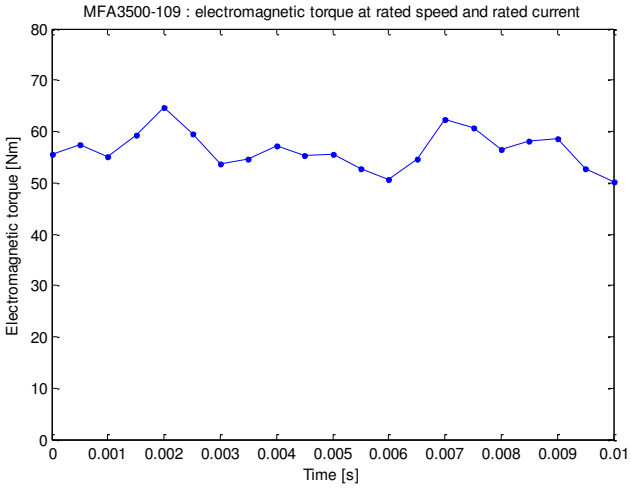

Fig.7.4 Electromagnetic torque obtained with a transient analysis at rated speed of 590 rpm and rated current of 5,6 A

The value of ripple torque can be reduced with the choice of different type of slot. In the previous machine an open slot was used and this permits to facilitate the insertion of windings and the realization of stator (for example it is possible to realize the stator with a machining of soft powdered magnetic materials). The semi-open slot permits to reduce the torque ripple and also the cogging torque, but the manufacture of the machine became more difficult.

4.1 Comparison between the obtained machines

In this paragraph, is reported the comparison between the three machines; in particular, the comparison is made considering the mean value of torque, the maximum value of cogging torque, the torque and the back emf constant, the fill factor of windings, the Joule and the iron losses of the machines. Referring to fig.8.4, each sized machine gives the minimum electromagnetic torque required. The lowest value regards the MFA3500-159CT; in fact these machine is different from the MFA3500-159 only for the tooth shape and the reduction of tooth area changes the total flux linked by the machine windings and therefore the machine torque is decreased. The mean value of torque is calculated at rated current and rated speed of the machine.

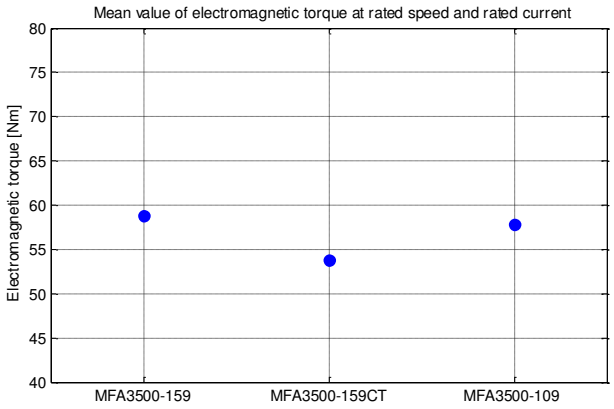

Fig.8.4Mean values of electromagnetic torque [Nm] computed for the three machine: MFA3500-159, MFA3500-159CT, MFA3500-109.

The fig.9.4shows the maximum values of cogging torque computed with a no-load 3D finite element analysis. The machine MFA3500-109 has the maximum value of cogging torque: this is due to fact that the machine is made with an high area of tooth which gives a variation of magnetic energy in the air gap greater than the other two cases and introducing also an high ripple in the torque.

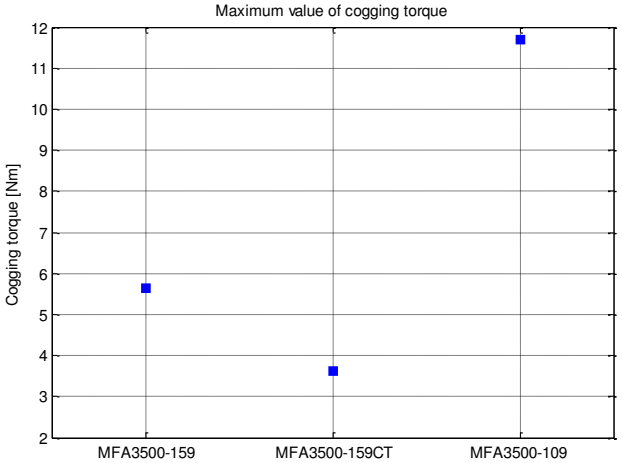

Fig.9.4 Maximum values of cogging torque [Nm] computed for the three machine: MFA3500-159, MFA3500-159CT, MFA3500-109.

Two important machine parameters useful for the comparison are the torque constant k_t and the back emf constant, k_e. Those parameters can be considered respectively as the proportional coefficient between the machine torque and machine current and between the back electromotive force induced in the phases and the speed of the machine. Both the parameters are strictly dependent by the number of turns.

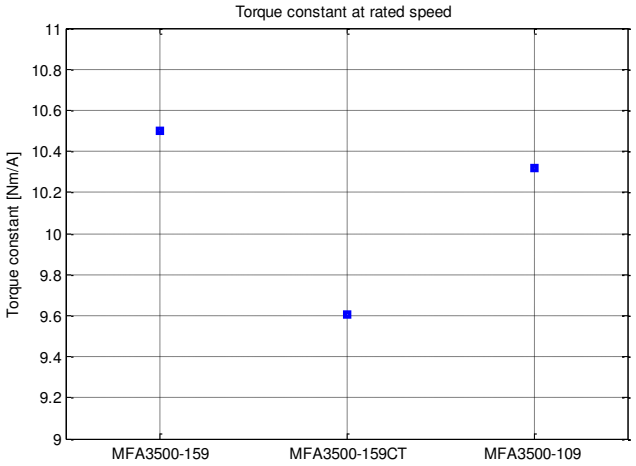

Fig.10.4 Torque constant [Nm/A] computed for the three machine: MFA3500-159, MFA3500-159CT, MFA3500-109.

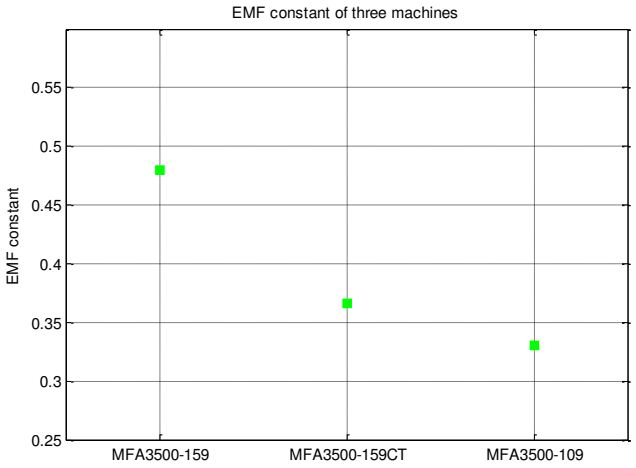

Fig.11.4 EMF constant [V/rpm] computed for the three machine: MFA3500-159, MFA3500-159CT, MFA3500-109.

The fig.10.4 puts in evidence that the higher value of k_t is reached by the first sized machine (MFA3500-159), but the last machine (MFA3500-109) has a similar value of k_t with a low number of turns (this is due to the greater sizes of machine which allows a greater value of linked flux). Instead the k_e has the maximum value for the machine "MFA3500-159" and the minimum value for the last machine and taking into account the rated speed of machine, in the first machine the back emf is equal to 283 V, in the second is equal to 215 V and in the last machine is 198V. Considering the phase to phase voltage imposed for the machine, it is evident that the first machine could not respect the voltage limit (the rated phase to phase voltage is 440 V).

Another important parameters for the comparison between two or more electrical machines are the electrical losses of the machines. The electrical losses in a permanent magnet machines are constituted by the Joule losses, the iron losses and the magnet losses. The last type of losses are usually negligible for low speed permanent magnet machine and become very important in high speed applications. Therefore the comparison shown in this chapter taking into account only the Joule Losses and the iron losses . Both the two type of losses are computed during the finite element analysis and for the Bertotti's coefficient are utilized [2],[3] to compute the iron losses. As it is possible to note from fig.12.4, the MFA3500-109 is the machine with the lowest values of iron losses but with the highest value of joule losses due to the high value of phase resistance.

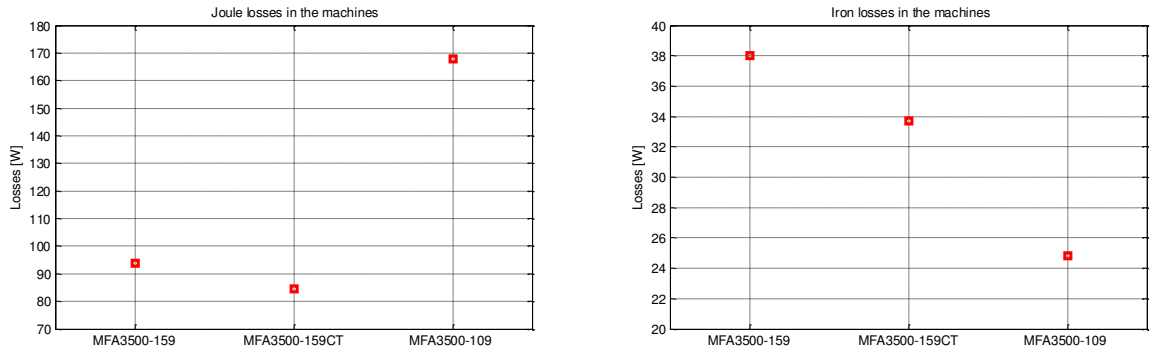

Fig.12.4 Joule losses [W] and Iron losses [W] computed for the three machine: MFA3500-159, MFA3500-159CT, MFA3500-109.

During the manufacturing of an electrical machines, the slots fill factor is one of the most important parameter to check before the realization of prototype. Depending by the type of conductor (round conductor or flat) and by the thickness of insulation, an high value of fill factor permits to exploit all the machine surface and to improve the machine performance. In fig.13.4 are reported the fill factor required by machines: probably the manufacturing of MFA3500-159 and MFA3500-159CT it is possible only with the use of flat conductors while the MFA3500-109 permits the use of round conductors.

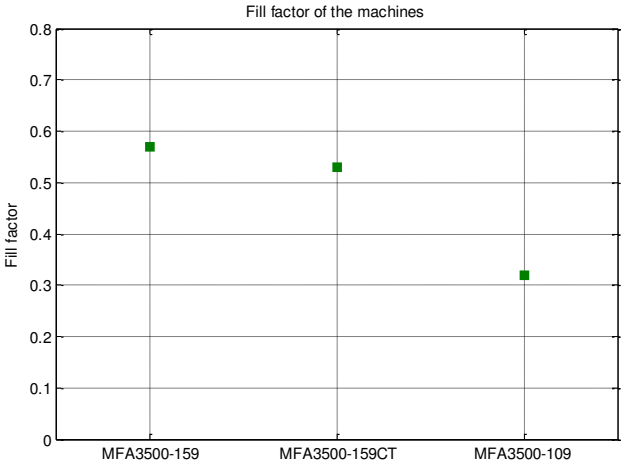

Fig.13.4 Fill factor of the three machine: MFA3500-159, MFA3500-159CT, MFA3500-109.

The fig.14.4 shows the synchronous inductance calculated in the machine. As it is possible to note, the MFA3500-109 machine has the lower value of synchronous inductance. This is due to the low number of turns respect the other two machine. The inductances difference between the other two machine with the same number of turn is related to the difference shape of the machine slots.

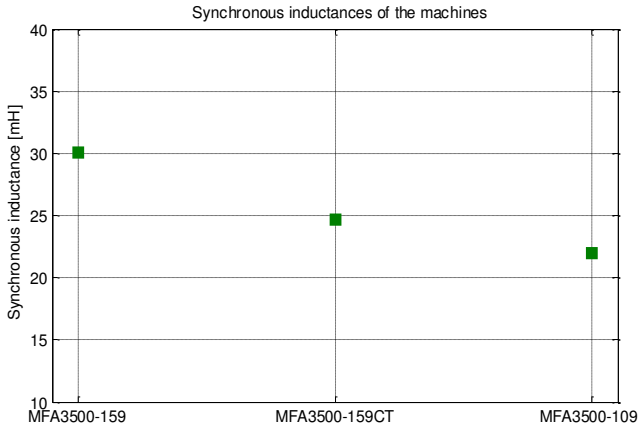

Fig.14.4 Synchronous inductances of the machines: MFA3500-159, MFA3500-159CT, MFA3500-109.

The final check realized with the finite element analysis is the verify of machine behavior in the flux weakening operation zone. The maximum speed allowable in the considered application is 900 rpm; taking into account the machine parameters and considering that in the flux weakening working point the machine works with the rated voltage and the rated current, in fig.15.4 is shown the electromagnetic torque developed by the three different machines:

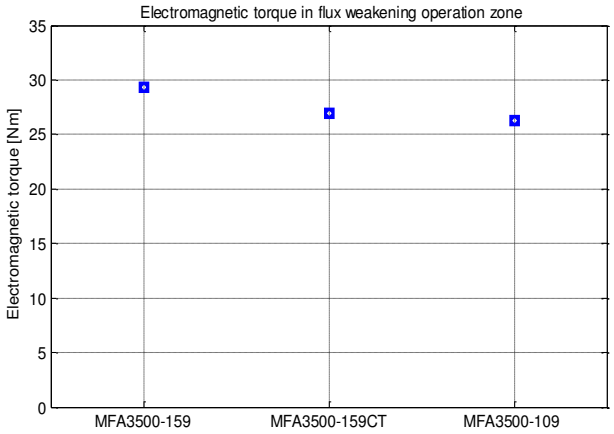

Fig.15.4 Electromagnetic torque in the flux weakning operation zone, at maximum speed of 900 rpm and Id equal to 6,86 A: MFA3500-159, MFA3500-159CT, MFA3500-109.

The higher electromagnetic torque is provided by the MFA3500-159 machine, but the other machines have an electromagnetic torque slightly lower than the MFA3500-159 and it is possible to affirm that the mechanical behavior in the flux weakening operation zone is the same for the three machines.

4.2 The prototyping of axial flux machine with the 3D printer

The rapid growth of 3D printers gives the opportunity to check the sizes of an electrical machines before the manufacturing of prototype. The most critical thing to check in an electrical machine is the correct insertion of coil and insulations in the slot. In fact, usually when a special electrical machine is designed, it is possible to impose a wrong value of fill factor which doesn't permits the correct insertion of the coils in the slots. In the following are reported the image related to the check of the slots size of machine MFA3500-109 through the prototyping process with the 3D printer.

Fig.16.4 Single coil of windings (each phase is constituted by four type of this coil). By courtesy of Umbra Cuscinetti SpA

Fig.17.4 In the figure is shown a single coil which is wrapped around the teeth of machine. By courtesy of Umbra Cuscinetti SpA

The fig. 17.4 shows the correct choice of slot sizes and the compatibility between the slot and the coil reported in fig.16.4. On the top and on the bottom of the slot it is possible to individuate a vacuum which is necessary to leave for the realization of neutral connection and for all the welds necessary for the coil. The fig.4.18 shows a frontal view of the coil inside the machine. It is clear that the coil is correctly inserted into the slot and it is evident the possibility to make a coil with more turns. In fig.19.4 a cross section of MFA3500-109 obtained with 3D printer is shown.

Fig.18.4 Frontal view of a single coil wrapped around the teeth of machine. By courtesy of Umbra Cuscinetti SpA

Fig.19.4 View of machine 3d printer prototype

Appendix of Chapter 4:

Finite element analysis of an axial flux permanent magnet machine

The finite element analysis is composed by three steps: the pre-processing , the analysis and the post-processing. In the pre-processing steps happens the choice of type of analysis (2D, 3D, quasi 3D), the cad modelling of geometry and the boundary conditions are imposed. The finite element simulation can be performed considering the field time invariant (magnetostatic analysis) or time variant (AC magnetostatic analysis), or considering that all the electrical (and also the mechanical parameter of an electrical machine) changing in the time (transient analysis). The final step of a finite element analysis is the post-processing where all the solutions are processed. Regarding the electrical machines analysis, in the post-processing operation it is possible to calculate all the electrical parameter and the electrical losses of the machine, the calculation of magnetic flux density permits also to check the machine saturation and the magnet working point. Considering the machine performance, the finite element analysis makes available the computation of electromagnetic torque developed by the machine. The electromagnetic torque is usually calculate in this different way:

- Maxwell stress tensor method

The Maxwell stress tensor provides the value (4.7) of normal F_n and tangential (4.8) components F_t of electromagnetic force which acts in the air gap region on the stator and rotor:

$$F_n = \frac{1}{2\mu_0}\int_S \left(B_n^2 - B_t^2\right)\hat{n}\, dS \qquad (4.7)$$

$$F_t = \frac{1}{\mu_0}\int_S B_n\, B_t\, \hat{t}\; dS \qquad (4.8)$$

In (4.7) and (4.8) B_n, B_t are respectively the normal and tangential components of magnetic flux density. The normal component of force doesn't create a torque component but acts only with an electromagnetic pressure on the stator and on the rotor and it is the mainly causes of vibrations and noise. The unique contribute to the torque is due to the tangential force (4.8), and considering the mean value of the air gap surface integral of (4.8), the torque expression for an axial flux machine is:

$$T = \frac{p}{2\,\mu_0\, g}\left(D_{out} - D_{in}\right)\int_S B_n\, B_t\, \hat{t}\; dS \qquad (4.9)$$

where p is the number of poles pairs, g is the air gap width, D_{out} and D_{in} are the external and the internal machine diameters.

- Method of virtual work

The method of virtual works is based on the calculation of magnetic co-energy variation for different rotor position and with a fixed current value:

$$T = -\left.\frac{\partial W_m^{'}}{\partial \theta_{mecc}}\right|_{i=\text{cost}} \qquad (4.10)$$

Both (4.9) and (4.10) can be utilized for the cogging torque computation. In this case it is necessary that the current in windings machine is zero and only the machine magnetization is only due to the permanent magnet motor.

The finite element analysis shown in this thesis are performed with the software *Flux Cedrat.*

Using the finite element analysis, the machine inductances can be calculated taking into account the total flux linkage along the d-q axis reference frame:

$$\begin{cases} \varphi_d = \varphi_m + L_d i_d \\ \varphi_q = L_q i_q \end{cases} \qquad (4.11)$$

In the relation (4.11) φ_d, φ_q and φ_m are respectively the linkage flux along the direct axis, the quadrature axis and the linkage flux due to the permanent magnets while L_d and L_q are the direct and quadrature inductances. With a finite element software, it is possible to eliminate the magnetization of permanent magnet and to impose a current along the direct axis. In this way the only component of flux is the direct axis component and it is easy to calculate the L_d. The same considerations are valid for the calculation of L_q. The difference betwenn Ld and Lq in the machine with superficial permanent magnet is very low; for this reason it is possible to evaluate only the synchronous reactance of the machine. The procedure is based on the calculation of magnetic energy stored in the machine airgap, and with the relation (4.12) it is possible to obtain the synchronous reactance:

$$L_s = \frac{2W_m}{3I_s} \qquad (4.12)$$

where W_m is the magnetic energy stored in the air gap, and I_s is the maximum value of current which flows in the phases.

The analysis of an axial flux machine could have some difficulties due to the geometry of machine. In particular it is possible to perform three different type of analysis: 2D, quasi 3-D and 3D analysis.

The 2D approach in an axial flux machine consists in the fact that the radial component of the magnetic flux density is neglected and the only considered components in a cylindrical coordinate system are the axial component and the circumferential component:

$$\mathbf{B} = B_\varphi(\varphi, z)\mathbf{e}_\varphi + B_z(\varphi, z)\mathbf{e}_z \qquad (4.13)$$

Assuming the relation (4.13), the potential vector **A** has a component only along radial direction. The considered Maxwell's equations are:

$$\nabla \cdot \mathbf{B} = 0 \qquad (4.14)$$

$$\nabla \times \mathbf{H} = 0 \qquad (4.15)$$

and the magnetic flux density is related to the magnetic field with the following equation:

$$\mathbf{B} = \mu_r \mathbf{H} + \mathbf{B_r} \qquad (4.16)$$

Assuming (4.14),(4.15),(4.16) and considering the Coulomb gauge , the final equation to solve in 2D analysis is:

$$\frac{1}{r^2}\frac{\partial^2 A}{\partial \varphi^2} + \frac{\partial^2 A}{\partial z^2} = -\frac{1}{r}\frac{\partial B_r}{\partial \varphi} \qquad (4.17)$$

The analysis is performed along a symmetry axis in the machine. The symmetry axis can be two: the first is obtained with a cutting plane which affects and divided the slots in two equal parts (fig.20.4), the latter could be obtained considering the average diameter and carry out a machine linearization (fig.21.4).

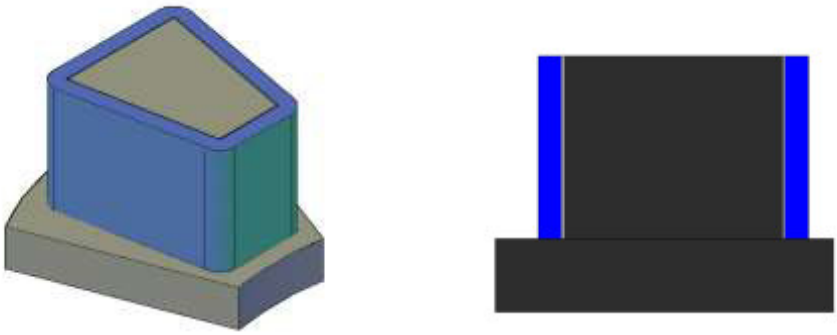

Fig.20.4 On the left is shown the 3D view of a slot and on the right 2D section of slot

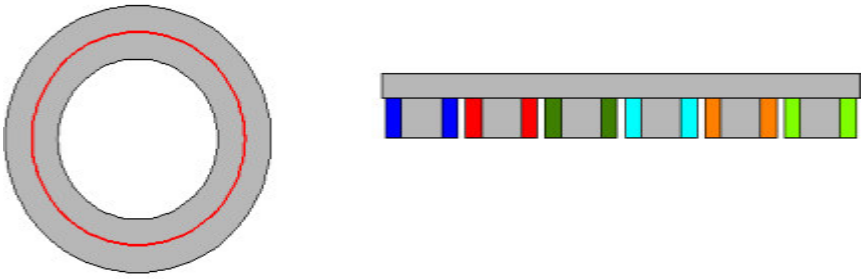

Fig.21.4 The average diameter (red circle) is linearized and the 2D view is shown on the right

The same consideration are made for the rotor and magnet whom overlooking the slot. The 2D analysis of an axial flux machine can introduces an high error, because there is a great uncertain in the definition of domain depth; in fact the domain depth is an equivalent depth which is calculated taking into account the total volume of machine.

The linearization of machine is also used in quasi 3-D modeling [1]. In quasi 3-D analysis, the axial flux machine can be considered as the composition of several linear machines and the sum of single linearized machines gives the total axial flux machine analysis. The procedure starts with the

selection of a computation plane in different point (for example it is possible to start from the external diameter and to create an iteration procedure until the average diameter). On the selected computation plane it is performed the transformation between the 3D machine in 3D linearized machine which is transformed in 2D plane.

Instead, the 3D analysis is the most complete analysis for an axial flux machine because takes into account all the boundaries effects neglected by the other analysis. In 3D analysis, the equation (5) used in 2D become:

$$\frac{1}{r}\frac{\partial}{\partial r}\left(r\frac{\partial A}{\partial r}\right)+\frac{1}{r^2}\frac{\partial^2 A}{\partial \varphi^2}+\frac{\partial^2 A}{\partial z^2}=-\frac{1}{r}\frac{\partial B_r}{\partial \varphi} \qquad (4.18)$$

The 3D analysis gives an high precision solutions respects to the 2D or quasi 3D analysis, but obviously this precision required an high computational cost and an increase of simulation time.

References of Chapter 4

[1] A. Parviainen, M. Niemelä, J. Pyrhönen, "*Modeling of Axial Flux Permanent-Magnet Machines*", IEEE Transactions on Industry Applications, Vol. 40, No. 5, September/October 2004

[2] G. Bertotti, "*Physical interpretation of eddy current losses in ferromagnetic materials: I. Theoretical considerations*", Journal of Applied Physics , Volume 57, Issue 6 ,1985

[3]F.Fiorillo, A. Novikov, "*An Improved Approach to Power Losses in Magnetic Laminations under Nonsinusoidal Induction Waveform* ", IEEE Transactions on Magnetics, Vol.26, No.5, September 1990

5. Mathematical model of concentrated single layer windings used in fault tolerant applications

In this chapter, the mathematical model of a machine with a tooth concentrated single layer windings is presented. The model is developed in a general manner and can be used for all slots and poles combinations. Usually, the machine with concentrated single layer windings are considered as fractional slot windings machines, because the main poles pairs considered are the rotor poles pairs. The proposed approach is based on the consideration that the machine is designed with a different number of stator (p_{sta}) and rotor (p_r) poles pairs and the coupling between the stator magnetic flux density and the rotor magnetic flux density occurs on the generic spatial harmonic of the stator. Considering a generic concentrated windings (the concentrated windings are obtained considering the maximum pitch obtainable by the full pitch of a single layer windings), the turn functions is:

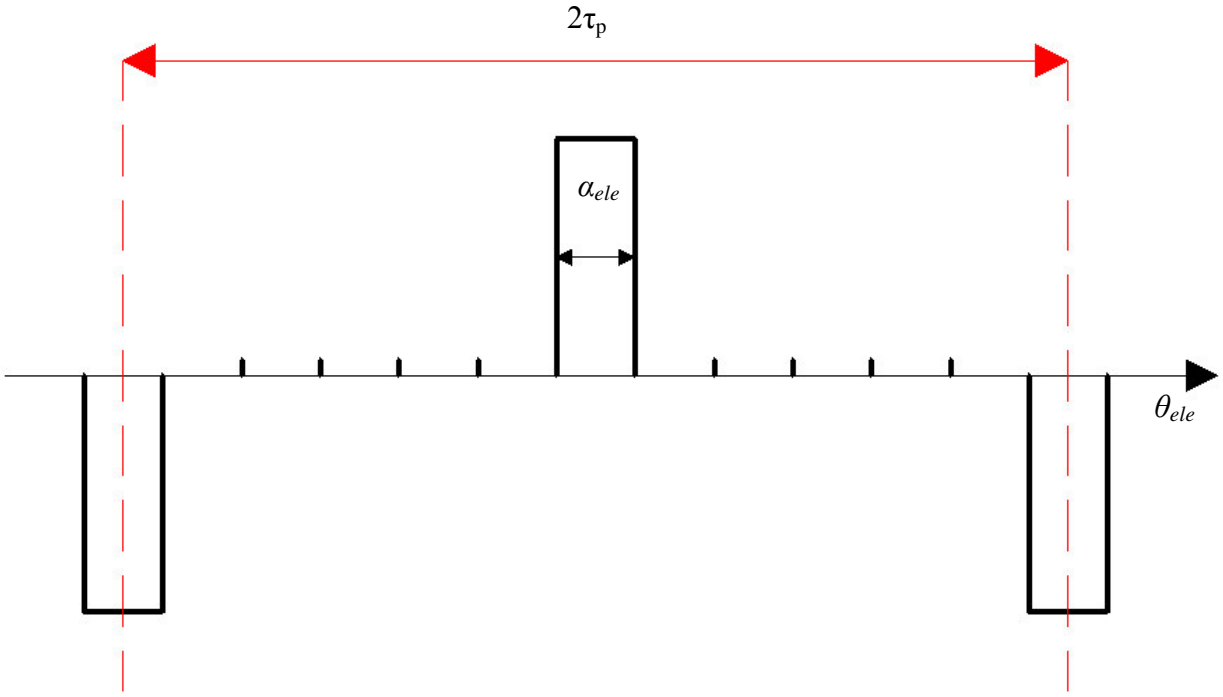

Fig.1.5 Stator linearization: τ_p is the polar pitch, α_{ele} is the slot electrical angle, θ_{ele} is the stator electrical angle.

$$N_k(\theta,t)=\frac{N}{\pi}\left[\int_{-\tau_p}^{-\tau_p+\frac{\alpha_{ele}}{2}}-\cos(n\theta_{ele})d\theta_{ele}+\int_{-\frac{\alpha_{ele}}{2}}^{\frac{\alpha_{ele}}{2}}\cos(n\theta_{ele})d\theta_{ele}-\int_{\tau_p-\frac{\alpha_{ele}}{2}}^{\tau_p}\cos(n\theta_{ele})d\theta_{ele}\right]\cos\left[np_{sta}\theta-(k-1)\frac{2\pi}{m}\right]$$

(5.1)

where α_{ele} is the stator electric angular slot, τ_p is the polar pitch, N is the number of turns for tooth, n is the generic harmonics, m is the number of phases, k is the considered phase, θ is the mechanical angle and θ_{ele} is the electrical angle. The relation (5.1) become:

$$N(\theta,t)=\sum_{k=1}^{m}\sum_{hn=1}^{+\infty}\frac{2N}{\pi h}\left\{\sin\left[h\left(\tau_p-\frac{\alpha_{ele}}{2}\right)\right]+\sin\left(h\frac{\alpha_{ele}}{2}\right)\right\}\cos\left[hp_{sta}\theta-(k-1)\frac{2\pi}{m}\right] \qquad (5.2)$$

From the turns function obtained in (5.2) it is possible to write the distribution of magneto motive force generated by the stator windings:

$$\Delta F(\theta,t)=\sum_{k=1}^{m}\sum_{h=1}^{+\infty}\frac{2N}{\pi h}\left\{\sin\left[h\left(\tau_p-\frac{\alpha_{ele}}{2}\right)\right]+\sin\left(h\frac{\alpha_{ele}}{2}\right)\right\}i_k(t)\cos\left[hp_{sta}\theta-(k-1)\frac{2\pi}{m}\right] \qquad (5.3)$$

Considering that the polar pitch τ_p in electrical angle is equal to π, the (3) is written as:

$$\Delta F(\theta,t)=\sum_{k=1}^{m}\sum_{h=1}^{+\infty}\frac{4N}{\pi h}k_{avv}i_k(t)\cos\left[hp_{sta}\theta-(k-1)\frac{2\pi}{m}\right] \qquad (5.4)$$

where :

$$k_{avv}=\sin\left(h\frac{\alpha_{ele}}{2}\right) \qquad (5.5)$$

The relation (4) become:

$$\Delta F(\theta,t)=\sum_{k=1}^{m}\sum_{h=1}^{+\infty}F_h\Re\left[e^{-jhp_{sta}\theta}\frac{2}{m}i_k(t)e^{j\left((k-1)\frac{2\pi}{m}\right)}\right] \qquad (5.6)$$

With:

$$F_h=\frac{2}{\pi}\frac{mN}{h}k_{avv} \qquad (5.7)$$

With the results provided by the relations (5.6) and (5.7), some examples are shown in the following. The figures 2.5a) and 2.5b) show the magneto motive distribution for two different three phase single layer windings machines and in the figures 3.5a) and 3.5b) are illustrated the magneto motive force of a single phase :

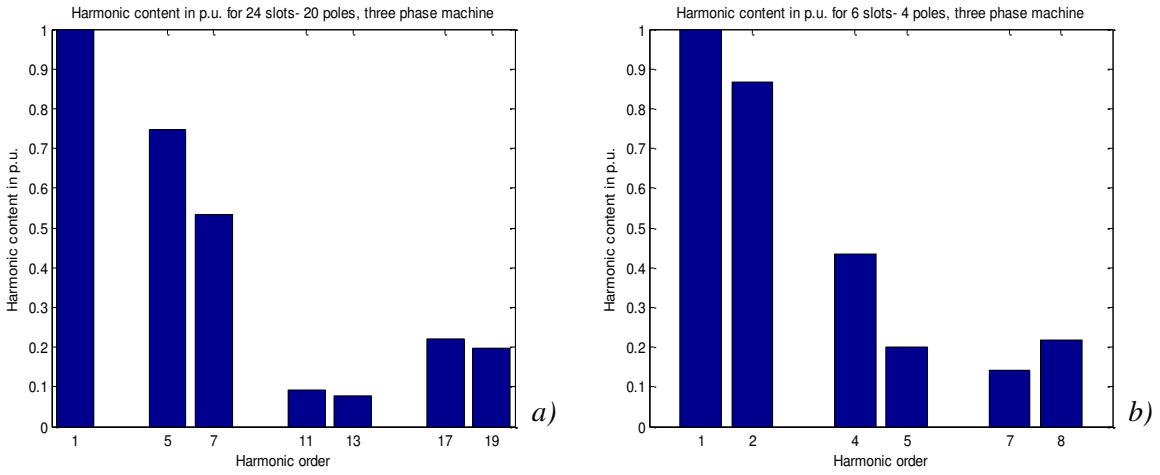

Fig.2.5 Magneto motive force distribution for 24 slots-20 poles three phase machine (a) and for 6 slots-4 poles three phase machine (b).

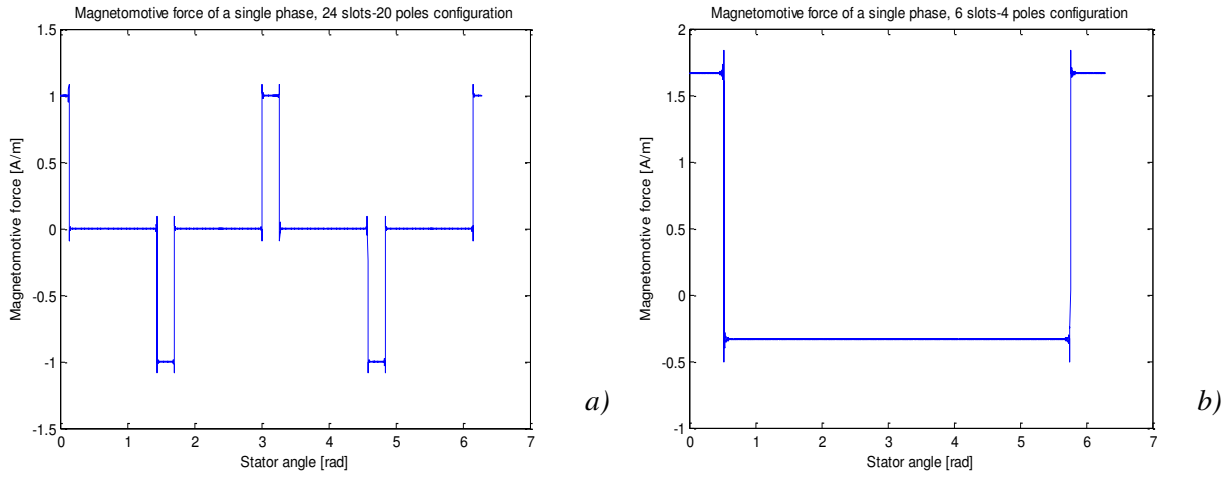

Fig.3.5 Magneto motive force distribution for 24 slots-20 poles three phase machine (a) and for 6 slots-4 poles three phase machine (b).

The first machine has 24 slots and 20 rotor poles, while the second machine is made with a configuration of 6 slots-4 poles machine. As is possible to note, the harmonic contain of first machine presents only the odd harmonics while in the second machine harmonic content all the harmonics orders are included (obviously only the third harmonic is not included).

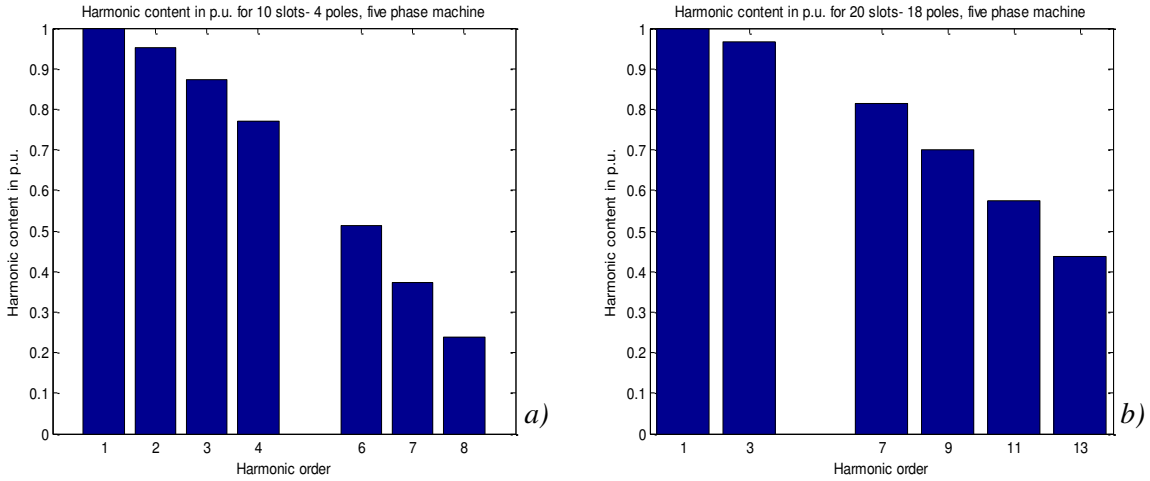

Fig.4.5 Magneto motive force distribution for10 slots-4 poles three five machine (a) and for 20 slots-18 poles five phase machine (b).

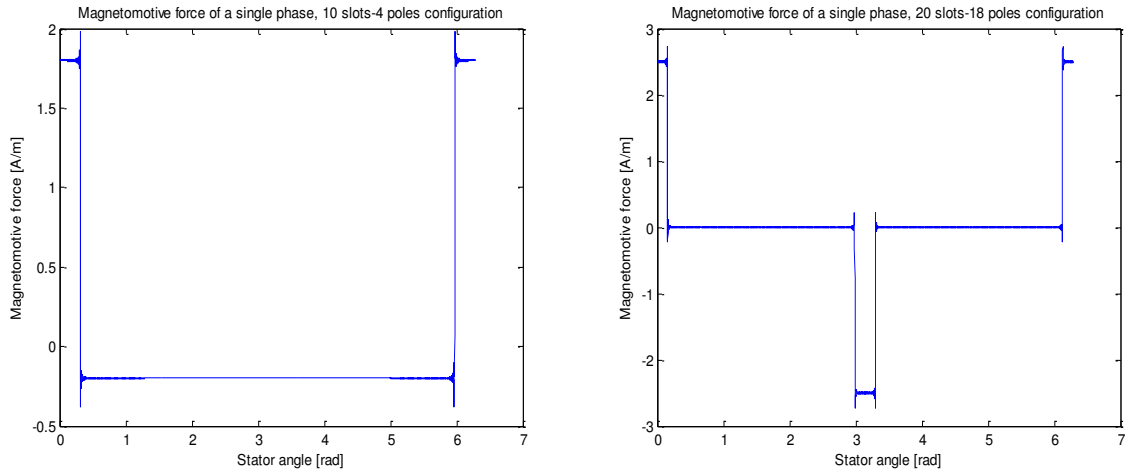

Fig.5.5 Magneto motive force distribution for10 slots-4 poles three five machine (a) and for 20 slots-18 poles five phase machine (b).

The figures 4.5a) and 4.5b) show the magneto motive distribution for two single layer windings , five phase machines with 10 slots-4 poles and 20 slots, while the fig. 5.5a) and 5.5b) represent the magneto motive force of a single phase of the machine.

Starting from the equation (5.6), the air gap flux density generated by the stator is obtained with the introduction of air gap permeance function evaluated as:

$$\lambda(\theta,\mathrm{t}) = \sum_{z=0}^{+\infty} \lambda_z \cos(2zhp_r\theta_r) \qquad (5.8)$$

with λ_h the generic harmonic of permeance function, , p_r is the number of magnet poles pairs and θ_r is the mechanical rotor angle; the following formula for the stator air gap flux density is obtained:

$$\mathrm{B_s}(\theta,t) = \lambda(\theta,\mathrm{t}) \sum_{k=1}^{m} \sum_{h=1}^{+\infty} F_h \Re\left[e^{-jhp_{sta}\theta} \frac{2}{m} i_k(t) e^{j\left((k-1)\frac{2\pi}{m}\right)} \right] = \lambda(\theta,\mathrm{t}) \sum_{h=1}^{+\infty} B_{s,h} \Re\left[e^{-jhp_{sta}\theta} \mathbf{i_s} \right] \qquad (5.9)$$

The air gap magnetic flux density in the air gap is calculated as:

$$\mathrm{B_r}(\theta,t) = \sum_{n_r=1}^{+\infty} \frac{2}{\pi} \frac{B_r}{n_r} \left\{ \sin\left[n_r \left(\frac{\pi}{2p_r} + \beta \right) \right] + \sin\left[n_r \left(\frac{\pi}{2p_r} - \beta \right) \right] \right\} \cos(n_r p_r \theta_r) = \sum_{n_r=1}^{+\infty} B_{n_r} \cos(n_r p_r \theta_r)\, 54 \qquad (5.10)$$

In (5.10) B_r is the residual magnetic flux density, n_r is the harmonic index, β is the half of magnet pole pitch.

The air gap magnetic flux density is computed as the sum of stator and rotor terms:

$$\mathrm{B_{airgap}}(\theta,t) = \lambda(\theta,\mathrm{t}) \sum_{h=1}^{+\infty} B_{s,h} \Re\left[e^{-jhp_{sta}\theta} \mathbf{i_s} \right] + \sum_{n_r=1}^{+\infty} B_{n_r} \Re\left[e^{jn_r p_r \theta_r} \right] \qquad (5.11)$$

Utilizing always the virtual works principle and starting from the relation (5.11), it is possible to calculate the value of torque for the case of isotropic machine (magnetic behavior constant in the

air gap) and in the case of anisotropic machine (there is a main magnetic path along one direction). The torque is calculate as:

$$T(\theta,t) = K^1 \int_0^{2\pi} B_{airgap}(\theta,t) \frac{\partial \Delta F(\theta,t)}{\partial \theta} d\theta \qquad (5.12)$$

where K^1 is a constant which depends by the type of machine (radial or axial flux machine), θ is the stator mechanical angle. In order to explain the coupling between the stator an rotor poles pairs which permits the generation of the torque, in fig. 6.5 the distribution of linear current density for a 24 slots-20 poles three phase machine is displayed:

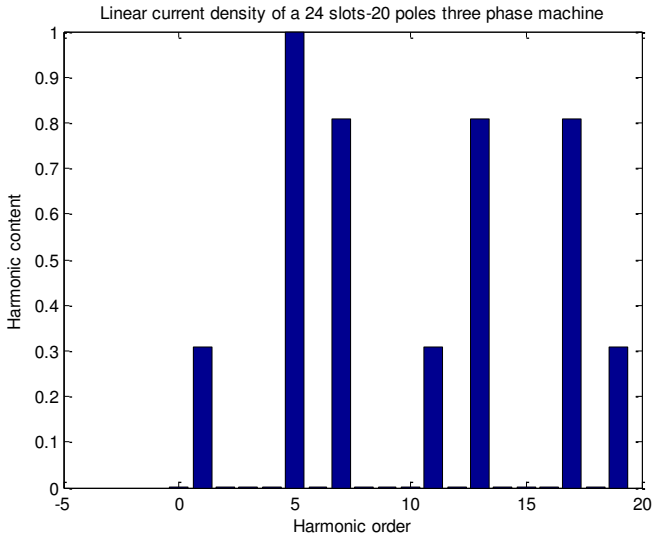

Fig.6.5 Magneto motive force distribution for10 slots-4 poles three five machine (a) and for 20 slots-18 poles five phase machine (b).

As is possible to note, the main harmonic of the stator linear current density distribution is the 5^{th} . In the examined case, the stator has two pole pairs therefore the fifth harmonic generates a magnetic flux density which the same period of the magnetic flux density creates by the ten pole pairs of the rotor.

In the case of isotropic machine, the relation (5.12) become:

$$\mathrm{T}=\mathrm{K}^1 \int_0^{2\pi} \left\{ \lambda_0 \sum_{n=1}^{+\infty} B_{s,n} \Re\left[e^{-jnp_{sta}\theta} \mathbf{i_s} \right] + \sum_{n_r=1}^{+\infty} B_{n_r} \Re\left[e^{jn_r p_r \theta_r} \right] \right\} \cdot \sum_{h=1}^{+\infty} h\, p_{sta} F_h \Im\left[e^{-jhp_{sta}\theta} \mathbf{i_s} \right] d\theta \qquad (5.13)$$

The product between the terms of (5.13) is equal to zero if the index h and n are different, therefore:

$$\mathrm{T}=\mathrm{K}^1 \int_0^{2\pi} \left\{ \sum_{h=1}^{+\infty} \lambda_0 h p_{sta} F_h B_{s,h} \Re\left[e^{-jhp_{sta}\theta} \mathbf{i_s} \right] \Im\left[e^{-jhp_{sta}\theta} \mathbf{i_s} \right] + \sum_{n_r=1}^{+\infty} \sum_{h=1}^{+\infty} h\, p_{sta} F_h B_{n_r} \Re\left[e^{jn_r p_r \theta_r} \right] \Im\left[e^{-jhp_{sta}\theta} \mathbf{i_s} \right] \right\} d\theta \qquad (5.14)$$

Assuming that the product between the real part and the imaginary part of two complex number is equal to the half sum of imaginary part of the product between the two complex number and the

imaginary part of the product between the complex conjugate of the first complex number and the second complex number, the relation (5.14) can be written as:

$$\mathrm{T}=\mathrm{K}\int_0^{2\pi}\left\{\sum_{n_r=1}^{+\infty}\sum_{h=1}^{+\infty}h\,p_{sta}F_hB_{n_r}\frac{1}{2}\Im\left[e^{j(n_r p_r\theta_r-hp_{sta}\theta)}\mathbf{i_s}\right]\right\}d\theta \qquad (5.15)$$

where $\mathrm{K}=\lambda_0\mathrm{K}^1$. Indicating with α the angle between the direct axis of rotor and the magnetic axis of the first phase:

$$\theta-\theta_r=\alpha \qquad (5.16)$$

the relation (5.15) become:

$$\mathrm{T}=\mathrm{K}\int_0^{2\pi}\left\{\sum_{n_r=1}^{+\infty}\sum_{h=1}^{+\infty}h\,p_{sta}F_hB_{n_r}\frac{1}{2}\Im\left[e^{-jn_r p_r\alpha}e^{j(n_r p_r-hp_{sta})\theta}\mathbf{i_s}\right]\right\}d\theta \qquad (5.17)$$

The (5.17) gives a value different from zero if and only if the following relation is respected:

$$n_r=h\frac{p_{sta}}{p_r} \qquad (5.18)$$

and the torque is expressed by the relation (5.19):

$$\mathrm{T}=\mathrm{K}\sum_{h=h1}^{+\infty}\pi h\,p_{sta}F_hB_{h\frac{p_{sta}}{p_r}}\Im\left[e^{-jhp_{sta}\alpha}\mathbf{i_s}\right] \qquad (5.19)$$

In order to particularize the model for an anisotropic machine, in the permeance function is considered the constant value of permeance and the first harmonic: in this way the air gap magnetic flux density become:

$$\mathrm{B}_{\mathrm{airgap}}(\theta,t)=\lambda_0\sum_{n=1}^{+\infty}B_{s,n}\Re\left[e^{-jnp_{sta}\theta}\mathbf{i_s}\right]+\lambda_1\sum_{n=1}^{+\infty}B_{s,n}\Re\left[e^{j2p_r\theta_r}\right]\Re\left[e^{-jnp_{sta}\theta}\mathbf{i_s}\right]+\sum_{n_r=1}^{+\infty}B_{n_r}\Re\left[e^{jn_r p_r\theta_r}\right] \qquad (5.20)$$

and the electromagnetic torque for an anisotropic machine become:

$$\mathrm{T}=\left[\sum_{h=h1}^{+\infty}\mathrm{K}\pi h\,p_{sta}F_hB_{r,h\frac{p_{sta}}{p_r}}\Im\left(e^{-jhp_{star}\alpha}\mathbf{i_s}\right)+\sum_{h=h1}^{+\infty}\mathrm{K}^1\lambda_1 hp_{sta}F_hB_{s,\frac{2p_r}{p_s}-h}\frac{\pi}{2}\Im\left(e^{-j2p_r\alpha}\mathbf{i_s}^2\right)\right] \qquad (5.21)$$

The torque expressed in (5.21) is composed by two terms: the firs is equal to the relation (5.19) , the latter is the term due to the anisotropy of the machine and is different from zero only for the harmonics of magnetic flux density which respect the following relation:

$$n=2\frac{p_r}{p_{sta}}-h \qquad (5.22)$$

6. Control strategies for an axial flux double rotor permanent magnet motor

In recent years, the use of AC electrical drives in industrial and in aerospace applications is rising; therefore it is necessary to develop new machine and new converter with faults tolerant features in order to increase the reliability of the drives. As cited in [1], the concept of a fault tolerant drive system is the possibility to operate with a minimum level of performance after a fault. In most of industrial applications, the electric motor is a three-phase induction motor or permanent magnet synchronous machine which is preferred in the applications where an high torque/power density is required. Usually each motors are fed by a voltage-source inverter supplied from a dc bus which can be substituted by a battery or a super capacitor. The increase of reliability level can be obtained with the usage of two motors in parallel (one master and another slave or in standby operation) or changing the converter and motor configuration as shown in [2]. In [2] is presented a simple and efficient reconfiguration of an AC drives composed by an three legs inverter and an induction motor; this configuration differs from the standard topology of a three phase AC drive because the neutral point of motor is linked to the midpoint of dc-link fig (1.6a).

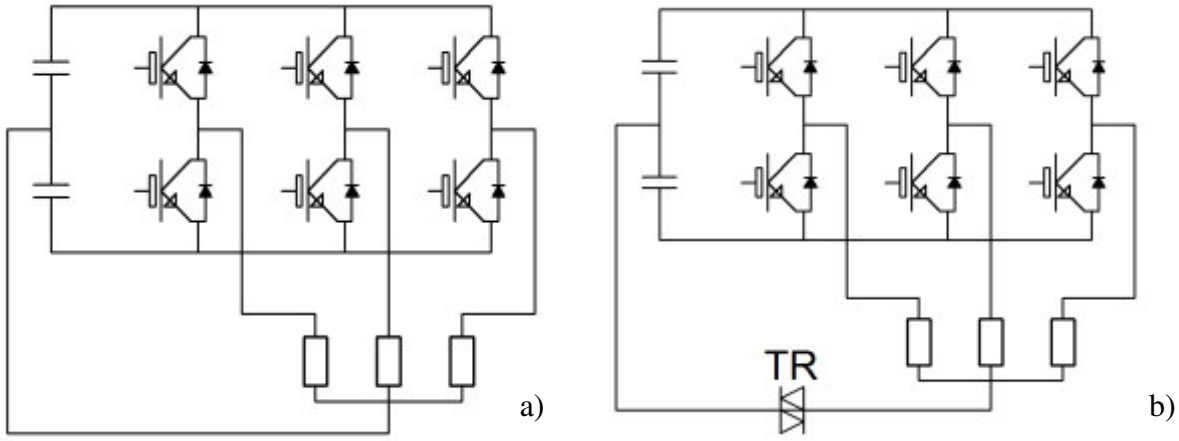

Fig.1.6Three phase AC Drives with a connection between the neutral point and the middle point of DC-Link; a)without triac on neutral b) with triac on the neutral.

In healthy operations, the current in neutral is practically zero while in the fault operations the current in the neutral become the sum of phases currents. In some application to guarantee that the neutral current is zero in normal mode operation, the neutral point of motors is separated to the dc-link by a triac fig.(1.6b), [2],[3], which is activated when a fault occurs in the motors windings or in the converter legs. As shown in [2], in order to obtain the same air gap rotating magnetic field is necessary that the following relations are respected:

$$\begin{aligned} i_s &= \frac{2}{3}\left(i_1 + i_2 e^{j\frac{2}{3}\pi} + i_3 e^{j\frac{4}{3}\pi} \right) = \frac{2}{3}\left(i_1 + i_2 e^{j\frac{2}{3}\pi} - i_1 e^{j\frac{4}{3}\pi} - i_2 e^{j\frac{4}{3}\pi} \right) = \\ &= \frac{2}{3}\left[i_1 \left(1 - e^{j\frac{4}{3}\pi} \right) + i_2 \left(e^{j\frac{2}{3}\pi} - e^{j\frac{4}{3}\pi} \right) \right] = \frac{2}{3}\sqrt{3}\left(i_1 e^{j\frac{\pi}{6}} + i_2 e^{j\frac{\pi}{2}} \right) \end{aligned} \tag{6.1}$$

In (6.1) it is assumed that the fault occurs on the third phase. To assure the same rotating magnetic field occurs that the currents must be increased by a factor of $\sqrt{3}$ and shifted by $\pi/6$. As it is

possible to note, the sum of new current i_1 and i_2 is different from zero and this implies the necessity to use the neutral connected to the middle point of dc-link. The fig. (2.6 a,b) and (3.6 a,b) shows the real and imaginary parts of symmetrical component in a normal operation and the symmetrical component with a fault occurs in the third phase. As it is possible to note, during the fault operation the symmetrical component parts (the blue dotted line) are not equal to the symmetrical component parts in normal operation and this determines a variation of rotating magnetic field in the air gap and then a worsening of machine performance.

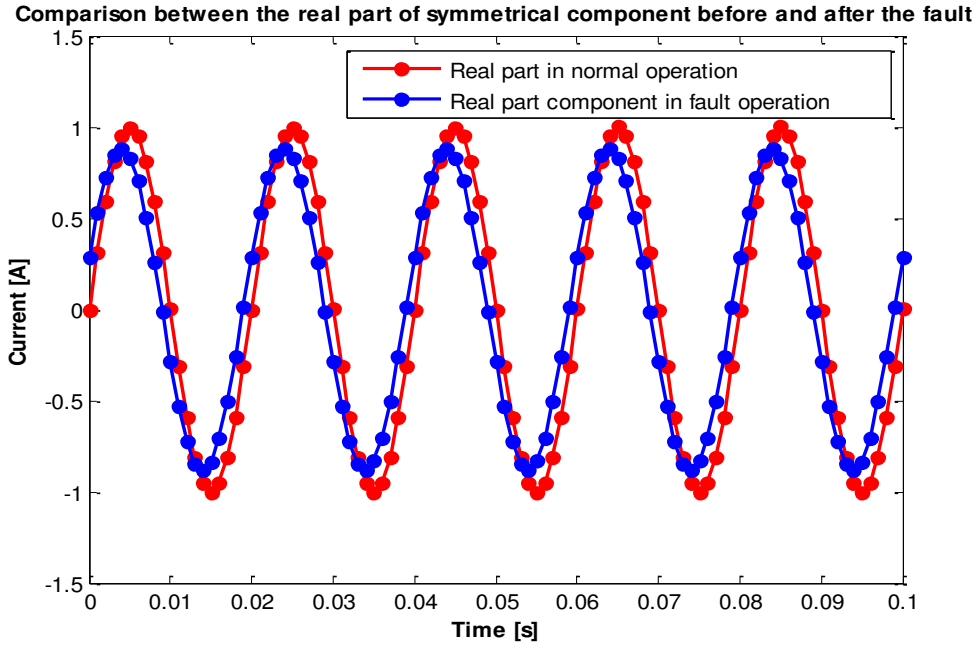

a)

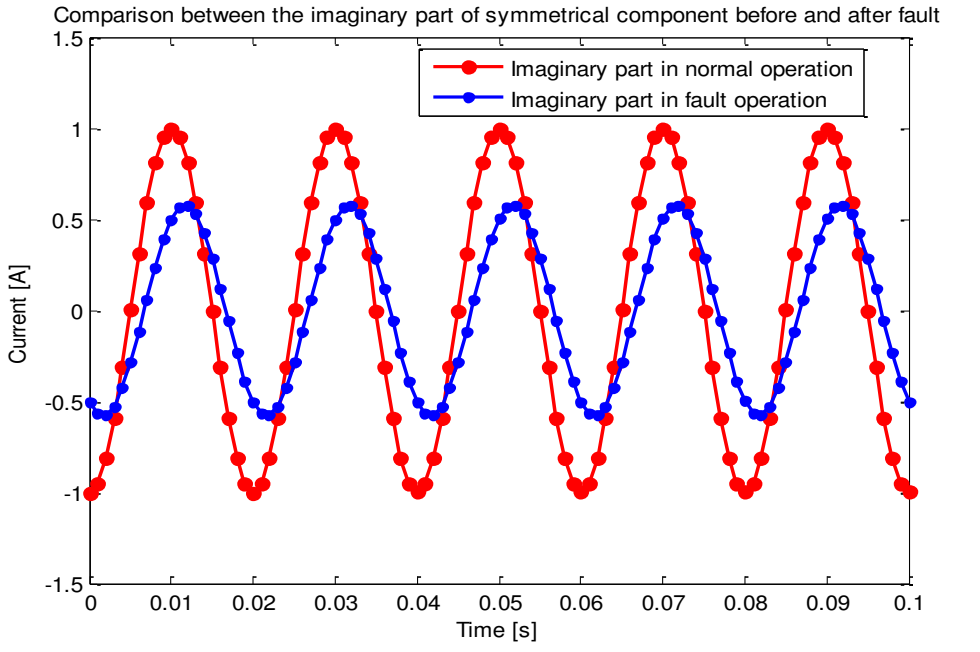

b)

Fig.2.6 Symmetrical component in normal and fault operation without the transformation of formula (6.1): a) real part of symmetrical component, b) imaginary part of symmetrical component

Instead in fig.3.6 a, b is made the comparison between the symmetrical component in normal operation and the symmetrical component in fault operation with the reconfiguration suggested by

relation (6.1). The symmetrical component obtained in fault operation coincides with the symmetrical component in normal operation.

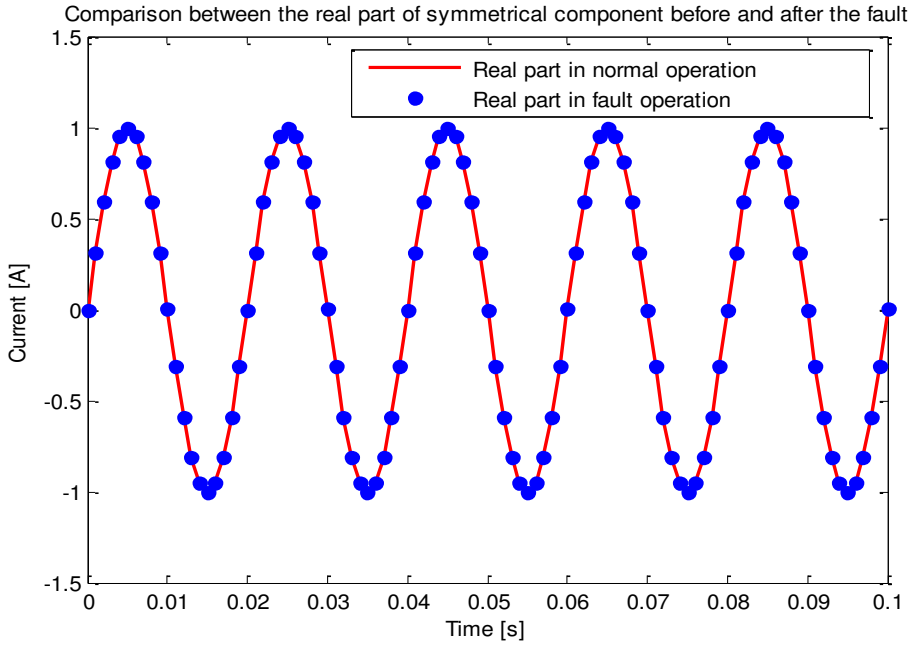

a)

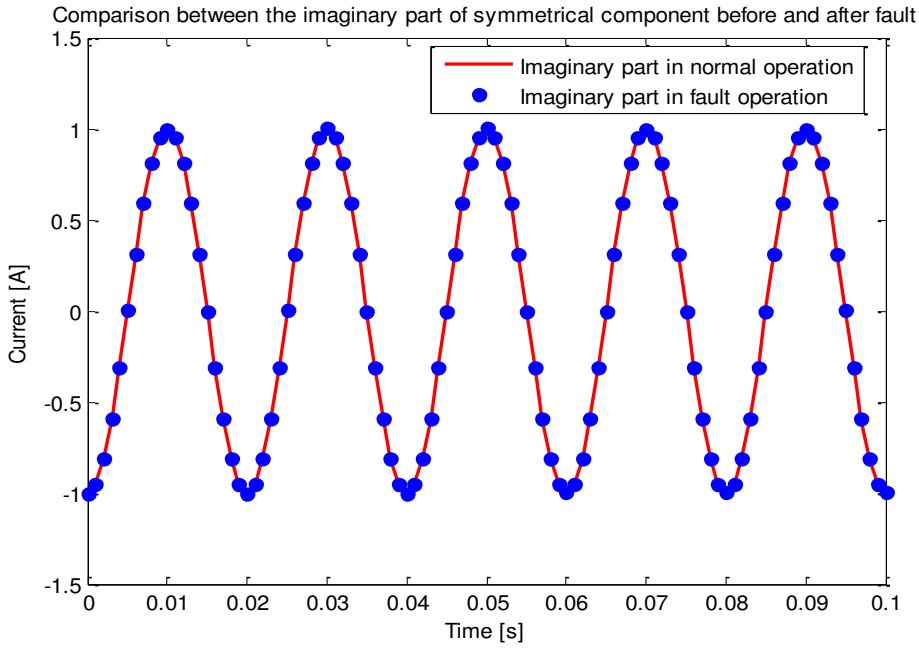

b)

Fig.3.6 Symmetrical component in normal and fault operation with the transformation of formula (6.1) : a) real part of symmetrical component, b) imaginary part of symmetrical component

Obviously, the application of reconfiguration proposed in [2] and [3] determines a reduction of machine operation domain in terms of maximum torque allowable and of maximum speed reached. In fault tolerant drives the three-phase motor is replaced by a motor with more than three phases. The needed reliability level is then reached by the fact that this motor can run on a reduced number of phases as shown for the three phase machine, but with a low degradation of performance respect the three phase motor.

In the technical literature are reported different applications of multiphase AC drives. For example in [4] is analyzed a two-motor five-phase drive system with series connection of stator windings: in this case is introduced an appropriate phase transposition in the series connection of two machines in order to create a complete decoupling of the flux/torque-producing currents between the two machines.
In [5] are reported an analytical current control strategies adopted to guarantee a safe drive operation after three different fault types: the open circuit condition of a single phase, the open circuit condition of two nonadjacent phases, and the open circuit condition of two adjacent phases. In particular are compared two motors with a double and single layers windings and the difference between the two different windings are highlighted.
The paper [6] proposes a global fault-tolerant control (FTC) for multiphase permanent-magnet machine drives and it is based on an optimization problem to produce ripple-free output torque with minimum joule losses. This approach has the important features of flexibility and simplicity in all possible fault conditions.
One of the most interesting features of double rotors axial flux machine is the double side stator. In the previous chapters, the benefits of this configuration are cited and in particular the main features regarding the possibility to make the machine with two separated windings fed by the same inverter or by two separated inverters. In fig.4.6 is shown the case of a four legs inverter with a three phase double rotor motor, while fig.5.6 shows the case of five legs inverter with the three phase motor:

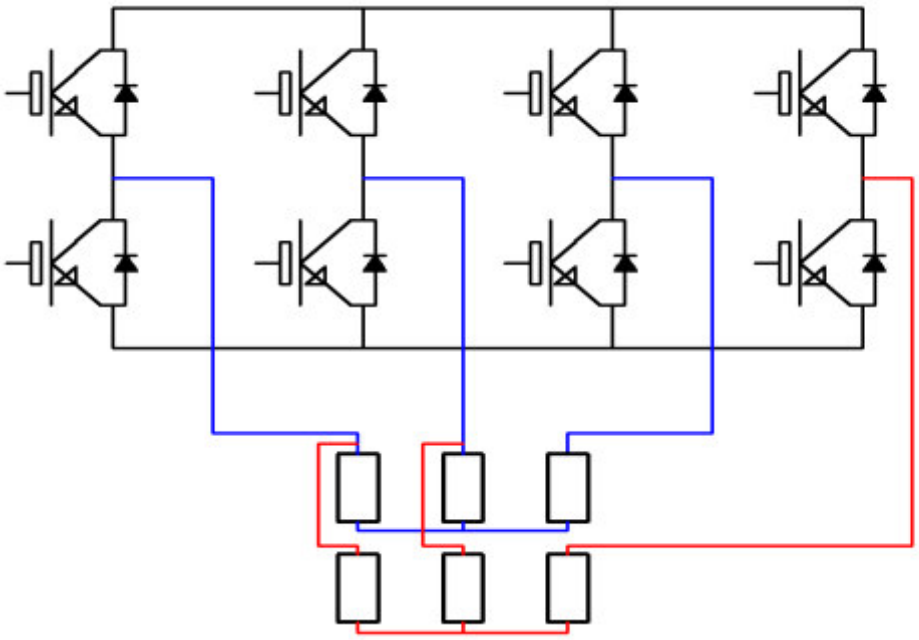

Fig.4.6 Four legs inverter and a three phase axial flux double rotor motor: the third phase of the two stator are separated and linked to two different inverter legs.

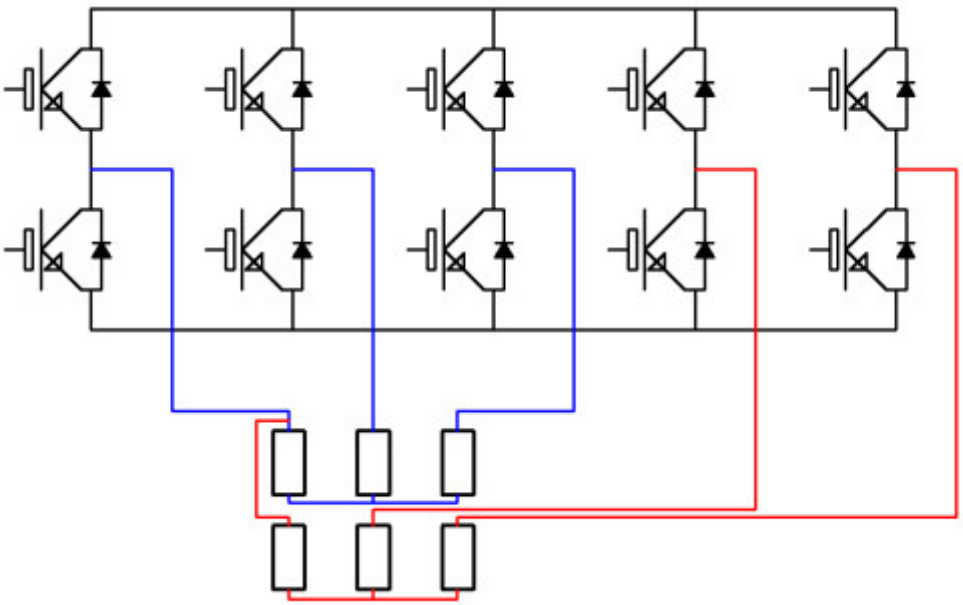

Fig.5.6 Five legs inverter and a three phase axial flux double rotor motor: the second and the third phase of the two stator are separated and linked to two different inverter legs.

In the following paragraphs are examined two different configurations which are able to control independently the two rotors.

6.1 Dual rotors axial flux permanent magnet machine fed by four legs inverter

The dual rotor axial flux machine allows the possibility to control two separated loads at two different speed. Obviously the possibility to control the rotors in two different manner depends also by the chosen inverter. For example, the usage of two independent inverters can guarantee a complete decoupling of the control of the two motor. In order to reduce the number of inverter legs, it was analyzed the configuration shown in fig.6.6 :

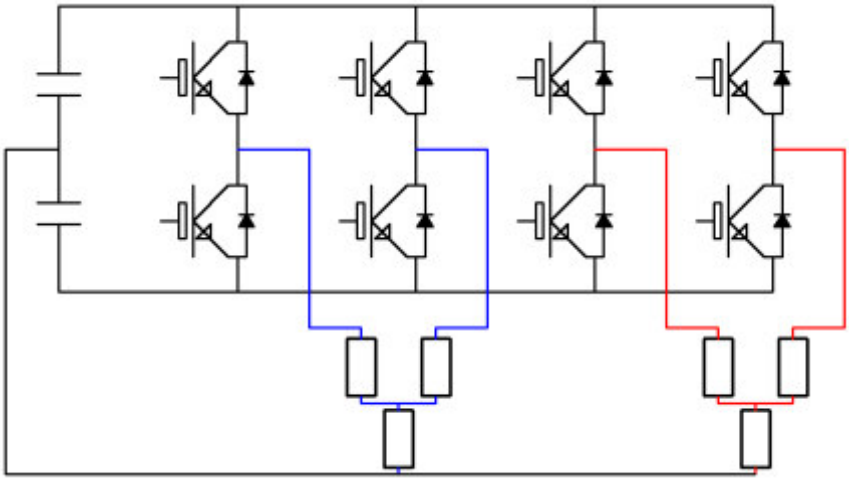

Fig.6.6 Four legs inverter and a three phase axial flux double rotor motor: only two phases for each side of stator are controlled

The four leg configuration permits to control in a separated manner the two rotors both in terms of speed and torque. The best advantages carried out by this configuration is the saving costs due to the fact that a four leg inverter supplies two three phase windings. The most important disadvantages are the limitation of voltage on a single phase coil and the absence of redundance in the inverter. The control of this configuration has been well examined in the literature: in [7] are investigated the possibilities for minimizing component cost in variable speed induction motor drives , with a technique called phase asymmetric PWM; in [8] is reported a new space-vector modulation strategy suitable for a four switches voltage-source inverter which minimizes the machine torque ripple, while in [9] the developed modulation strategy permits to reduce the dc-link voltage ripple.
Considering the results obtained in [8] - [9] and referring to fig. 7.6, the voltages between the point *a*,*b*,*c* and the neutral point n are:

$$\begin{cases} u_{an} = u_{a0} - u_{n0} \\ u_{bn} = u_{b0} - u_{n0} \\ u_{cn} = u_{c0} - u_{n0} \end{cases} \qquad (6.2)$$

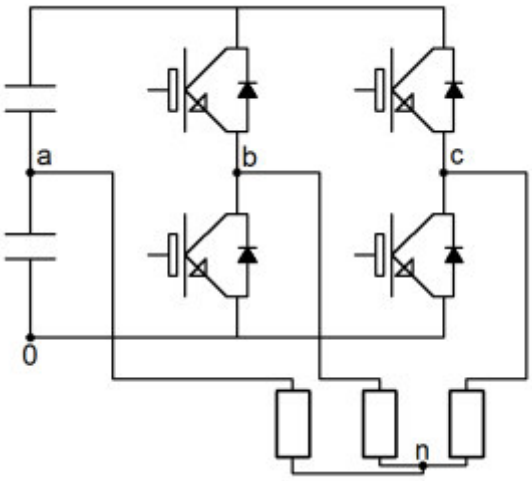

Fig.7.6 Four leg inverter configuration with the neutral point and legs.

Applying the Millman theorem to calculate the voltage u_{n0} and taking into account that the sum of the line to neutral voltages is zero, the relation (6.2) becomes:

$$\begin{cases} u_{an} = \frac{2}{3}u_{a0} - \frac{1}{3}(u_{b0} + u_{c0}) \\ u_{bn} = \frac{2}{3}u_{b0} - \frac{1}{3}(u_{a0} + u_{c0}) \\ u_{cn} = \frac{2}{3}u_{c0} - \frac{1}{3}(u_{a0} + u_{b0}) \end{cases} \qquad (6.3)$$

The u_{a0} is equal to $V_{dc}/2$ while the values of u_{b0} and u_{c0} can be V_{dc} or zero. In the table 1 are reported the value of phase voltages with different values of u_{b0} and u_{c0} . Referring to the case of a three phase inverter legs and taking into account the table 6.1, it is easily to note that the

configuration analyzed introduced some limits in the maximum voltage allowable in the phases. In the fig.8.6 is reported a simple control scheme based on an hysteresis current control for this inverter topologies.

The connections between the four legs of the inverter and the two windings of the two stator sides allows a separated control for the two rotors of the machine. The choice of an hysteresis current control is due to the fact that this configuration can be applied in low power applications where a contra rotating rotors are utilized, for example in low power unmanned aerial vehicles propellers [10].

		$\mathbf{u_{bo}}$		$\mathbf{u_{co}}$	
		0	V_{dc}	0	V_{dc}
$\mathbf{u_{bo}}$	0			$u_{an}=V_{dc}/3$ $u_{bn}=-V_{dc}/6$ $u_{cn}=-V_{dc}/6$	$u_{an}=0$ $u_{bn}=-V_{dc}/2$ $u_{cn}=V_{dc}/2$
	V_{dc}			$u_{an}=0$ $u_{bn}=V_{dc}/2$ $u_{cn}=-V_{dc}/2$	$u_{an}=-V_{dc}/3$ $u_{bn}=V_{dc}/6$ $u_{cn}=V_{dc}/6$
$\mathbf{u_{co}}$	0	$u_{an}=V_{dc}/3$ $u_{bn}=-V_{dc}/6$ $u_{cn}=-V_{dc}/6$	$u_{an}=0$ $u_{bn}=V_{dc}/2$ $u_{cn}=-V_{dc}/2$		
	V_{dc}	$u_{an}=0$ $u_{bn}=-V_{dc}/2$ $u_{cn}=V_{dc}/2$	$u_{an}=-V_{dc}/3$ $u_{bn}=V_{dc}/6$ $u_{cn}=V_{dc}/6$		

Table 6.1: Values of voltage u_{an}, u_{bn} and u_{cn}

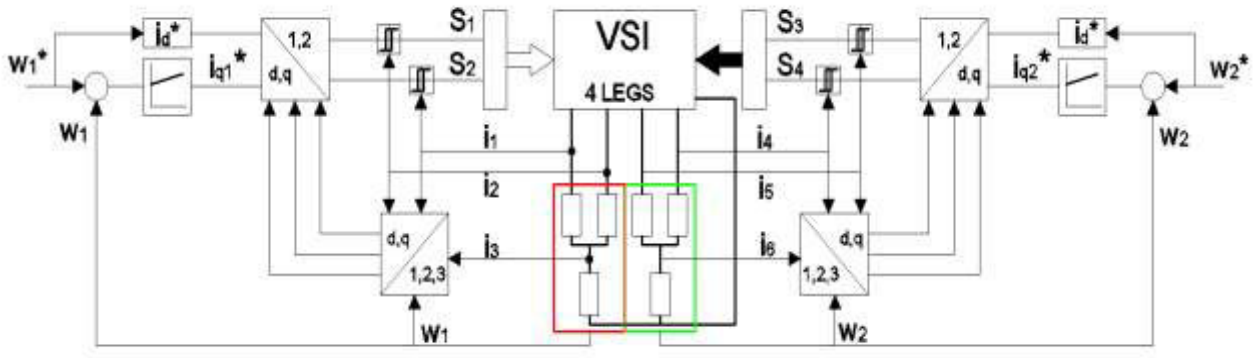

Fig.8.6 Control scheme of four leg inverter configuration based on hysteresis modulation of current

In the figures 9.6 and 10.6, are shown some results about the simulation of control scheme of fig.8.6.
The fig.9.6 shows a speed variation of the second rotor: the initial speeds are different (the angular speed of first rotor is 20 rad/s while the angular speed of second rotor is 40 rad/s) and at t=2s the second rotor was braked (the torque in fig.6.11 become negative).
The fig.10.6 well highlighted the separation of the control between the two rotor: in fact during the load variation the first rotor is not interested by torque or angular speed perturbations.

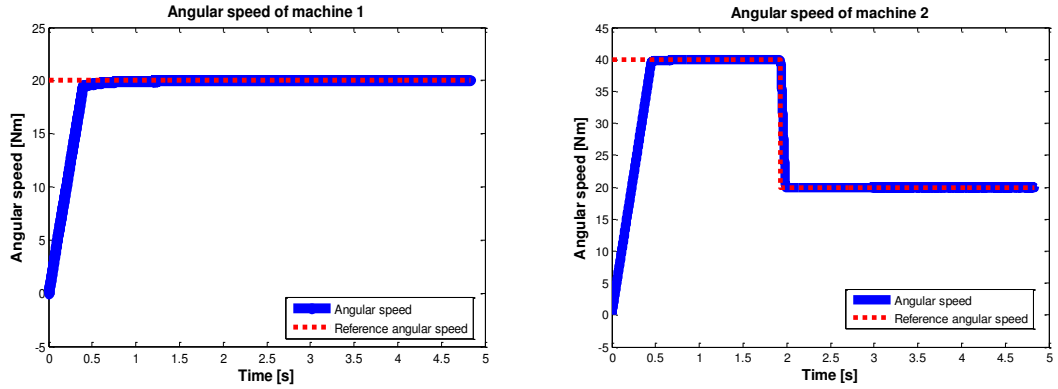

Fig.9.6 Angular speed of the two rotors: the initial speeds are different but a time t=2s the second rotor is braked and reached the same speed of first rotor

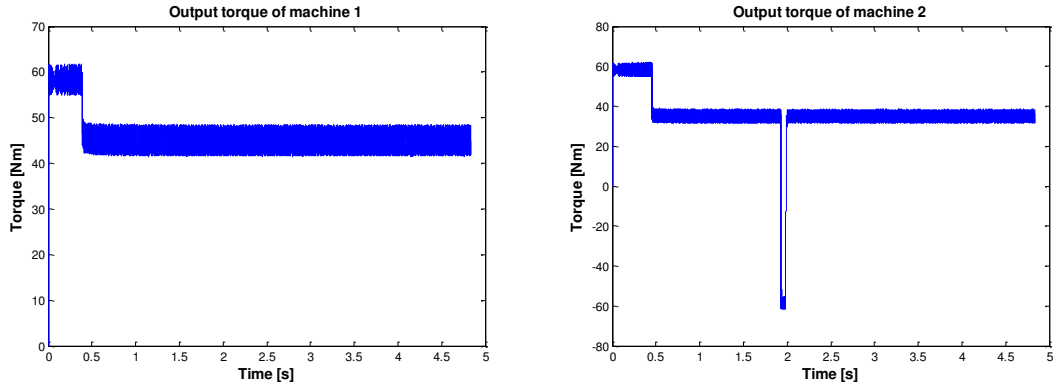

Fig.10.6 Output torque of machines: the variation of torque of second rotor machine doesn't influence the first rotor

6.2 Dual rotors axial flux permanent magnet machine fed by five legs inverter

Some application of dual three phase permanent magnet machine fed by a five legs inverter can be found in [11] and in [12]. In [11] is implemented a position control for the two motor, while in [12] is developed a model predictive control necessitating a state-space modeling based on the direct and quadrature axis of the two machine. The five legs configuration proposed in fig.11.6 allows the

possibility to control the machine with two different loads on the rotors, introducing a redundance in the drive and reducing the voltage limits which affected the four switch configuration, but the limitation of this configuration is inherent the angular speed of the two rotors which must be the same.

The proposed five legs configuration is made with a double rotor machine with two corresponding phase of the two stator sides places in an open phase configuration and linked to the dc-link. The other phases are connected to the middle point of dc-link. The connections to the dc-link permits to feed the windings of the machine with three unbalanced currents.

The presence of a common leg between the two windings of the stator implies that the current in this leg must be the same and this can create a problem specially when the two rotors work with different loads and a standard control determines two different currents in the common phases. To solve this is used a simple algorithm which identifies the two rotors as “master” and the “slave”. The master-slave algorithm identification is based on the comparison between the angular position of the two rotors as shown in fig.12.6: the master rotor is identified as the most loaded rotor. After the selection of master rotor and slave rotor, the reference currents for the master windings are calculated in a regular manner, while the reference currents of slave windings are reported in formula (6.4):

$$\begin{cases} i_{1,s} = \frac{3}{2} i_{sx,s} + \frac{\sqrt{3}}{2} i_{sy,slr} + i_3 \\ i_{2,s} = \sqrt{3} i_{sy,s} + i_3 \end{cases} \qquad (6.4)$$

where i_3 is the current in the common phase of master and slave windings and it is determined by the master control; $i_{sx,s}$ and $i_{sy,s}$ are respectively the real and the imaginary part of symmetrical component of slave rotor, $i_{1,s}$ and $i_{2,s}$ are the currents of the other two phases of slave windings.

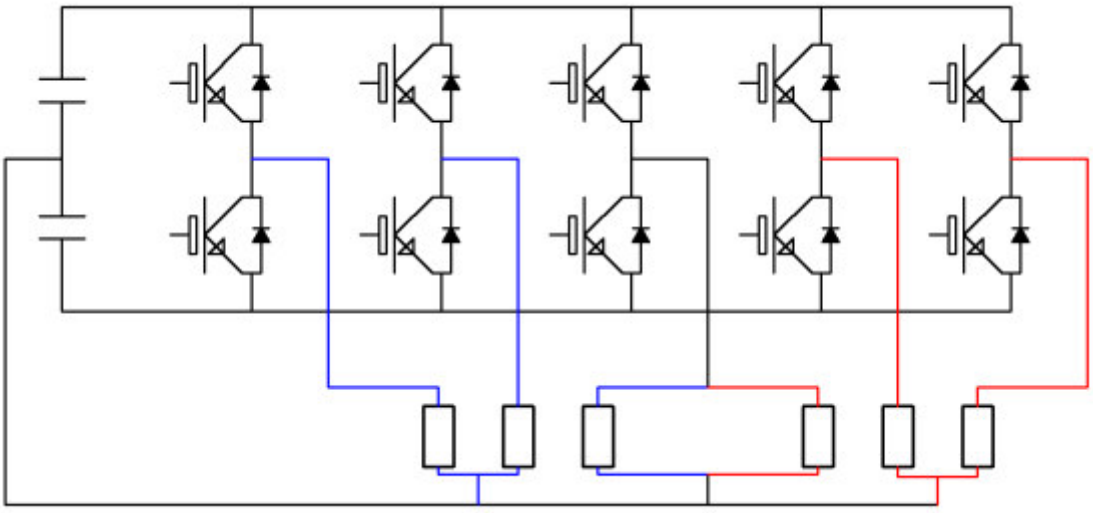

Fig.11.6 Five legs inverter with three phase axial flux double rotor motor: the third phase of each winding is separated from the other two phases.

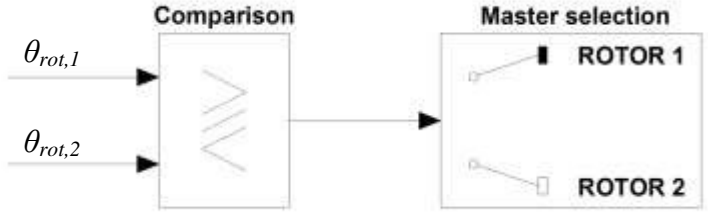

Fig.12.6 Master and slave rotors identification

The fig.13.6 shows the control scheme utilized. As mentioned before, in this configuration the angular speed of the two rotors must be the same. This can create some problems during the master and slave control, because the slave machine can reached the angular speed before the master machine (which is the most loaded machine) and synchronism between the two rotors is lost.
The necessity to guarantee the synchronism is due to the fact that the current in the third phase of the two windings is the same and only the synchronism permits to avoid that the currents in the other two phases have the same frequency of current in the common leg. The synchronism is guaranteed by a PI regulator which compare the speed of master and slave and acts on the slave quadrature current, in order to regulate the current and to simulate an increased mechanical inertia on the axis of slave rotor which permits to reach the desired speed in the same instant of master rotor.

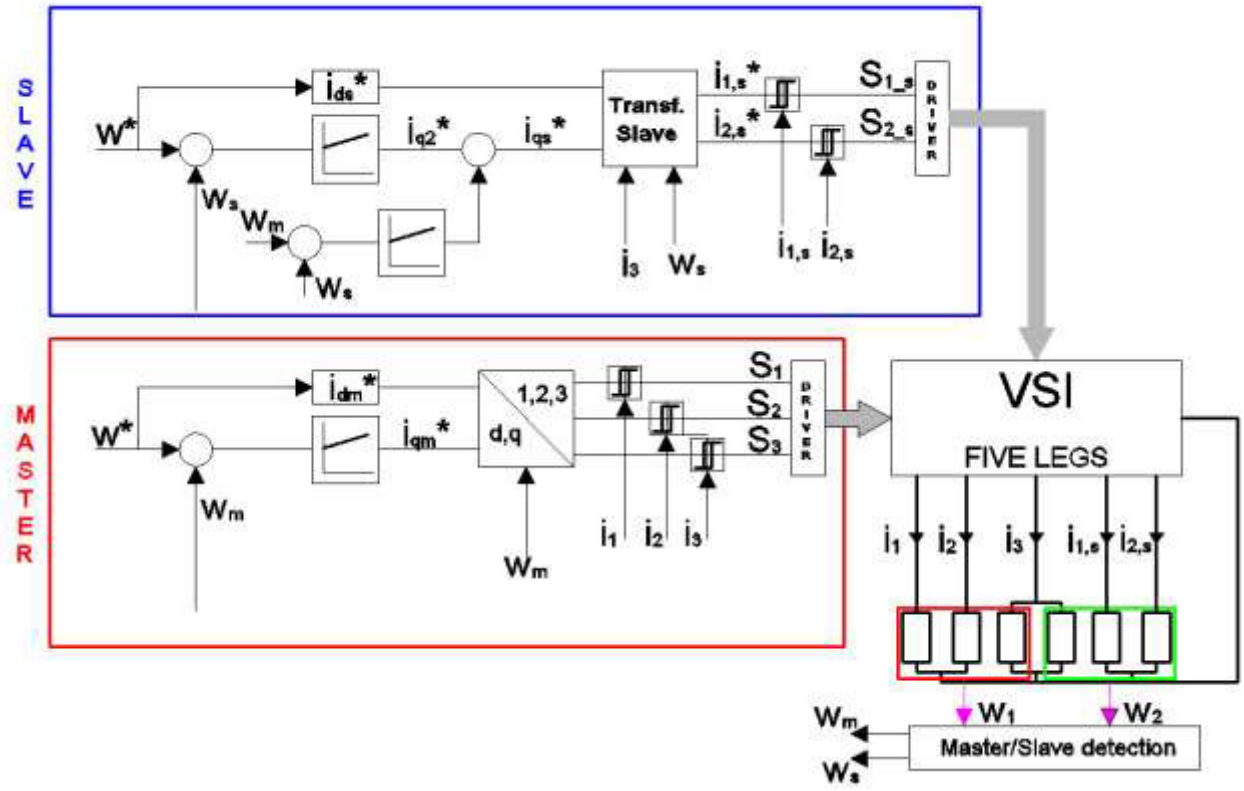

Fig.13.6 Control of five legs dual rotor axial flux machine

Various simulations were performed and the results are shown in fig.14.6, 15.6, 16.6. In fig.14.6 and 15.6 are reported respectively the torque and angular speed profiles for the two rotors.
A load variation step is introduced at t=2s.

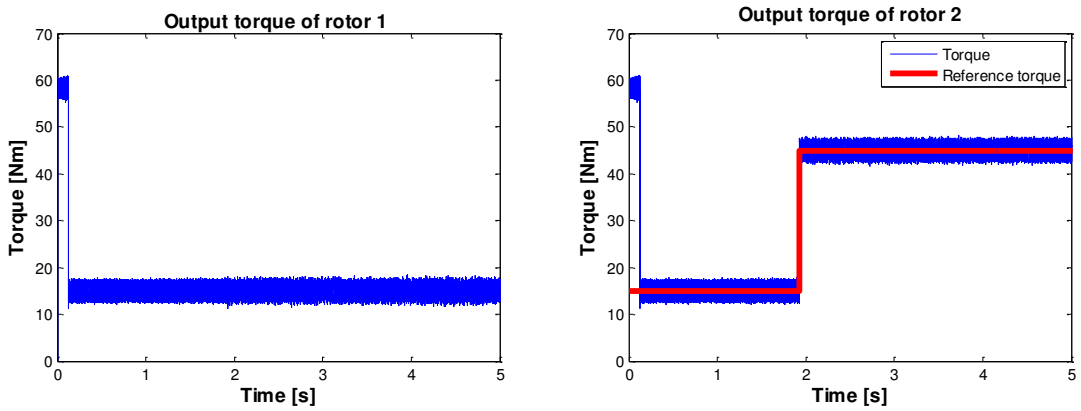

Fig.14.6 Torque profile of the two rotors: at t=2 there is a load variation and the second rotor become the master

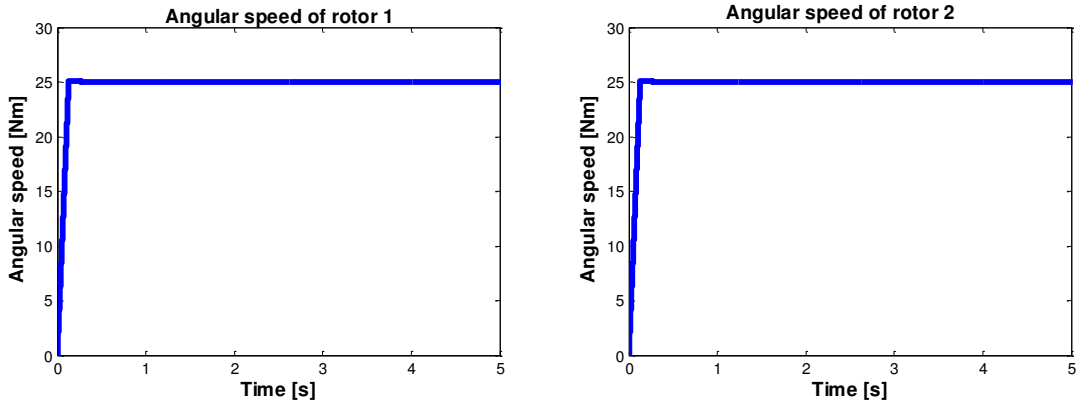

Fig.15.6 Angular speed of the two rotors during the simulation

The fig. 16.6 shows clearly the operation of the synchronization algorithm.

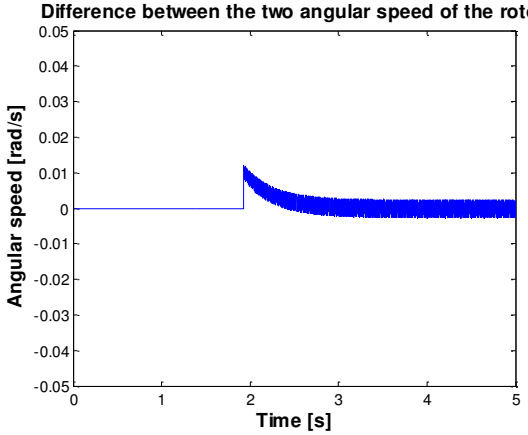

Fig.16.6 Difference between the angular speed of the two rotors: at time t=2s the load variation occurs and the synchronization algorithm permits to keep the synchronism between the two rotors

When the load variation occurs at t=2s, a difference of angular speed is carried out in the two rotors and the control identifies the master rotor and the slave rotor. In the control of slave rotor is introduced another PI with the aim to limit the quadrature axis current and to decelerate the rotor: in this way the control restores the synchronism between the two rotors.

References of Chapter 6

[1]Welchko B.A., Lipo T.A., Jahns T.M., Schulz S.E., "Faul tolerant Three-Phase AC Motor Drive Topologies: A Comparison of Features, Cost, and Limitations", IEEE Transactions on Power Electronics, Vol.19, No.4, July 2004

[2]Liu T.H., Fu J.R., Lipo T.A., "*A Strategy for Improving Reliability of Field Oriented Controlled Induction Motor Drives*", IEEE Transactions on Industry Applications, Vol.29, No.5, September/October 1993

[3] Fu J.R., Lipo T.A., "*A Strategy to isolate the switching device fault of a current regulated motor drive*", in Conf. Rec. IEEE IAS Annu. Meeting, Vol.2 , 1993,pp.1015-1020

[4] Levi E., Jones M. , Vukosavic S.N. , Iqbal A., Toliyat A.H., "*Modeling, Control, and Experimental Investigation of a Five-Phase Series-Connected Two-Motor Drive With Single Inverter Supply*", IEEE Transactions on Industrial Electronics, Vol. 54, NO. 3, June 2007

[5] Bianchi N., Bolognani S., Dai Pré M., "*Impact of Stator Winding of a Five-Phase Permanent Magnet Motor on Postfault Operations* ", IEEE Transactions on Industrial Electronics, Vol. 55, No. 5, May 2008

[6] Mohammadpour A., Parsa L., "*Global Fault-Tolerant Control Technique for Multiphase Permanent Magnet Machines*", IEEE Transactions on Industry Applications, Vol. 51, No. 1, January/February 2015
[7]Van der Broeck H.W., Van Wyk J.D., "*A Comparative Investigation of a Three-Phase Induction Machine Drive with a Component Minimized Voltage- Fed Inverter under Different Control Options*", IEEE Transactions on Industry Applications, Vol. IA-20, No. 2, March/April 1984
[8] Blaabjerg F., Freysson S., Hansen H.H. , Hansen S., "*A New Optimized Space-Vector Modulation Strategy for a Component-Minimized Voltage Source Inverter*", IEEE Transactions on Power Electronics, Vol. 12, No. 4, July 1997
[9] Blaabjerg F., Neacsu D.O., Pedersen J.K., "*Adaptive SVM to Compensate DC-Link Voltage Ripple for Four-Switch Three-Phase Voltage-Source Inverters*", IEEE Transactions On Power Electronics, Vol. 14, No. 4, July 1999
[10] Brando G., Dannier A., Del Pizzo A., Di Noia L.P., "*A Direct Drive Solution for Contra-Rotating Propellers in Electric Unmanned Aerial Vehicle*", 3rd International Conference on electrical systems for aircraft, railway, ship propulsion and road vehicles (ESARS'15), March 3rd-5th 2015, Aachen (Germany)
[11] Nozawa Y., Oka K., Omata R., Matsuse K., "*Performance for Position Control of Two Permanent Magnet Synchronous Motors with the Five-Leg Inverter* " 32nd Annual Conference on IEEE Industrial Electronics IECON 2006, 6-10 Nov. 2006, Paris
[12] Lim C.S., Rahim N.A.,Hew W.P., Levi E., "*Model Predictive Control of a Two-Motor Drive With Five-Leg-Inverter Supply*" IEEE Transactions on Industrial Electronics, Vol. 60, No. 1, January 2013

Conclusions

The particular configuration of axial flux machine can be useful in all the application where an high reliability is required. In this thesis work has been proposed a multi stack machine which combines both the rapid manufacturing of axial flux machine and give an high reliability to the drive.
In the thesis is presented a mathematical model for the single layer tooth concentrated windings, a design procedure of the axial flux machine, a study for the coupling between the axial flux machine and a ball screw actuator.
The design of a double rotor axial flux machine and the prototyping with the 3D printer is presented in chapter 4; in chapter 6 are shown two different control configurations for a multi stack machine made with a double rotor axial flux machine.
The final result of this thesis work is that the axial flux permanent magnet machines are a valid alternative to the radial flux machines for the use in linear mechatronic actuators. The attractiveness of the axial flux machine for industrial purposes is due to the compactness along the axial dimension and due to the high torque density in low speed applications which allows the possibility to make a direct drive actuators.

Acknowledgments

I want to express my gratitude to my supervisor Prof. Andrea Del Pizzo and to the coordinator of PhD in Electrical Engineering Prof. Claudio Serpico .

Moreover I want to thanks Prof. Elio Chiodo, Prof, Davide Lauria, Prof. Gianluca Brando, Prof. Adolfo Dannier and Prof. Renato Rizzo for their support in these years.

I want to thanks the company Umbra Cuscinetti SpA for the realization of the machine prototype; in particular I'm grateful to: Ing. Federico Perni, Ing. Luca Castellini, Ing. Moreno D'Andrea, Ing. Gianni Caiafa.

In the end, I am immensely grateful to my family for their support, their encouragement and their infinite patience.